TRIAXIAL BEHAVIOUR OF LAYERED SOIL AT SMALL STRAIN LEVEL

By **WEI LIU,** B. Eng.

SUPERVISORS: Peijun Guo and Dieter F.E. Stolle

A Thesis
Submitted to the School of Graduate Studies
in Partial Fulfilment of the Requirements
for the Degree of
Master of Applied Science

McMaster University

July 2017

Master of Applied Science (2017) McMaster University
(Civil Engineering) Hamilton, Ontario

TITLE: Triaxial Behaviour of Layered Soil at Small Strain Level

AUTHOR: Wei Liu, B.Eng.

SUPERVISORS: Peijun Guo and Dieter F.E. Stolle

NUMBER OF PAGES: xiv, 119

ABSTRACT

The purpose of this study was to analyze the anisotropic behaviour of layered soil at small strain level. This thesis comprised experimental, numerical, and theoretical aspects and provided an insight to the concept of the 'equivalent' homogeneous cross-anisotropic material indicating that the layered soil can be replaced by an equivalent transversely isotropic material under certain conditions.

In the experimental program, this study extended Vaid's work (1971) to conduct K_0-compression tests in a rigid triaxial cell with a flexible lateral boundary for the determination of the K_0-value of normally consolidated soil. The error induced by the compliance of the cell-water system that always existed in the previous study was successively eliminated by attaching a compliance correction system (i.e., GDS controller) to the triaxial cell. Three stress path tests (i.e., the K_0-compression test, the plane strain compression test, and the hydrostatic pressure compression test) were conducted consecutively in a rigid triaxial cell for a layered soil specimen to determine the elastic cross-anisotropic properties of the equivalent homogeneous material. The applicability of the proposed approach was demonstrated by conducting the tests on two types of soil (i.e., the homogeneous soil and the layered soil).

A three-parameter constitutive equation for describing the soil's cross-anisotropic elastic behaviour was modified in a basic FEM program. Based on the material properties determined by the experimental study as an input, numerical simulations (i.e., the numerical K_0-test) using FEM were conducted to compare numerical results with the test results.

In the theoretical part, this study made use of the Reuss and the Voigt approximations and proposed a simple, yet physically meaningful, approach to determine the equivalent cross-anisotropic elastic properties of a multilayered medium. To simplify the exposition, a multilayered medium with two constituent materials that were both isotropic was examined.

ACKNOWLEDGEMENT

I really want to express my greatest gratitude to my Master's supervisors, Dr. Peijun Guo and Dr. Dieter Stolle, Professors of Civil Engineering at McMaster University. Their guidance and support during these years of research have been invaluable. I am grateful for their great patience and encouragement. I am also very proud that I have this wonderful opportunity to be their Master student. Without them, this thesis would not have been completed.

I am grateful to Mr.Peter Koudys, Geotechnical laboratory technician, for his wonderful help and advice during the experimental study.

I would like to express my thanks to the Department of Civil Engineering, McMaster University for consistent support, and also I would like to thank my several colleagues, Xing Li, Yaqian Liu, Jingshan Shi, Sina Moallemi, who gave me a lot of help, suggestions and feedback.

Special thanks to my parents for their consistent financial support and consistent help through the whole period of study. Without them, this thesis would not have been completed.

TABLE OF CONTENTS

LIST OF FIGURES

LIST OF TABLES

LIST OF SYMBOLS

α	Degree of anisotropy
A	Cross-sectional area of the soil specimen
B	Degree of saturation
C	Compliance of cell-water system
C_{ijkl}	Compliance tensor for the stress-strain relation
D_{ijkl}	Stiffness tensor for the stress-strain relation
E	Elastic modulus
E_v	Elastic modulus in the vertical direction
E_h	Elastic modulus in the horizontal direction
E_{Voigt}	Voigt average elastic modulus
E_{Reuss}	Reuss average elastic modulus
E_i	Elastic modulus of the *i*-th constituent layer.
$\bar{E}_c$	Equivalent elastic modulus of a multilayered medium
G	Shear modulus
G_{vh}	Shear modulus in vertical plane
G_{hh}	Shear modulus in a horizontal plane
H	Height of the soil specimen
h_i	Thickness and the elastic modulus of the *i*-th constituent layer
$\dot{h}$	Axial displacement rate
J	Coupling modulus
K	Bulk modulus
K_0	Coefficient of earth pressure at rest

K_{v0} Stress ratio of vertical effective stress to horizontal effective stress in PSC test

K_0^{NC} K_0-value of the normally consolidated soil

K_0^{OC} K_0-value of the over-consolidated soil

m_v Coefficient of volumetric compressibility

M_{vz} Constrained modulus

M_{vx} Soil property determined from PSC test

OCR Over-consolidation ratio

p' $=\sigma_v' + 2\sigma_h'$, Mean effective stress

q $=\sigma_v' - \sigma_h'$ Deviatoric stress

R Radius of the soil specimen

u_{b0} Back pressure required to fully saturate the soil specimen

$\bar{u}_x$ Average lateral displacement of the element

Δu Pore pressure change

V Volume of the soil specimen

$\dot{V}_2$ Rate of injecting water for making a compliance correction

ΔV Volume change of the fluid in the triaxial cell

ΔV_1 Volume change of the soil specimen

ΔV_2 Required volume of injecting water

σ_{kl} Stress tensor

σ Applied hydrostatic pressure

σ_v' Vertical effective stress

σ_h' Horizontal effective stress

σ_{v0}' Initial vertical effective stress

σ'_{h0} Initial horizontal effective stress

σ'_m $= \sigma'_v + 2\sigma'_h$, Mean normal effective stress

$\Delta\sigma'_v$ Vertical effective stress increment

$\Delta\sigma'_h$ Horizontal effective stress increment

$\Delta\sigma'_c$ Actual increase in horizontal effective stress due to the compliance

ε_{ij} Strain tensor

$\overline{\varepsilon}_x$ Average lateral strain of the element on the boundary

ε_{vol} Volumetric strain

ε_q $= \frac{2}{3}(\varepsilon_v - \varepsilon_h)$, Deviatoric strain

ε_v Vertical/Axial strain

ε_h Horizontal/Lateral strain

$\Delta\varepsilon_{vol}$ Volumetric strain increment

$\Delta\varepsilon_v$ Vertical/axial strain increment

$\Delta\varepsilon_h$ Horizontal/Lateral strain increment

ν Poisson's ratio

ν_{vh} Poisson's ratio for the effect of vertical strain on horizontal strain

ν_{hv} Poisson's ratio for the effect of horizontal strain on vertical strain

ν_{hh} Poisson's ratio for the effect of horizontal strain on horizontal strain

φ_i Volume fraction/Normalized thickness of the *i*-th constituent layer

ϕ' Effective friction angle

ABBREVIATIONS

ASTM	America Standard Test Method
CTC	Conventional Triaxial Compression Test
GDS	Global Digital System
HCA	Hollow Cylinder Apparatus
HPC	Hydrostatic Pressure Compression Test
KC	K_0-Compression Test
LVDT	Linear Variable Differential Transducer
PSC	Plane Strain Compression Test
REV	Representative Elementary Volume
SGSS	Japanese Geotechnical Society Standards
TTC	Toronto Transportation Commission

Chapter 1 INTRODUCTION

1.1 Background

With the rapid development of computing power and numerical modeling software over last 20 years, it is possible to more realistically analyze and make predictions for complex geotechnical problems in practice. Although commercial software provides a broad range of constitutive models, engineers need to select proper material models that can reasonably describe the mechanical behaviour of soil under different conditions. In addition, some parameters adopted in the constitutive models need to be obtained by experiments.

For structures designed to work under conditions far from soil failure, the strain level in the ground is small. The soil elastic stiffness at small strain level plays an important role in making accurate predictions of ground movement that can affect the performance of adjacent buildings, including underground structures.

In geotechnical engineering practice, soil is most commonly assumed to be isotropic and linearly elastic at stress levels that do not produce yielding of the soil (Clayton, 2011). The description of the characteristics of isotropic elastic soil requires two independent material properties among four parameters; i.e., elastic modulus E Poisson's ratio ν, bulk modulus K, and shear modulus G.This common assumption is based on the merit of simplicity and convenience. However, Bishop and Hight (1977) indicate that there are reasons that soil is actually anisotropic, or at least, cross-anisotropic. One of the main reasons is that soil tends to be deposited naturally through a one-dimensional consolidation process under accumulated overburden pressure over a long period. Thus, it is reasonable to assume that soil particles are oriented nearly parallel to the plane on which the major principal stress acts during consolidation. The normal to this plane should be an axis of radial symmetry. Seven constants are required to fully describe the stress-strain behaviour of a cross-anisotropic material, compared

with twenty-one constants for a full description of the anisotropic constitutive relation. For a cross-anisotropic soil, the mechanical behaviour in the horizontal plane is considered to be isotropic, but it is different from the behaviour in the vertical plane. Moreover, not all of these seven parameters are independent. Some constraints, which are introduced later in the literature review, must be satisfied and hence reduce the number of independent parameters.

Lee and Rowe (1989) and Simpson et al. (1996) demonstrated the importance of considering anisotropic elastic stiffness to obtain good numerical modeling results, especially for the case of ground deformations above tunnels. Since the 1980's, different approaches have been used to determine cross-anisotropic elastic properties of soil, including seismic field testing, dynamic laboratory testing, advanced triaxial testing with bender elements, and tests using the torsional shear hollow cylinder apparatus; e.g., Jardine, et al. (1984), Knodel et al. (1991), Hoque and Tatsuoka (1998), Chaney et al. (2000), Kuwano and Jadine (2002), Gaspare et al. (2007), and Nishimura (2014). Nevertheless, there is still limited reported data on the complete determination of cross-anisotropic elastic parameters of clays (Lings et al., 2000; Gaspare et al., 2007), and of sands (Bellotti et al., 1996; Kuwano and Jadine, 2002). In addition, there is no study on the equivalent cross-anisotropic elastic parameters of the undisturbed, layered soil.

Layered soil normally consists of a series of parallel layers of varying thickness in either a random or systematic pattern that is associated with the natural sedimentation process; as illustrated in Figure 1-1. Each constituent layer has isotropic properties with the thickness of each layer varying from several millimeters to several meters. When the thickness of each individual layer is much smaller than the characteristic length of interest, the multilayered system may be modeled as an equivalent cross-anisotropic homogeneous medium (Niemunis et al., 2000).

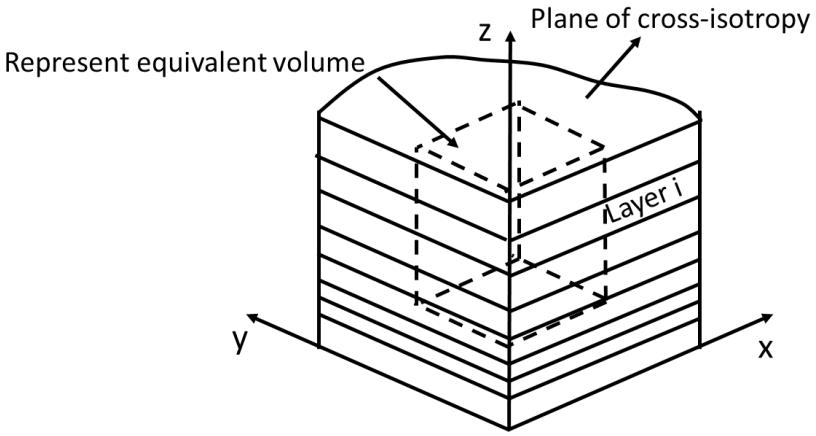

Figure 1-1 System of parallel homogeneous cross-anisotropic layers

Homogenisation is an effective and efficient approach to deal with the heterogeneous materials when the scale of the engineering problem is significantly larger than the dimension of each constituent and the focus is on the overall behaviour of the system, rather than on the details. The applicability of this approach is supported by previous studies on the modeling of the behaviour of layered materials (e.g., Gerrad,1982; Hornung, 1997; Niemunis et al., 2000; Milton, 2004; Stolle and Guo, 2007).

Salamon (1968) considered a multilayered medium composed of a series of parallel layers, each being homogeneous with different isotropic elastic properties. From the conservation of strain energy point of view, the multilayered medium can be represented by an equivalent homogeneous material. He showed that the equivalent material has cross-anisotropic symmetry, with the axis of symmetry coinciding with the direction perpendicular to layer interfaces. Its stress-strain relation can be described by the constitutive relation of 'general' cross-anisotropic materials.

In addition to small-strain elastic stiffness and deformation characteristic, the initial stress states in the naturally deposited ground are also affected by the nature of soil layering and deformation history. In many geotechnical problems, such as excavations, or the construction of retaining walls and tunnels, the initial stress state in the ground is important and must be known for design and analysis. The vertical effective stress at any depth can be easily determined according to the equilibrium in

the vertical direction. In geotechnical engineering, the horizontal effective stress is generally related to the vertical effective stress through the earth pressure coefficient at-rest defined as

$$K_0 = \frac{\sigma'_h}{\sigma'_v} \tag{1-1}$$

in which σ'_h and σ'_v are the horizontal and vertical effective stress, respectively.

However, the horizontal effective stress and hence the K_0-value are relatively difficult to determine for multilayered soils, either from measurements in field tests or through existing empirical relations that are mostly for homogeneous isotropic soils.

This study examines the K_0-value and the complete set of cross-anisotropic elastic properties of a layered soil when it is considered as an equivalent homogeneous soil through experimental and analytical investigations. On the experimental side, tests along three stress paths (i.e., K_0-compresstion test, plane strain compression test, and hydrostatic pressure compression test) are carried out in a rigid triaxial cell to determine the cross-anisotropic elastic properties of the layered soil. Among these stress path tests, the K_0-compression test is the most complicated to conduct in the laboratory and will be interpreted in details. Using the data obtained by each individual stress path test, the cross-anisotropic elastic properties of the soil are determined by applying the elastic cross-anisotropic constitutive equations via the least squares method.

Following the experimental study, the experimental process of the K_0-test is simulated by FEM. Two strategies for determining the average strain of the elements on the lateral boundary are proposed. After that, according to a theoretical analysis based on the Reuss and the Voigt models, a simple, yet physically meaningful homogenization approach is proposed to determine the ‘equivalent’ cross-anisotropic elastic properties for a layered material. A parameter sensitivity analysis is performed to investigate the dependence of the equivalent cross-anisotropic properties on the elastic properties of each constituent layer in a multilayered medium.

1.2 Research objectives

The main objective of this thesis is to study the small-strain cross-anisotropic elastic behaviour of layered soils, which is significantly different from that of homogeneous soils. The findings are expected to improve the analysis and design of geotechnical structures built in or on ground consisting of multilayered soils. This goal is achieved in this research by focusing on the following tasks:

- Demonstrate the experimental setup adopted in this study is capable of performing tests following a variety of selected stress paths (either compression or extension, by strain control or stress control, under drained or undrained conditions).
- Determine the equivalent cross-anisotropic elastic parameters of layered soils from measured data, by performing tests along three stress paths (i.e., the K_0-compresstion test, the plane strain compression test, and the hydrostatic pressure compression test) in the designed triaxial apparatus.
- Carry out FEM numerical simulations to interpret the behaviour of the layered soil and to compare with test results.
- Provide a theoretical homogenisation approach to determine the equivalent cross-anisotropic elastic properties for a layered medium given that the isotropic elastic properties and the volume fraction of each layer are known.

1.3 Thesis layout

Following a brief introduction in this chapter, Chapter 2 presents a review of the elasticity theory and a general description of elastic stress-strain relations for a cross-anisotropic soil. Different approaches to determine the cross-anisotropic elastic parameters are summarized, including the use of the traditional triaxial apparatus combined with other advanced instruments, such as bender elements and sensors for local strain measurement, and the use of advanced Hollow Cylinder Apparatus (HCA).

This is followed by a review of the homogenization technique for dealing with multilayered materials. Then, different methods to determine the coefficient of earth pressure at rest K_0 are discussed, including the use of the traditional oedometer apparatus and the triaxial apparatus.

Chapter 3 describes the experimental setup, tested materials, specimen preparation methods, and testing procedures for three types of stress-path tests. Typical experimental results are used to demonstrate the consistency and repeatability of the test results.

Chapter 4 provides analyses and interpretations of test results for different materials, along with the use of various strain and stress paths to acquire sufficient measured data to determine material properties. Following the presentation of three types of mathematical descriptions for the determination of the equivalent cross-anisotropic elastic properties, typical results obtained from these approaches are compared, with limitations of each method being discussed.

Chapter 5 conducts FEM simulations for the behaviour of layered soils and compares the numerical results to test results. A theoretical homogenisation approach to determine the equivalent cross-anisotropic elastic properties for a multilayered medium is also proposed by making use of the Reuss and the Voigt approximations. The applicability of the theoretical approach is examined by analyzing a multilayered medium with two constituent materials that are both isotropic. After that, a parameter sensitivity analysis is performed to investigate the dependence of the equivalent cross-anisotropic properties on the elastic properties of each constituent layer in a multilayered medium.

Chapter 6 provides conclusions and suggested future work.

Chapter 2 LITERATURE REVIEW

2.1 Anisotropic elasticity of soils

Natural soils are usually formed through a process of sedimentation and geological activities, including consolidation of sediments over a long period. During this process, non-spherical particles tend to align themselves with the longer axis in the horizontal plane at either microscopic or macroscopic scales. The preferential orientation of particles causes some degree of anisotropy in the macroscopic engineering properties of soil, including small strain stiffness, strength characteristics, and permeability (Liu, 2010).

The anisotropy of soil is generally categorized into two types: inherent anisotropy and induced anisotropy (Hoque and Tatsuoka, 1998). Inherent anisotropy results from the inherent grain structure and soil fabric, which are formed with preferential directions during the deposition process. Induced anisotropy comes from the change of soil fabric induced by certain stress or deformation history.

In engineering practice, the stiffness anisotropy and strength anisotropy both have significant influences on the analysis of many geotechnical engineering problems, such as the stability of slopes, the bearing capacity of footings, and the stability of underground structures.

The use of the elasticity theory plays an important role in soil mechanics for the calculation of deformation of geotechnical structures under working loads, where the shear stress level is much lower than the shear strength of soil. In this stress range, the anisotropic behaviour of soil, either linear or nonlinear, can be described within the framework of elasticity. Within the linear elastic region, the relation between stress and strain is described by Hooke's law (Hooke, 1675). For three-dimensional stress states, the generalized Hooke's law for an anisotropic elastic material is expressed in the Cartesian coordinate system as

$$\begin{Bmatrix} \Delta\varepsilon_{xx} \\ \Delta\varepsilon_{yy} \\ \Delta\varepsilon_{zz} \\ \Delta\gamma_{yz} \\ \Delta\gamma_{zx} \\ \Delta\gamma_{xy} \end{Bmatrix} = \begin{bmatrix} a_{11} & a_{12} & a_{13} & a_{14} & a_{15} & a_{16} \\ a_{21} & a_{22} & a_{23} & a_{24} & a_{25} & a_{26} \\ a_{31} & a_{32} & a_{33} & a_{34} & a_{35} & a_{36} \\ a_{41} & a_{42} & a_{43} & a_{44} & a_{45} & a_{46} \\ a_{51} & a_{52} & a_{53} & a_{54} & a_{55} & a_{56} \\ a_{61} & a_{62} & a_{63} & a_{64} & a_{65} & a_{66} \end{bmatrix} \begin{Bmatrix} \Delta\sigma_{xx} \\ \Delta\sigma_{yy} \\ \Delta\sigma_{zz} \\ \Delta\tau_{yz} \\ \Delta\tau_{zx} \\ \Delta\tau_{xy} \end{Bmatrix} \quad (2\text{-}1)$$

where, without loss of generality, ***x, y*** represent horizontal directions, and ***z*** indicates vertical direction.

In Eq. (2-1), the strain components are related to stresses through a compliance matrix with 36 components. The thermodynamic requirement that strain energy must be positive requires symmetry of the compliance matrix. As a result, only 21 independent constants are needed to entirely describe a fully anisotropic material. When a material has three mutually perpendicular planes of symmetry, then there are only 9 independent components of compliance matrix. This type of material is termed an orthotropic material (Love, 1927; Heyman, 1982). An isotropic elastic material has only two independent constants.

2.2 Cross-anisotropic elasticity of soils

As illustrated previously, an entire description of a general anisotropic, linearly elastic material requires the specification of 21 independent elastic constants. But analyses using such general material characteristics are very limited in engineering practice. The adoption of cross-anisotropy is the most prevalent type of anisotropy in soil due to the manner in which soils are deposited (Crampin, 1981). Most soils have anisotropy imposed through the processes through which they are formed. More specifically, soils are deposited naturally through a one-dimensional vertical consolidation process under accumulated overburden pressure over a long period. Thus, it is reasonable to realize that soil particles are oriented nearly parallel to the plane on which the major principal stress acts during consolidation. Such depositional history introduces an axis of radial symmetry which is normal to the horizontal bedding plane. As a result, the elastic

parameters in the horizontal plane are isotropic, but they are different from the parameters in the vertical direction. This type of anisotropy is generally referred to as the cross-anisotropy or the transverse isotropy.

The full description of the stress-strain relations of a cross-anisotropic soil require seven elastic constants. When introducing the elastic constants and Poisson's ratios, the stress-strain relations of a cross-anisotropic material are as follows:

$$\begin{Bmatrix} \Delta\varepsilon_{xx} \\ \Delta\varepsilon_{yy} \\ \Delta\varepsilon_{zz} \\ \Delta\gamma_{yz} \\ \Delta\gamma_{zx} \\ \Delta\gamma_{xy} \end{Bmatrix} = \begin{bmatrix} \frac{1}{E_h} & \frac{-\nu_{hh}}{E_h} & \frac{-\nu_{vh}}{E_v} & & & \\ \frac{-\nu_{hh}}{E_h} & \frac{1}{E_h} & \frac{-\nu_{vh}}{E_v} & & & \\ \frac{-\nu_{hv}}{E_h} & \frac{-\nu_{hv}}{E_h} & \frac{1}{E_v} & & & \\ & & & \frac{1}{G_{hv}} & & \\ & & & & \frac{1}{G_{hv}} & \\ & & & & & \frac{1}{G_{hh}} \end{bmatrix} \begin{Bmatrix} \Delta\sigma_{xx} \\ \Delta\sigma_{yy} \\ \Delta\sigma_{zz} \\ \Delta\tau_{yz} \\ \Delta\tau_{zx} \\ \Delta\tau_{xy} \end{Bmatrix} \tag{2-2}$$

where， E_v : Elastic modulus in the vertical direction;

E_h : Elastic modulus in the horizontal direction;

ν_{vh} : Poisson's ratio for the effect of vertical strain on horizontal strain, $\nu_{vh} = -\frac{\varepsilon_{xx}}{\varepsilon_{zz}}$;

ν_{hv} : Poisson's ratio for the effect of horizontal strain on vertical strain, $\nu_{hv} = -\frac{\varepsilon_{zz}}{\varepsilon_{xx}}$;

ν_{hh} : Poisson's ratio for the effect of horizontal strain on horizontal strain, $\nu_{hh} = -\frac{\varepsilon_{xx}}{\varepsilon_{yy}}$;

G_{hv} : Shear modulus in any vertical plane;

G_{hh} : Shear modulus in any horizontal plane.

For clarity, the zero terms in the elasticity matrix in Eq. (2-2) are omitted. Not all

of these seven parameters are independent. Because the horizontal plane is a plane of isotropy, the shear modulus G_{hh} is related to E_h and ν_{hh} via

$$G_{hh} = \frac{E_h}{2(1+\nu_{hh})} \tag{2-3}$$

The symmetry of the elastic stiffness matrix requires (Love, 1927)

$$\frac{\nu_{hv}}{E_h} = \frac{\nu_{vh}}{E_v} \tag{2-4}$$

When examining the 3rd row and column of the elasticity matrix in Eq. (2-2). As a result, five independent constants are required to describe a cross-anisotropic elastic material. Although the five necessary parameters are independent, there are bounds on the values that they can take because of the thermodynamic requirement that strain energy of an elastic material must be positive. Pickering (1970) showed that E_v, E_h, and G_{vh} must be positive, and $-1 < \nu_{hh} < 1$. He also indicated that E_v, E_h, ν_{hh}, and ν_{hv} must satisfy an inequality, which was equivalent to an expression given by Raymond (1970) in the form of

$$\frac{E_v}{E_h}(1-\nu_{hh}) - 2\nu_{vh}^2 \geq 0 \tag{2-5}$$

Raymond (1970) showed that G_{vh} is bounded by

$$G_{vh} \leq \frac{E_v}{2\nu_{vh}(1+\nu_{hh}) + 2\sqrt{(E_v/E_h)(1-\nu_{hh}^2)\left[1-(E_h/E_v)\nu_{vh}^2\right]}} \tag{2-6}$$

Referring to Eq. (2-2), consider the stress-strain relations with respect to the compliance tensor $\varepsilon_{ij} = C_{ijkl}\sigma_{kl}$, the elastic compliance tensor in the space of principal stresses or strains is expressed as

$$C_{ijkl} = \begin{bmatrix} \frac{1}{E_h} & -\frac{\nu_{hh}}{E_h} & -\frac{\nu_{vh}}{E_v} \\ -\frac{\nu_{hh}}{E_h} & \frac{1}{E_h} & -\frac{\nu_{vh}}{E_v} \\ -\frac{\nu_{hv}}{E_h} & -\frac{\nu_{hv}}{E_h} & \frac{1}{E_v} \end{bmatrix} \tag{2-7}$$

which involves five independent constants. By applying Eq. (2-4), the symmetry of C_{ijkl} is ensured, thus Eq. (2-7) becomes

$$C_{ijkl} = \begin{bmatrix} \frac{1}{E_h} & -\frac{\nu_{hh}}{E_h} & -\frac{\nu_{vh}}{E_v} \\ -\frac{\nu_{hh}}{E_h} & \frac{1}{E_h} & -\frac{\nu_{vh}}{E_v} \\ -\frac{\nu_{vh}}{E_v} & -\frac{\nu_{vh}}{E_v} & \frac{1}{E_v} \end{bmatrix} \tag{2-8}$$

The corresponding elastic stiffness tensor D_{ijkl} is expressed as (Guo and Stolle, 2016)

$$D_{ijkl} = \begin{bmatrix} D_{11} & D_{12} & D_{13} \\ D_{21} & D_{22} & D_{23} \\ D_{31} & D_{32} & D_{33} \end{bmatrix} \tag{2-9}$$

with

$$D_{11} = D_{22} = \frac{E_h(E_v - E_h\nu_{vh}^2)}{(1+\nu_{hh})\left[E_v(1-\nu_{hh}) - 2E_h\nu_{vh}^2\right]}$$

$$D_{12} = D_{21} = \frac{E_h(\nu_{hh}E_v + E_h\nu_{vh}^2)}{(1+\nu_{hh})\left[E_v(1-\nu_{hh}) - 2E_h\nu_{vh}^2\right]}$$

$$D_{13} = D_{31} = D_{23} = D_{32} = \frac{E_hE_v\nu_{hh}}{E_v(1-\nu_{hh}) - 2E_h\nu_{vh}^2}$$

$$D_{33} = \frac{E_v^2(1-\nu_{hh})}{E_v(1-\nu_{hh}) - 2E_h\nu_{vh}^2}$$

2.3 Experimental schemes to determine cross-anisotropic elastic parameters of soil

It has been observed that, for a wide range of soils, the stiffness is sufficiently constant below a strain level of about 0.001%, which is a threshold value for the elastic behaviour of soil (Clayton and Heymann, 2001). The exact 'threshold value' is open to debate, but elasticity is considered to be closely approximated for the behaviour at strains smaller than 0.001% (Nishimura, 2014). All calculations that follow for the determination of cross-anisotropic elastic parameters are considered to be at small strain levels, with the exception for that of Graham and Houlsby (1983), who considered the soil stiffness at large strain levels.

Extensive laboratory tests were performed in the past to investigate anisotropic behaviour of different types of soils, including clay (Graham and Houlsby, 1983; Ling et al.,2000; Gasparre et al.,2007; Nishimura,2014), granular materials (Hoque and Tatsuoka, 1998; Kuwano et al.,2000; Kuwano and Jardine, 2002; Liu,2010). In the various laboratory testing methods, the conventional triaxial apparatus is widely used. However, not all the cross-anisotropic elastic parameters can be determined from the results of conventional triaxial tests.

Graham and Houlsby (1983) proposed a mathematical technique for describing the pre-yield mechanical properties of clays using the cross-anisotropic elastic theory, and for determining appropriate material properties. Different from the common elastic constants used to describe the cross-anisotropic material, they adopted bulk modulus K, shear modulus G, and the coupled modulus J to define cross-anisotropic soil properties. Herein the coupled modulus J is used for a cross-anisotropic soil to establish relations between the mean stress and the shear strain, and between the shear stress and the volumetric strain. The least squares method was adopted to solve a set of equations that are mathematically redundant because four equations can be obtained from triaxial tests along two stress paths but there are only three unknowns defining the

elastic parameters (K , G ,and J). In addition, a ratio of elastic modulus in the horizontal and vertical direction is defined as a measure to quantify the degree of anisotropy of a soil. With this ratio, the elastic properties (K , G , and J) determined from the triaxial tests can be converted to the five more common engineering parameters (E_v , E_h , ν_{hh} , ν_{hv} ,and G_{vh}). This approach provides a theoretical framework for describing the elastic anisotropy of soil as measured in the triaxial test. However, the limitation of the approach is that the modulus in the horizontal direction E_h, and Poisson's ratio ν_{hh} cannot be obtained directly, because uniaxial horizontal loading cannot be applied in the triaxial apparatus (Kuwano et al., 2000).

Seyhan and Tuturmluer (2005) explored the stress path dependency of resilient modulus for granular materials at various anisotropic initial stress states under triaxial stress conditions. A three-parameter model was used to describe the linearly elastic stress-strain relation of a cross-anisotropic material. The cross-anisotropic parameters were determined by performing three triaxial tests along slightly different stress paths. Subsequently, the least squares method was used for a linear regression analysis on the data to determine three elastic parameters (i.e., E_v , E_h , and ν_{vh}). Liu (2010) used the same approach to determine the above three cross-anisotropic elastic properties.

Hoque and Tatsuoka (1998) developed a large triaxial apparatus to host a large square-prismatic specimen (57cm × 23cm × 23cm) with measurements of local axial and lateral strain to determine the cross-anisotropic elastic properties of reconstituted gravel specimens. Both inherent and stress-induced anisotropy were explored. In this method, the vertical elastic modulus E_v and Poisson's ratio ν_{vh} under a constant confining pressure were directly determined from the experimental data. However, the horizontal elastic modulus E_h cannot be obtained directly from the test results. ν_{hh} was estimated by assuming $\nu_{hh} = \nu_{vh}$ for the isotropic stress state. Owing to the limitation of the equipment, ν_{hv} and the shear modulus terms were not determined.

When considering the symmetry of the compliance matrix, only three independent cross-anisotropic elastic parameters can be directly determined from the data of traditional triaxial tests (Ling et al., 2000). To determine all five cross-anisotropic elastic constants, considerable effort has been made to combine data from the static triaxial tests and other tests (Jiang et al., 1997; Kuwano et al., 2000; Ling et al., 2000; Gasparre et al., 2007).

Kuwano et al. (2000) added bender elements to a conventional triaxial testing system to measure multi-directional shear wave velocities without sacrificing the ability to perform standard triaxial tests. With both the static triaxial test results and shear wave velocities from bender element tests, this approach could determine all the cross-anisotropic elastic properties through a simple manipulation of the elastic theory. In addition to the measurement of the overall axial deformation of the sample, Kuwano et al. (2000) also measured local axial strain and local lateral strains of the sample, which helped eliminate potential effects from the compliance of the apparatus and improve the accuracy of the measured deformation of the specimen. The same technique was adopted around the same time by Ling et al. (2000), and Kuwano and Jardine (2002) for sand, later by Gasparre et al. (2007) for London Clay.

The hollow cylinder apparatus (HCA) is the ideal testing equipment for the experimental study of anisotropic soil behaviour. Since the HCA offers independent control of four stress components (i.e., σ_r , σ_θ , σ_z , τ_{rz} with $\tau_{r\theta} = \tau_{\tau\theta} = 0$), and accurate strain measurements (ε_r , ε_θ , ε_z , γ_{rz}), the cross-anisotropic elastic parameters can be easily determined for the measured data (Zdravkovic and Jardine, 1997; Minh et al., 2011). However, in engineering practice, HCA is still rarely used due to the complex operation of a HCA and costly instrumentation.

One of the primary difficulties in determining the elastic constants of soil through laboratory tests using a triaxial apparatus is the non-reliable measurement of lateral strain. Nishimura (2014) explored a simplified approach to complete the parameter determination in a triaxial apparatus by establishing the relation between the undrained

elastic modulus and drained elastic parameters in saturated soil without radial strain measurement. A horizontally cut specimen was used to validate the reliability of this approach by comparing the elastic modulus determined on a vertically cut sample. Bender elements were installed to measure the shear moduli.

2.4 Three-parameter description of cross-anisotropy

Referring to Eq. (2-8), the compliance matrix of a cross-anisotropic material has five independent parameters for a description in the principal stress space. Owing to difficulties in determining all five anisotropic parameters through experimental work, simplified three-parameter models are proposed to account for the anisotropy of soil, particularly for cross-anisotropic soil under triaxial stress conditions (see, e.g., Graham and Houlsby,1983; Atkinson et al.,1990; Wood, 1990; Ling et al.,2000).

In the triaxial plane, the mean effective stress p' and the deviatoric stress q are related to the vertical and horizontal effective stress σ_v' and σ_h' via

$$\begin{bmatrix} p' \\ q \end{bmatrix} = \begin{bmatrix} \frac{1}{3} & \frac{2}{3} \\ 1 & -1 \end{bmatrix} \begin{bmatrix} \sigma_v' \\ \sigma_h' \end{bmatrix} \tag{2-10}$$

The corresponding volumetric strain ε_{vol} and deviatoric strain ε_q are related to vertical and horizontal strain ε_v and ε_h by

$$\begin{bmatrix} \varepsilon_{vol} \\ \varepsilon_q \end{bmatrix} = \begin{bmatrix} 1 & 2 \\ \frac{2}{3} & -\frac{2}{3} \end{bmatrix} \begin{bmatrix} \varepsilon_v \\ \varepsilon_h \end{bmatrix} \tag{2-11}$$

Referring to Atkinson et al. (1990), the incremental stress-strain relation at a small strain level can be expressed as

$$\begin{bmatrix} \Delta\varepsilon_{vol} \\ \Delta\varepsilon_q \end{bmatrix} = \begin{bmatrix} \frac{1}{K'} & \frac{1}{J'_{qp}} \\ \frac{1}{J'_{qp}} & \frac{1}{3G'} \end{bmatrix} \begin{bmatrix} \Delta p' \\ \Delta q \end{bmatrix} \tag{2-12}$$

where, K' is a bulk modulus, G' is a shear modulus, and J'_{qp} is the coupling modulus that links changes in deviatoric and volumetric behaviours.

When the material is isotropic, there is no coupling between the volumetric and distortional behaviour, which requires $\frac{1}{J'_{qp}}=0$, or equivalently $J'_{qp}=\pm\infty$. The three parameters (K', G', and J'_{qp}) in Eq. (2-12) can be evaluated separately by conducting drained triaxial tests at either constant p' or constant q.

Alternatively, Graham and Houlsby (1983) proposed a different form of three-parameter incremental stress-strain relation in terms of stiffness, which is expressed as

$$\begin{bmatrix} \Delta p' \\ \Delta q \end{bmatrix} \begin{bmatrix} K^* & J \\ J & 3G^* \end{bmatrix} = \begin{bmatrix} \Delta\varepsilon_{vol} \\ \Delta\varepsilon_q \end{bmatrix} \tag{2-13}$$

where, K^* is a bulk modulus, G^* is a shear modulus, and J is the coupling modulus.

It should be mentioned that there is no equivalence between K', G', J'_{qp} and K^*, G^*, J. However, conversion between these two sets of parameters can be obtained by inverting the matrix.

Without taking the shear terms into account, considering the condition in a triaxial cell with $\Delta\sigma_{xx}=\Delta\sigma_{yy}=\Delta\sigma_h$, $\Delta\sigma_{zz}=\Delta\sigma_v$, $\Delta\varepsilon_{xx}=\Delta\varepsilon_{yy}=\Delta\varepsilon_h$, and $\Delta\varepsilon_{zz}=\Delta\varepsilon_v$, Eq. (2-2) can be rewritten as

$$\begin{bmatrix} \Delta\varepsilon_v \\ \Delta\varepsilon_h \end{bmatrix} = \begin{bmatrix} \frac{1}{E_v} & \frac{-2\nu_{vh}}{E_v} \\ \frac{-\nu_{vh}}{E_v} & \frac{1-\nu_{hh}}{E_h} \end{bmatrix} \begin{bmatrix} \Delta\sigma'_v \\ \Delta\sigma'_h \end{bmatrix} \tag{2-14}$$

By making use of Eqs. (2-12) and (2-14), and Eqs. (2-13) and (2-14), Ling et al.

(2000) built a relation between the two sets of parameters (i.e., K', G', J'_{qp} and K^*, G^*, J) and cross-anisotropic elastic constants as

$$\begin{aligned} G' &= \frac{3}{4\left[\left(1+2\nu_{vh}\right)/E_v + (1-\nu_{hh})/2E_h\right]} \\ K' &= \frac{1}{\left[\left(1-4\nu_{vh}\right)/E_v + 2(1-\nu_{hh})/E_h\right]} \\ J'_{qp} &= \frac{3}{2\left[\left(1-\nu_{vh}\right)/E_v - (1-\nu_{hh})/E_h\right]} \end{aligned} \tag{2-15}$$

and

$$\begin{aligned} G^* &= \frac{E_v}{6}\left[\frac{2(1-\nu_{hh})E_v + (1-4\nu_{vh})E_h}{(1-\nu_{hh})E_v - 2\nu_{vh}^2 E_h}\right] \\ K^* &= \frac{E_v}{9}\left[\frac{(1-\nu_{hh})E_v + 2(1+2\nu_{vh})E_h}{(1-\nu_{hh})E_v - 2\nu_{vh}^2 E_h}\right] \\ J &= \frac{E_v}{3}\left[\frac{(1-\nu_{hh})E_v + (1-\nu_{vh})E_h}{(1-\nu_{hh})E_v - 2\nu_{vh}^2 E_h}\right] \end{aligned} \tag{2-16}$$

It is clear that two sets of parameters (i.e., K', G', J'_{qp} and K^*, G^*, J) are functions of the four independent parameters E_v, E_h, ν_{vh}, and ν_{hh}. Although K', G', J'_{qp} and K^*, G^*, J can be separately determined from standard triaxial tests, the four independent elastic parameters (E_v, E_h, ν_{vh}, and ν_{hh}) cannot be obtained unless an additional assumption or constraint is provided.

Graham and Houlsby (1983) proposed an alternative three-parameter (E^*, ν^*, α) description for the cross-anisotropic material by introducing an anisotropic factor α, which is defined as

$$\alpha = \sqrt{\frac{E_h}{E_v}} = \frac{\nu_{hh}}{\nu_{vh}} = \frac{G_{hh}}{G_{vh}} \tag{2-17}$$

With this assumption, the conventional cross-anisotropic elastic properties are determined as

$$
\begin{aligned}
E_v &= E^* \\
E_h &= \alpha^2 E^* \\
\nu_{vh} &= \nu^* / \alpha \\
\nu_{hh} &= \nu^* \\
G_{hv} &= \alpha E^* / 2(1+\nu^*) \\
G_{hh} &= \alpha^2 E^* / 2(1+\nu^*)
\end{aligned}
\tag{2-18}
$$

Regarding the laboratory tests to determine the cross-anisotropic elastic constants, Graham and Houlsby (1983) suggested that two different stress path tests should be carried out using triaxial apparatus. As a result, four equations obtained from Eq. (2-13) can be used to determine three parameters (K^*, G^*, J) by using the least squares procedure to eliminate the mathematical redundancy. Thereafter, all the cross-anisotropic elastic properties can be determined from Eq. (2-16) with the help of one extra assumption given in Eq. (2-17a). Wood (1990) presented the relations between parameters (E^*, ν^*, α) and cross-anisotropic elastic constants as

$$
\begin{aligned}
E^* &= E_v \\
\nu^* &= \frac{\nu_{vh} E_h \left[-\nu_{vh} + \sqrt{\nu_{vh}^2 + 4(E_v / E_h)(1-\nu_{hh})} \right]}{2E_v(1-\nu_{hh})} \\
\alpha &= \frac{E_h \left[-\nu_{vh} + \sqrt{\nu_{vh}^2 + 4(E_v / E_h)(1-\nu_{hh})} \right]}{2E_v(1-\nu_{hh})}
\end{aligned}
\tag{2-19}
$$

2.5 Homogenization approaches for equivalent elastic properties of a multilayered material

Stratified rock or soil is often encountered in engineering practice. The thickness of individual constituent layers may vary from several millimeters up to meters. Depending on the dimension of a geotechnical structure, consideration for all details of each constituent layer may become impossible in numerical modeling or structural design. The complexity in numerical modeling mostly comes from the use of a dense mesh to discretize a thin layer and from limitations of the computer capacity, especially

for three-dimensional boundary valued problems. The multilayered material can, however, be modelled as an equivalent cross-anisotropic homogeneous material under certain conditions (Salamon, 1968), thereby making an analysis computationally more efficient. In general, the following four assumptions are made to determine the equivalent elastic properties of a layered soil (Salamon, 1968; Wardle and Gerrard, 1972 and Gerrard, 1982):

1) Each constitutive layer is isotropic and bonded by parallel planes. A multilayered medium is axisymmetric being normal to the bounding planes.
2) The thickness of each constitutive layer must be much smaller than the characteristic length of the multilayered medium.
3) All interface planes between layers remain in contact, and no relative displacement takes place between layers at the interface.
4) The thickness and material properties of the layers vary randomly with respect to their respective positions within the system

Studies have been conducted on determining the equivalent cross-anisotropic elastic properties of the multilayered medium through various homogenisation methodologies (Hornung, 1997; Milton, 2004; Skrzypek and Ganczarski, 2015). They follow the work of Postma (1955) and Salamon (1965) by adopting traditional volume-averaging techniques to investigate the equivalent cross-anisotropic elastic constants, which depend on the elastic constants and volume fraction of the constituent layers. Among these studies, the simple models of Voigt (1907) and Reuss (1929) are still of considerable interest owing to their simplicity and clear physical meaning.

The Voigt model (1907) is applicable for determining the elastic modulus of a layered medium when loading is parallel to layering with an assumption of ‘equal strains’ in the loading direction. The Reuss model (1929) can be used when loading is perpendicular to layering with an assumption of ‘equal stresses’ in the loading direction. More specifically, Voigt (1907) proposed the use of a mixture rule to determine the equivalent properties of the composite material in the direction parallel to the layering.

The equivalent elastic modulus is expressed in terms of the elastic modulus and volume fraction of each layer as

$$\bar{E}_c = \sum_{i=1}^{N} \varphi_i E_i, \ \sum_{i=1}^{N} \varphi_i = 1, \ \varphi_i = \frac{h_i}{\sum_{i=1}^{N} h_i} \tag{2-20}$$

where $\bar{E}_c$ specifies the equivalent elastic modulus of the composite material, φ_i, h_i and E_i are the volume fraction, thickness and the elastic modulus of the *i*-th constituent layer.

Similarly, Reuss (1929) proposed a mixture rule to state the overall properties of the composite material in the direction perpendicular to the layering, which is expressed in terms of isotropic properties of each layer as

$$\frac{1}{\bar{E}_c} = \sum_{i=1}^{N} \frac{\varphi_i}{E_i}, \ \sum_{i=1}^{N} \varphi_i = 1, \ \varphi_i = \frac{h_i}{\sum_{i=1}^{N} h_i} \tag{2-21}$$

In engineering practice, the Voigt and the Reuss equivalent elastic moduli are considered appropriate to represent the upper and lower bounds for the elastic moduli of a composite material composed of different constituents (Mavko et al., 2009).

Postma (1955) considered a stratified medium consisting of many parallel layers, each of which on a smaller scale can be considered as isotropic homogeneous. When the number of layers is large and the characteristic length of interest is much larger than individual layer thickness, the multi-layered system can be replaced by an equivalent homogeneous, transversely isotropic (cross-anisotropic) material when only the average elastic behaviour is concerned. The applicability of such an approach is examined by analyzing a multilayered medium consisting of a large number of alternating layers of different homogeneous, isotropic materials for which the elastic properties are known. By applying the requirement of energy conservation between the systems and considering different deformation mechanisms, the theoretical expressions are derived for the five elastic constants of the equivalent homogeneous cross-

anisotropic material. In addition, limits for the elastic constants' values for equivalent cross-anisotropic material are discussed.

Salamon (1965) considered a stratified rock mass composed of a large number of parallel homogeneous isotropic layers. From the strain energy conservation point of view, a homogeneous cross-anisotropic medium, whose behaviour is equivalent to that of the rock mass, can be defined. He shows that the homogeneous equivalent material has the cross-anisotropic symmetry, with the axis of symmetry coinciding with the direction perpendicular to the layer's interface. More specifically, the stress-strain relations of the equivalent medium are derived from the condition that the strain energy stored in two cubes cut from rock mass and equivalent cross-anisotropic medium are equal. It should be mentioned that the auxiliary stress and strain components, which satisfy the stress equilibrium and deformation compatibility on the interface, are taken into account when determining the strain energy for the cube of the layered rock mass. The five independent elastic constants of the equivalent cross-anisotropic medium are expressed in terms of the elastic properties and normalized thickness of each constituent layer as follows:

$$
\begin{aligned}
&E_h = \left(1-\nu_{hh}^2\right)\sum \frac{\varphi_i E_{hi}}{1-\nu_{hhi}^2}, \quad \frac{1}{E_v} = \sum \frac{\varphi_i}{E_{hi}}\left(\frac{E_{hi}}{E_{vi}} - \frac{2\nu_{vhi}^2}{1-\nu_{hhi}}\right) + \frac{2\nu_{hv}^2}{\left(1-\nu_{hh}\right)E_h} \\
&\nu_{hh} = \frac{\sum \frac{\varphi_i \nu_{hhi} E_{hi}}{1-\nu_{hhi}^2}}{\sum \frac{\varphi_i E_{hi}}{1-\nu_{hhi}^2}}, \quad \nu_{hv} = \left(1-\nu_{hh}\right)\sum \frac{\varphi_i \nu_{hvi}}{1-\nu_{hhi}}, \quad \frac{1}{G_{hv}} = \sum \frac{\varphi_i}{G_{hvi}}
\end{aligned}
\tag{2-22}
$$

If each individual layer is isotropic with $E_{hi} = E_{vi} = E_i$, $\nu_{hhi} = \nu_{hvi} = \nu_i$ and $G_{hvi} = G_{vhi}$, the expressions of elastic properties of the equivalent material are simplified from Eq. (2-22) as

$$E_h = \left(1-\nu_{hh}^2\right)\sum\frac{\varphi_i E_i}{1-\nu_i^2},\quad \frac{1}{E_v}=\sum\frac{\varphi_i}{E_i}\left(1-\frac{2\nu_i^2}{1-\nu_i}\right)+\frac{2\nu_{hv}^2}{\left(1-\nu_{hh}\right)E_h}$$
$$\nu_{hh}=\frac{\sum\frac{\varphi_i\nu_i E_i}{1-\nu_i^2}}{\sum\frac{\varphi_i E_i}{1-\nu_i^2}},\quad \nu_{hv}=\left(1-\nu_{hh}\right)\sum\frac{\varphi_i\nu_i}{1-\nu_i},\quad \frac{1}{G_{hv}}=\sum\frac{\varphi_i}{G_i} \tag{2-23}$$

Following closely the approach of Salamon (1968) and adopting the same assumption, Gerrard (1982) determined the equivalent elastic properties for a system of parallel layers, each of which consists of a homogeneous orthorhombic elastic material. This means that each constituent layer has three mutually perpendicular planes of symmetry. It is shown that the system of parallel, orthorhombic layers can be regarded as a single 'equivalent' homogeneous orthorhombic material. The elastic properties of the equivalent material are expressed in terms of the elastic properties and the volume fraction of each constituent layer.

It should be noted that the homogeneous volume averaging technique has some limitations as follows (Farhad, 2009):

1) In reality, the stiffness of a material is not a property that can be averaged.
2) When a very thin and weak layer exists in a multilayered system, such layer dominates the overall behaviour of the multilayered medium. For example, this weak layer may facilitate failure, however, this layer has little influence on average parameters if the thickness of the layer is taken as a weighting factor. As a result, a discrepancy is expected to occur between the predicted results, based on the homogenisation technique and the real behaviour of the multilayered medium.

2.6 Laboratory testing method for the determination of the K_0-value

In geotechnical engineering practice, the K_0-value is important for the determination of geostatic stresses induced by the natural deposition and consolidation process in which the soil has no lateral deformation. In laboratory tests, the K_0-value of a soil can be

determined via the oedometer test that is one-dimensional compression test with zero lateral strain. The measurement of the lateral stress is crucial for the determination of K_0 in the oedometer test.

Wood (1990) found that K_0-value is constant for the normally consolidated soil. Jaky (1944) proposed an equation that can be used to estimate the K_0-value for normally consolidated soils based on the internal friction angle ϕ' of the soil; i.e.,

$$K_0^{NC} = 1 - \sin\phi' \tag{2-24}$$

where, K_0^{NC} implies the K_0-value for the normally consolidated soil. In general, the internal friction angle ϕ' is understood as the friction angle obtained from triaxial compression tests.

However, the K_0-value for a particular soil varies with the over-consolidation ratio. Numerical investigations have been carried out to estimate the coefficient of earth pressure at rest for the over-consolidated soils, yielding various empirical relations to estimate the K_0-value. Not all of them are listed here as this is not a focus of this study. Mayne (1982) reviewed experimental data for over 170 different soils and suggests an empirical equation

$$K_0^{OC} = K_0^{NC} * OCR^{\sin\phi'} \tag{2-25}$$

for predicting the K_0-value of the over-consolidated soil, in which K_0^{OC} is the K_0-value for the over-consolidated soil and OCR represents the over-consolidation ratio.

The oedometer test is the most common test to measure the K_0-value of a soil. The soil sample is placed in an oedometer that has a rigid boundary to constrain lateral deformation, and simultaneously the corresponding lateral stress can be measured. Pressure transducers have been successfully used to measure the lateral pressure in oedometer tests (Ladd, 1965; Abdelhamid, 1976). In addition, the lateral stress can also be measured by strain gauges attached to the outer wall of the consolidation ring. The strain gauges are calibrated with the horizontal stress measurement before conducting the K_0-compression test (Fahad, 2008). However, the wall friction of the oedometer

may affect the measured K_0-value.

To eliminate the effect of the wall friction in an oedometer test, Davis and Poulos (1963), and Head (1986) came up with the idea to use the traditional triaxial cell with a flexible boundary around the specimen and adopt a feedback system to maintain the zero lateral strain condition by adjusting the cell pressure. In other words, this method is to load a sample axially in a triaxial cell, and continuously adjust the cell pressure with a pneumatic system to maintain the zero lateral strain condition. The major shortcoming of this method is the oscillation of the cell pressure when it is adjusted to constrain the lateral strain. In addition, this method requires accurate local lateral strain measurements using a local displacement transducer attached to the outer periphery of the soil sample. Additionally, the installation of the transducer for local lateral strain measurements is complex and tends to cause disturbance to the soil sample.

Mesri and Hayat (1992) conducted the K_0-test using a special oedometer cell. In this method, a soil sample is trimmed and directly put into a highly polished stainless steel confining ring using a sharp cutting edge assembly. The central half of the confining ring is machined to a 0.254 mm diaphragm and the strain gauge on the outside of the ring detects any lateral deformation, which is prevented by controlling pressure in the silicon oil that surrounds the diaphragm.

All methods reviewed above require direct measurements of the lateral deformation at a point or points on the side surface of the soil sample, although the measurement devices are different. In these methods, displacement measurement at a point or points may not be representative of the average radial deformation of the sample when the deformation is not uniform (Okochi and Tatsuoka, 1984). This source of error may affect the measured K_0-value.

To minimize the error from the direct measurement of the lateral deformation, alternative methods have been developed where no lateral strain measurement is required (Vaid, 1971; Lo and Chu, 1991; and Eliadorani et al., 2005). Instead of running tests in a flexible triaxial cell with lateral strain measured and controlled directly, Vaid

(1971) developed a rigid cell that allows the K_0-condition to be automatically obtained. In this rigid cell, the loading shaft has the same cross-section area as the sample. Since the volume change of the rigid cell is negligible, if the water in the cell is considered incompressible, the sample would have no lateral deformation during compression. To obtain a low compliance for the system, the triaxial cell has to be assembled under water to avoid the inclusion of air bubble into the triaxial cell, and the rigid cell has to be extremely rigid against expansion during the increase in cell pressure. However, there is always some compliance of cell-water system that can affect the measured K_0-value.

On the other hand, Lo and Chu (1991) and Eliadorani et al. (2005) measured the K_0-value of soil by performing a controlled strain-path test, in which the ratio of axial strain and volumetric strain are controlled to be unity, which means the volume change of the soil sample is always equal to the axial deformation times the original average cross-sectional area. These methods only work for fully saturated soil.

Okochi and Tatsuoka (1984) and Dariusz and Chu (2006) proposed two alternative approaches to estimate the K_0-value of saturated soil, where the lateral strain was indirectly obtained from measured axial strain and volume strain. Following Bishop's work (1965), Okochi and Tatsuoka (1984) used a double-cell triaxial apparatus to control zero lateral strain. Dariusz and Chu (2006) adopted a plane-strain testing apparatus, in which the cell pressure was applied through a digital pressure-volume controller (DPVC) and another DPVC was used to control the volumetric change of the specimen, and four pressure transducers were mounted on the outer surface of the sample to measure the lateral stress due to vertical loading. For details of the testing arrangement, see Okochi and Tatsuoka (1984) and Dariusz and Chu (2006).

Chapter 3 EXPERIMENT STUDY

This chapter presents details of the testing program for the experimental investigation of soil behaviour along different stress and strain paths. It includes a detailed description of the experimental equipment, tested materials, sample preparation methods, sample installation process and testing procedures. Thereafter, the performance of the experimental setup and the repeatability of the test results are examined.

3.1 Testing program

To investigate the equivalent cross-anisotropic elastic parameters of soils, either homogeneous or layered soils, three tests along different stress and strain paths were carried out under triaxial stress conditions to determine E_v, E_h, ν_{hh}, and ν_{hv}; i.e.,

1) K_0-compression (KC) test in which $\Delta\varepsilon_{xx}=\Delta\varepsilon_{yy}=0$;

2) Plane strain compression (PSC) test with $\Delta\varepsilon_{zz}=0$, and $\Delta\sigma_{xx}=\Delta\sigma_{yy}$;

3) Hydrostatic pressure compression (HPC) test in which $\Delta\sigma_{xx}=\Delta\sigma_{yy}=\Delta\sigma_{zz}$.

Unless otherwise noted, for convenience it is assumed that the ***x-y*** plane is horizontal and the ***z***-direction is vertical.

The three stress and strain path tests above were selected because the results can be interpreted with clear physical meaning. More specifically, for a K_0-compression test, the coefficient of lateral earth pressure at rest and the constrained compressibility (or constrained modulus) of soil in the vertical direction could be determined directly from measured data. From the test results of the plane strain compression test, plane strain compressibility of soil in the horizontal direction could be measured. The difference between the results of these two tests with respect to the compressibility of soil provides evidence for material anisotropy. Additional confirmation of anisotropy was found in a hydrostatic pressure compression test. The directional dependence of

soil behaviour can be interpreted properly from the three tests.

Given that we focused on 'elastic' deformation, one specimen for each soil was used for the three tests along the different strain and stress paths, provided that the permanent vertical strain of the specimen did not exceed 1%. This allowed a reduction in the variability of results due to variation between specimens. After each individual test, the specimen was unloaded back to the original initial stress state, and several hours were allowed for the specimen to stabilize itself. This helped to reduce measurement errors from the potential oscillation of unstable initial stress conditions.

3.2 Description of testing equipment

3.2.1 Testing system

A modified rigid triaxial cell similar to that designed by Vaid (1972) was used to carry out all tests in this study. A brief description of the testing system is presented in this section.

Figure 3-1 shows all components of the testing system, which allows a variety of stress paths during shear (either passive or active, compression or extension, loading by strain control or stress control, under drained or undrained conditions). A volume change transducer was used to measure the volume change of a sample and an injecting water system was used to offset the potentially negative influence of compliance to obtain a K_0-condition. A digital data acquisition system was used to record the response of a soil sample every 15 seconds and to monitor the satisfaction of the K_0 constraint. The axial load, cell pressure, and back pressure were applied through an air pressure supply and controlled through pneumatic valves. Axial displacement, volume change, excess pore water pressure, and cell pressure were measured by different transducers. The measurement of total friction through the loading ram connected to the rolling diaphragm double acting piston gave a maximum recorded value of 50 grams, which was considered negligible since it gave an error in the axial stress of 0.5 kPa for a 60-

mm diameter sample. The performance of the various loading and measuring devices is summarized in Table 3-1. The measuring range and resolution of each device are specified as well.

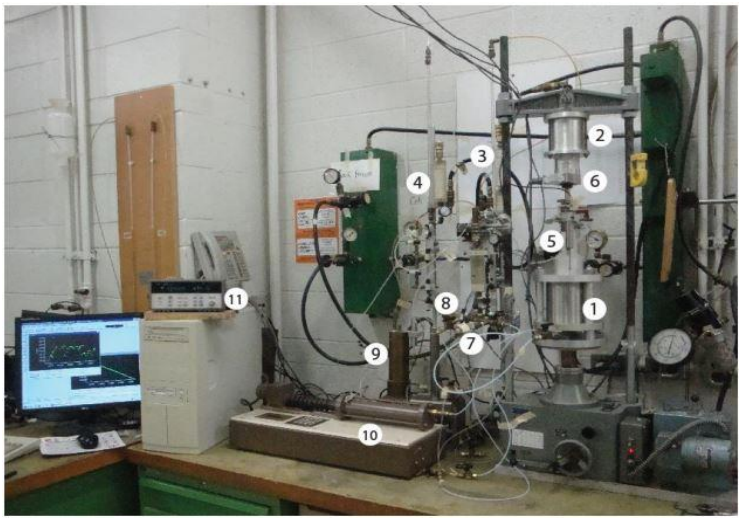

Figure 3-1 Overview of the testing system

1-Rigid triaxial cell; 2- Rolling Bellofram piston for axial load; 3-Pipette for volume measurement and back pressure control; 4-Pipette for correction of cell-water compliance; 5-LVDT; 6-Load cell; 7-Cell pressure transducer; 8-Pore (back) pressure transducer; 9-Volume change transducer; 10-GDS digital controller for compliance correction; 11-data logger

Table 3-1 Specifications for loading and measuring devices

	Range	Resolution	Manufacturers
Loading devices:			
Axial motor	30mm	0.0001mm	Canadian Duff-Norton
(Axial Strain)	60%	0.001%	
Cell pressure	700kPa	0.01kPa	
Measuring devices:			
LVDT	5mm	0.0001mm	SE Labs, Model SE373/15
(Vertical strain)	10%	0.001%	
Volumetric transducer	6ml	0.0001ml	Hewlett Packard Model 7DCDT-500
(Volumetric strain)	4%	0.001%	
Presure transducers	700kPa	0.01kPa	
(Cell pressure)	1200kPa	0.01kPa	Data Instruments, Model AB,200psi
(Back pressure)	700kPa	0.01kPa	Data Instruments, Model AB,100psi
Load cell	2500N	0.01N	
(Deviator stress)	880kPa	0.01kPa	

A simplified schematic of the entire experimental system is presented in Figure 3-2 to provide a better understanding of the setup.

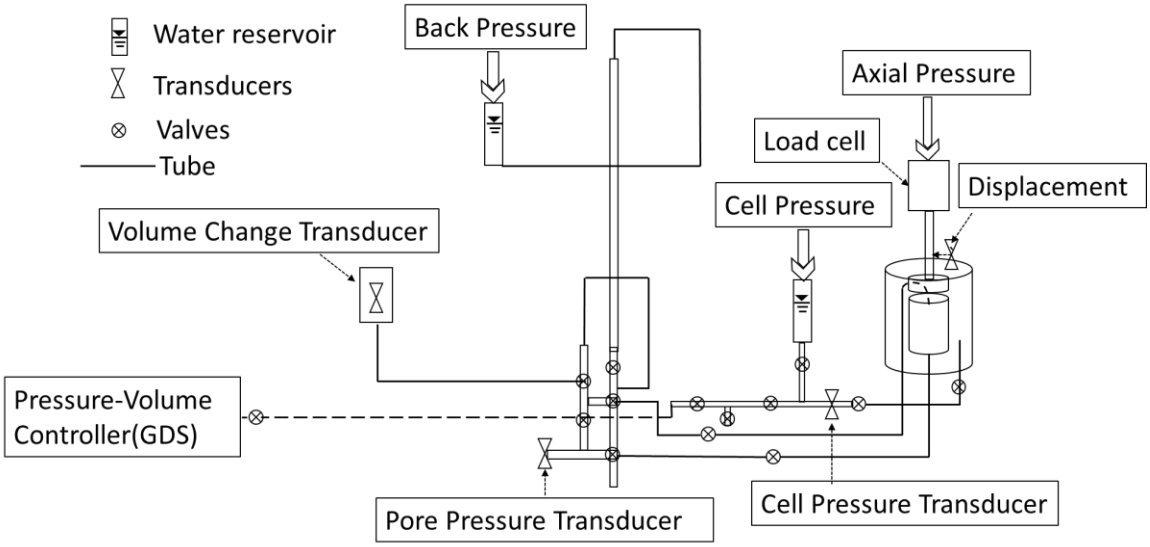

Figure 3-2 A simplified schematic of entire testing system

3.2.2 Rigid triaxial cell

1) Description of main components

The rigid triaxial cell with all essential details is shown in Figure 3-3. The cylinder was machined from a heavy stainless steel pipe to keep the compliance of the cell-water system to a minimum. The cell could host a specimen of 60.9 mm in diameter and 50-mm in height. A special design feature in this triaxial cell was that the loading ram used to transfer axial force from the loading rod to the specimen had an effective area equal to the area of the sample. The special design allowed for good control to maintain zero lateral deformation in the K_0–compression test if the compliance of the cell-water system was low. The remaining components of the triaxial cell were similar to those in the conventional triaxial cell. An explanation of the rigid cell is provided in Figure 3-4.

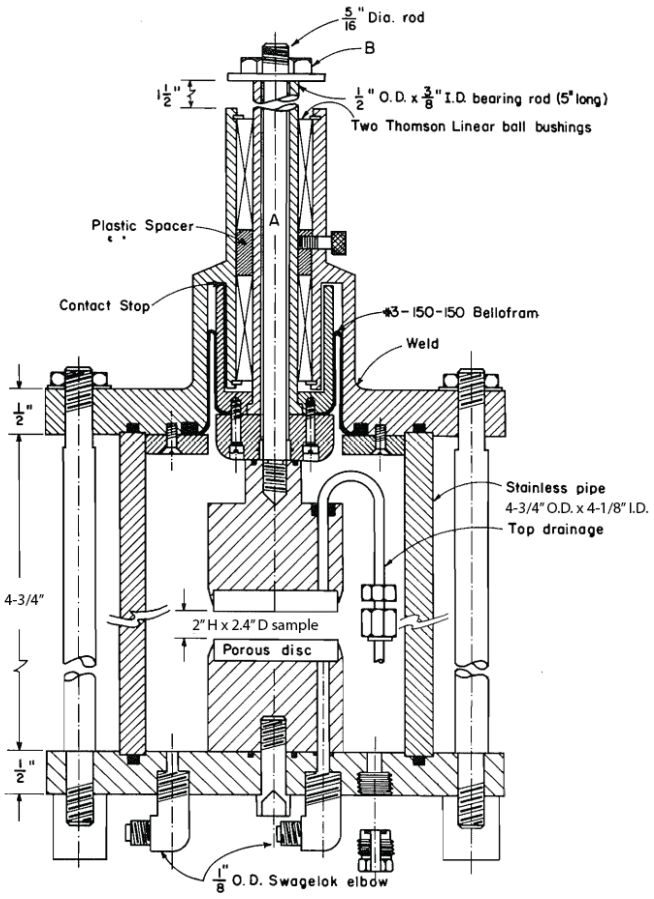

Figure 3-3 Overview of triaxial cell (modified from Vaid, 1972)

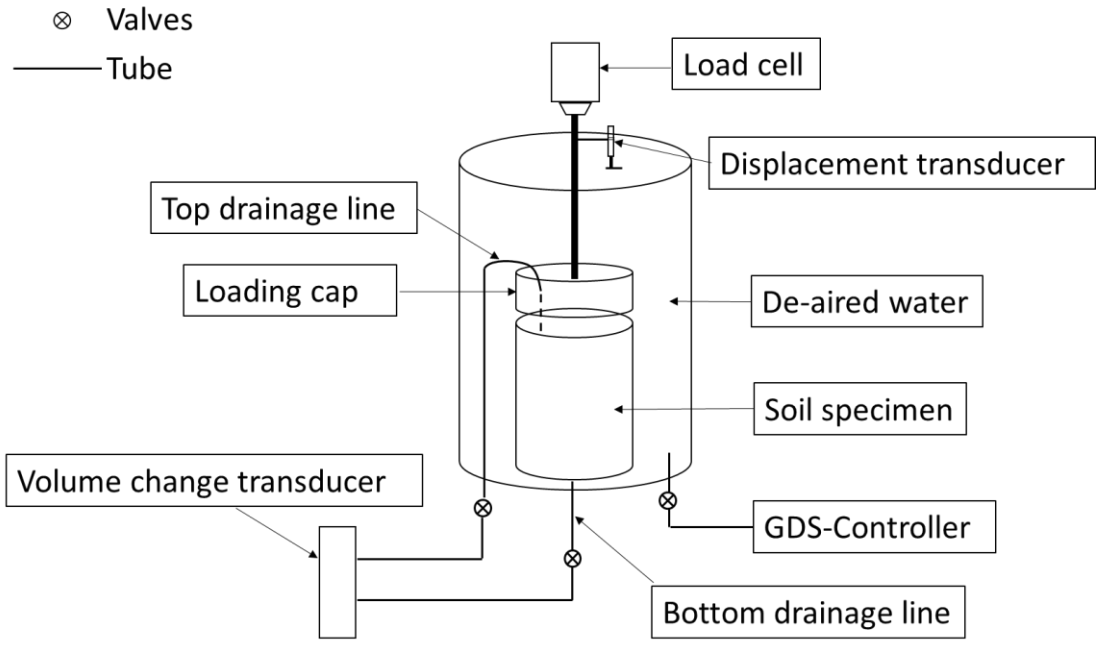

Figure 3-4 Simplified schematic of the rigid triaxial cell

2) Drainage conditions

This apparatus provided the flexibility for controlling the drainage conditions during a test. It permitted drainage from both ends or drainage from one end and pore pressure measurement at the other. Following Head (1986), side drains were not used to avoid the development of non-uniform strains in the radial direction during consolidation. It should be noted that for each load increment, sufficient time was allowed for excess pore pressure to dissipate before the next load increment was applied.

3) Flexibility of operation

This apparatus had been originally designed to conduct the K_0-test because of its low compliance of the cell-water system required to achieve near zero lateral deformation. However, it was also suitable to perform a variety of stress path tests under triaxial stress conditions. In this study, plane strain compression with $\varepsilon_{zz} = 0$ and consolidation test under hydrostatic pressure were also carried out using this testing system.

3.2.3 Compliance of the cell-water system

An essential requirement of the equipment is a very low compliance of the cell-water system during a K_0-test, which minimizes the lateral strain induced by the volume change of the cell-water system associated with pressure changes. More specifically, when performing a K_0-test by controlling the lateral pressure, a small but finite compliance of the cell-water system can cause a slight departure from conditions of ideal zero lateral strain. The compression of the entrapped air in the water due to continuously increasing pressure also permitted compression of the fluid in the cell and hence produced lateral deformation of the specimen. Therefore, one could argue that the lateral pressure measured was not consistent with the pressure that would have been generated under a truly one-dimensional consolidation condition.

The compliance of the water-cell system was estimated through a series of tests, in which the cell pressure was alternatively increased and decreased while the resulting

volume change of the fluid in the triaxial chamber was measured. For the calibration test, the triaxial cell was fully filled with de-aired water and no specimen was installed. This eliminated the effect of compliance induced by the compressibility of soil (due to the change of effective stress). The test allowed us to establish the relation between pressure change in the triaxial cell and the change in volume of the fluid introduced into the cell due to the compressibility of the fluid and the potential volume change of the cell induced by cell pressure change.

Two loading and three unloading tests with several pressure increments were carried out to minimize the influence of potential random errors. Figure 3-5 presents the measured volume change of the fluid in the cell at different pressure increments (relative to initial value) in several tests. The different slopes represent the compliance of the cell-water system.

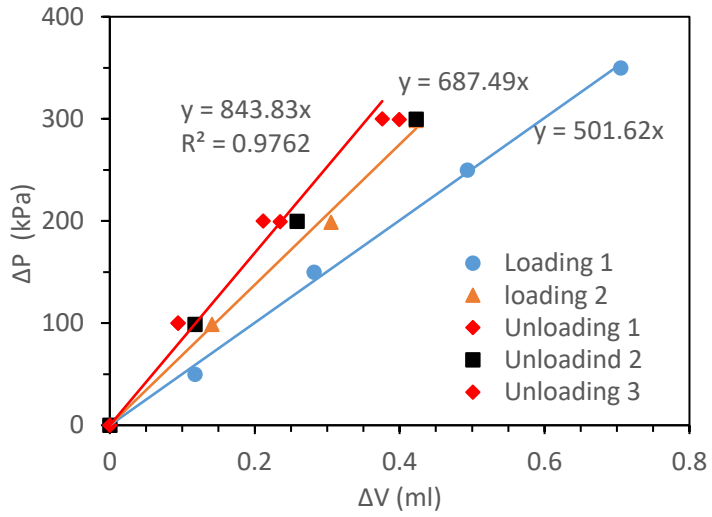

Figure 3-5 Measured volumetric compliance of the cell-water system

The compliance of the cell-water system is given by

$$C = \frac{\Delta V}{\Delta P} \tag{3-1}$$

where C is the compliance of cell-water system in $cm^3/kg/cm^2$, ΔP is the pressure change in the triaxial cell, and ΔV is the sum of volume change of the triaxial cell and the fluid in the chamber of the triaxial cell.

The volumetric compliance of the cell-water system was estimated to be in the range of 0.15-0.20 cm^3/100 kPa, which was two times higher than 0.06 cm^3/100 kPa reported by Vaid (1972). Following Vaid (1972), the error in measured K_0-value induced by the compliance of the system was investigated by the following analysis.

Considering a clay sample is in equilibrium under vertical and horizontal effective stress of σ_v' and $K_0\sigma_v'$ respectively. If the compliance of the system is equal to zero (C=0), for a vertical effective stress increment $\Delta\sigma_v'$, the increase in the horizontal effective stress is

$$\Delta\sigma_h' = K_0\Delta\sigma_v' \tag{3-2}$$

However, since $C \neq 0$ in reality, the actual increase in horizontal stress will not equal $K_0\Delta\sigma_v'$, but $\Delta\sigma_c'$, where $\Delta\sigma_c' < K_0\Delta\sigma_v'$. The change in volume of the sample is

$$\Delta V_1 = m_v V \frac{1}{3}(\Delta\sigma_v' + 2\Delta\sigma_c') \tag{3-3}$$

where V is the volume of sample, m_v is the coefficient of volumetric compressibility of the sample with respect to changes in mean normal effective stress σ_m' under the K_0-condition, and $\sigma_m' = \frac{1}{3}(\Delta\sigma_v' + 2\Delta\sigma_c')$. The corresponding expansion of the lateral pressure system is

$$\Delta V_2 = C\Delta\sigma_c' \tag{3-4}$$

When a specimen is subjected to compression, the change in the volume of the specimen at the condition of C=0 is

$$\Delta V_3 = m_v V \frac{1}{3}(\Delta\sigma_v' + 2K_0\sigma_v') \tag{3-5}$$

The deficiency in volume change $\Delta V_3 - \Delta V_1$ equals to the expansion of the cell-water system ΔV_2; that is,

$$C\Delta\sigma_c' = \frac{2}{3} m_v V(K_0\Delta\sigma_v' - \Delta\sigma_c') \tag{3-6}$$

This equation can be rewritten as

$$\Delta\sigma_c' = K_0 \Delta\sigma_v' \eta \tag{3-7}$$

where $\eta = \dfrac{1}{1+\dfrac{1.5}{V}\dfrac{C}{m_v}}$. As a result, the ratio of the lateral to vertical effective stress after applying the stress increment $\Delta\sigma_v'$ is

$$\left(K_0\right)_m = \frac{K_0\sigma_v' + \Delta\sigma_c'}{\sigma_v' + \Delta\sigma_v'} = K_0 \frac{\sigma_v' + \eta\Delta\sigma_v'}{\sigma_v' + \Delta\sigma_v'} \tag{3-8}$$

where $\left(K_0\right)_m$ represents the measured value of K_0.

Eq. (3-8) shows that the error in measured K_0-value depends on the current value of the vertical effective stress σ_v', the vertical effective stress increment $\Delta\sigma_v'$, and the parameter η, which is a function of the ratio of the compliance of the system C to the compressibility of a certain soil m_v. When $C = 0$ (zero compliance of the system) and $\eta = 1$, the measured K_0-value is the same as the actual K_0-value of the soil sample. When $C \neq 0$, the magnitude of η is less than unity. During the loading process of a K_0-test, $\Delta\sigma_v'$ is always positive, which results in $\left(K_0\right)_m < K_0$.

According to the theoretical analysis, the compliance of the apparatus adopted in this study (0.15-0.20 cm^3/100 kPa) brought approximately 5%-10% error for the measured K_0-value, depending on the various coefficient of volumetric compressibility of soils. More specifically, for the normally consolidated soil with high volumetric compressibility, the compliance of the system does not cause significant error in the measured K_0-value, but the error would be significant when the volumetric compressibility of soils is very small, for example, for heavily over-consolidated soils.

An example calculations and details with respect to the determination of the error in measured K_0-value can be found in the Appendix.

3.2.4 Compliance correction system

In order to minimize the error induced by the cell-water compliance, an unique

compliance system was introduced to make compliance corrections. The working principle of the compliance correction system was to inject the same volume of water into the triaxial cell when the fluid in the triaxial cell was compressed or the triaxial cell expanded owing to an increase of the cell pressure. A GDS standard pressure controller shown in Figure 3-6 was used to do a necessary compensation to reduce the effect of compliance of the cell-water system. It was capable of measuring and regulating liquid pressure, as well as measuring and regulating the flow rate of the liquid. It was connected to the triaxial chamber through a short plastic tube of 1/8 inch in diameter with high stiffness. By using the GDS pressure controller, we could inject the same volume of water into the triaxial chamber when the volume of the fluid (de-aired water) in the triaxial chamber was compressed, owing to the air entrapped in the triaxial chamber or dissolved into the water, and the increase of cell pressure.

Figure 3-6 GDS digital controller for compliance compensation

The rate of water injection for proper compliance correction from the GDS pressure controller was estimated as

$$\frac{\dot{V}_2}{\dot{h}} = \frac{2\varepsilon_h V}{\varepsilon_v H} = \frac{\varepsilon_h}{\varepsilon_v} 2A \tag{3-9}$$

where $\dot{V}_2$ is the rate of injecting water for proper compliance correction, $\dot{h}$ is axial displacement rate resulted from axial loading, $\varepsilon_h / \varepsilon_v$ is the ratio of the lateral and

vertical strain of the specimen, and V, H, A are the volume, height, and cross-sectional area of the specimen, respectively.

The ratio of the lateral and vertical strain of the specimen is a function of soil properties (i.e., the coefficient of volumetric compressibility and the K_0-value), the compliance of the system and the volume of the specimen. Mathematically, it is expressed as

$$\frac{\varepsilon_h}{\varepsilon_v} = \frac{K_0}{1+2K_0}\left(1+\frac{2m_vV}{3C}\right)^{-1} \tag{3-10}$$

Details about the derivation can be found in the Appendix. Once the soil properties (m_v and K_0) were estimated, the rate of injection for proper compliance correction $\dot{V}_2$ can be estimated from Eqs. (3-9) and (3-10).

Alternately, the rate of injecting water for proper compliance correction without taking into account the volumetric compressibility of the specimen can be estimated as

$$\frac{\Delta V_2}{\Delta t} = C\frac{\Delta \sigma_c'}{\Delta t} \tag{3-11}$$

where ΔV_2 and $\Delta \sigma_c'$ are the required volume of injecting water and the variation of cell pressure in the period of Δt, respectively.

It should be mentioned that the first method is only used to estimate the initial rate of water injection for proper compliance correction. As a K_0-test proceeds, the rate of water injection needs to be changed properly, depending on the measured volume change and the axial deformation of the specimen. Once the variation of cell pressure $\Delta \sigma_c'$ is measured in the period of Δt from the test, the proper rate of injecting water to make compliance correction can be determined from Eq. (3-11). The test results showed that the system controlled the lateral strain of the specimen in the range of ± 0.02%, which was much less than the requirement for lateral strain (±0.05%) suggested by Japanese Geotechnical Society Standards (JGS0525-2000).

3.3 Test materials

All tests were conducted on specimens obtained from high-quality undisturbed soil samples, either homogeneous soils or layered soils that were provided by the Toronto Transportation Commission from different construction sites.

3.3.1 Homogeneous sandy soil

Real soils tend to be non-homogeneous in nature. Even uniformly graded soils vary somewhat from point to point in the ground; as shown in Figure 3-7. Owing to the height of the specimen (50 mm), uniformly-graded sandy soils were considered to be homogeneous, when compared to layered soils with the strong layering structure that contributed to an apparent anisotropic behaviour of the soil samples.

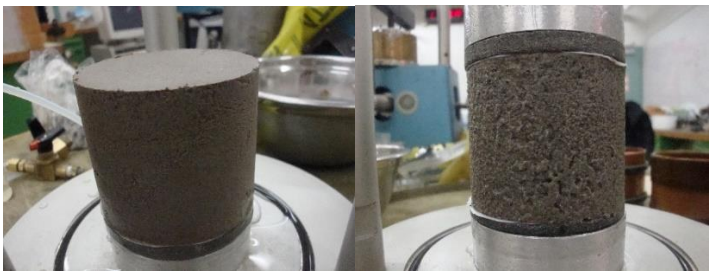

(a) Specimen 3002# (b) Specimen #2004

Figure 3-7 Appearance of homogeneous sandy soils

3.3.2 Layered soil

Sedimentation processes most often lead to soil formation of alternating texture and fabric, for example, the varve structure of clayey or silty soils. In this study, layered soils consisted of a series of parallel layers of different thicknesses (as thin as a few millimeter) and different properties. The stiffer layer was clay of high cohesion, with the soft layer being a silt or fine sand of no cohesion. Figure 3-8 shows layered soils with apparent anisotropic structures. The layers displayed contrasting colours when the sample was air-dried. The anisotropic mechanical properties were attributed to the

layered structure and the different mechanical properties of each material layer.

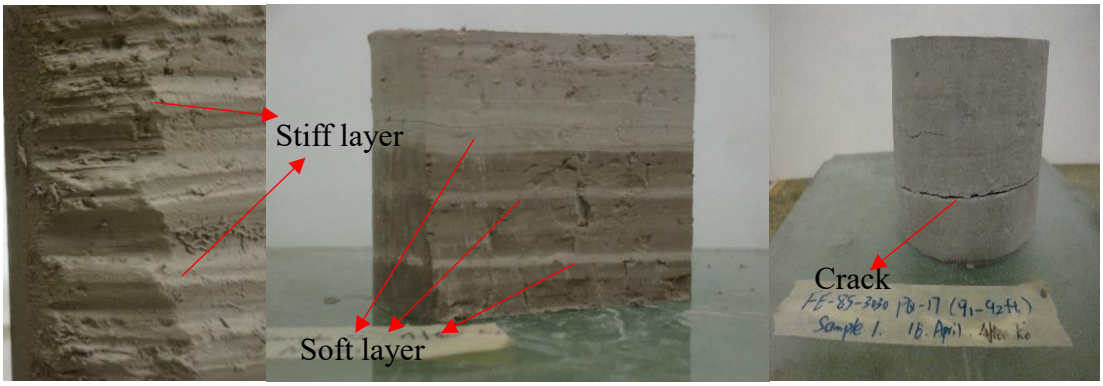

(a) (b) (c)

Figure 3-8 Appearance of layered soils
(a) Undisturbed soil specimen #6011 with natural water content
(b) Air-dried specimen #1004 after testing
(c) Air-dried specimen #3030 with a crack in the weak layer (after testing)

3.4 Specimen preparation methods

3.4.1 Specimen preparation method for clayey soil

The following steps were followed to make specimens for laboratory tests from samples obtained from boreholes:

(1) After taken from sampling tubes, soil samples were immediately wrapped in plastic to minimize any changes in water content, and were then placed into a 1.5-meter long plastic tube to reduce sample disturbance; as illustrated in Figure 3-9(a). The tube samples were delivered to the lab and stored in a moist room.

(2) The required soil was removed from the tube for sample preparation, see Figure 3-9 (b). Some soil samples were disturbed during the sampling process with fissures developing at the periphery of the sample; as shown in Figure 3-9 (c). The portion of highly disturbed soil sample was discarded.

(3) After removing the plastic wrap, the segment of a sample of approximately 80 mm long was cut carefully from the core by using a sharp blade. The expected

height of the specimen to be tested was 50 mm. Any leftover material was wrapped in the plastic wrap immediately and stored in the moist room for later use.

(4) The top and bottom surfaces of the sample segment were cut perpendicular to the axis to allow the sample to stand vertically in the soil lathe. The upper platen of the trimmer was brought down to sit firmly on the top surface of the sample to protect the sample from moving around during the trimming process; as shown in Figure 3-9 (d).

(5) The sample was rotated slowly while trimming vertically using a wire-saw. After the periphery of the specimen was trimmed smoothly; as shown in Figure 3-9 (e), the sample was removed from the lathe and placed on a flat plastic plate.

(6) The top and bottom surfaces of the sample were trimmed in the mold; as shown in Figure 3-9 (f). The height of the mold was 50mm and its inner diameter was 62 mm, slightly larger than that of the specimen. The objective was to make the top and bottom surfaces perfectly flat and perpendicular to the sides. The final dimension of the specimen; as shown in Figure 3-9 (g), was 50 mm in height and 60.9 mm in diameter. The excess soil that was trimmed off was used to determine the natural water content.

(7) After measuring the weight and dimensions, the trimmed specimen was transported to the base of the triaxial cell for testing. If the test could not be carried out immediately, the specimen was placed on a plastic plate and sealed in a plastic bag before placing the sample in the moist room where it was kept until it was required for a test.

(a) (b) (c)

(d) (e)

(f) (g)

Figure 3-9 Trimming specimen to the proper diameter and length

3.4.2 Specimen preparation method for homogeneous sandy soil

For sandy soils with low cohesion, the recommended method for clay samples of using a wire saw to cut the specimen to the desired diameter and length was not possible as the sample could not stand by itself under self-weight on the trimming lathe. For this type of soil, specimens were prepared using a thin-wall aluminum mold by following

the procedures described below:

(1) Lubricate the inner-side of the thin-wall aluminum mold with thin grease. The mold, which is 50 mm high and 61.2 mm in inner diameter, is sharpened at one end to act as a cutting blade; as shown in Figure 3-10 (a).

(2) Trim both ends of the soil core. Both ends must be parallel to the bottom surface and perpendicular to the axis of the cylindrical soil core; as shown in Figure 3-10 (b).

(3) Gently push the mold into the soil sample manually using a loading frame at a slow velocity. Remove extra soil outside the mold when necessary. The extra soil removed from the mold is to be collected and saved in a sealed plastic bag to measure the natural water content.

(4) Trim the top and bottom surfaces of the specimen to be perfectly flat; as shown in Figure 3-10 (c). The sample in the mold is then placed in a freezer with a temperature of -20℃ for at least half an hour, which allows the sample to freeze and develop some strength so that it can stand on the base of the triaxial cell by itself for specimen installation.

(5) Push the partially frozen specimen down out of the mold onto the base of the triaxial cell chamber, and carefully position it in the center of the base; as shown in Figure 3-10 (d).

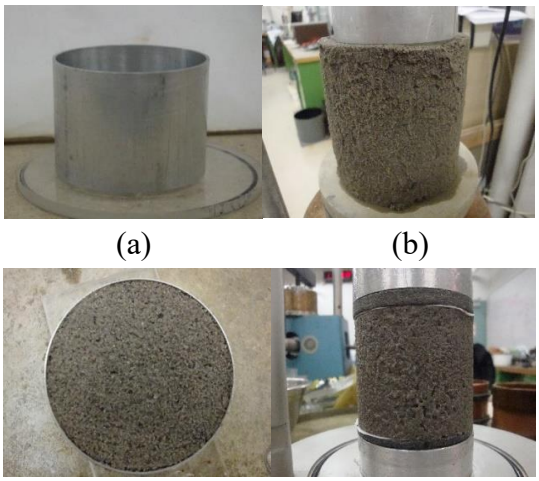

(a) (b)

(c) (d)

Figure 3-10 Specimen preparation for sandy soils

3.5 Specimen installation and saturation

The installation of a specimen and proper assembling of the rigid cell are important to minimize the compliance of the cell-water system. Care must be exercised to reduce the amount of air entrapped into the triaxial cell during this process. The following steps were followed to assemble the rigid cell:

(1) Put the trimmed specimen on a porous stone with filter paper on the base of the triaxial cell, and put another porous stone and filter paper with a loading cap on top of the specimen; as shown in Figure 3-11 (b).

(2) Wrap the soil specimen using a membrane of 1.5mm thickness. The membrane is sealed to the bottom of the base and the top cap by two O-rings on each end; as shown in Figure 3-11 (c). To ensure a complete seal, a thin layer of silicon grease is applied on the side of the loading cap and the base, where it is possible for some tiny soil particles to adhere to the surface.

(3) Connect a drainage tube to the cap. A 10-20 kPa vacuum is applied to the soil specimen through the top drainage line to stabilize and fix the position of the specimen and to reduce potential disturbance during the remaining installation process.

(4) Assemble the triaxial cell under water in a 55cm deep water tank; as shown in Figure 3-12, to prevent air from getting trapped in the cell-water system. Remove any air bubbles sticking to the membrane. Thereafter, position the stainless steel cylinder of the triaxial chamber around the sample. After all visible air bubbles are eliminated from the Bellofram by pushing the loading rod up and down, the head is carefully slipped around the rod until the top plate sits on the triaxial chamber.

(5) Put all parts of the triaxial cell together by tightening the nuts. Thereafter, remove the assembly from the container.

(6) Position the triaxial cell on the base of the loading platform and connect all pressure and water lines. Then, a small cell pressure of 20 kPa is applied to the

sample, with drainage valves closed and the negative pressure in the specimen being released at the time.

(7) Connect the compliance correction system to the triaxial cell and connect the volume change transducer to the drainage lines of the specimen.

(8) Position the LVDT to the loading rod to measure axial deformation of the specimen.

(a) (b) (c)

Figure 3-11 Installing the soil specimen to the base of the triaxial cell

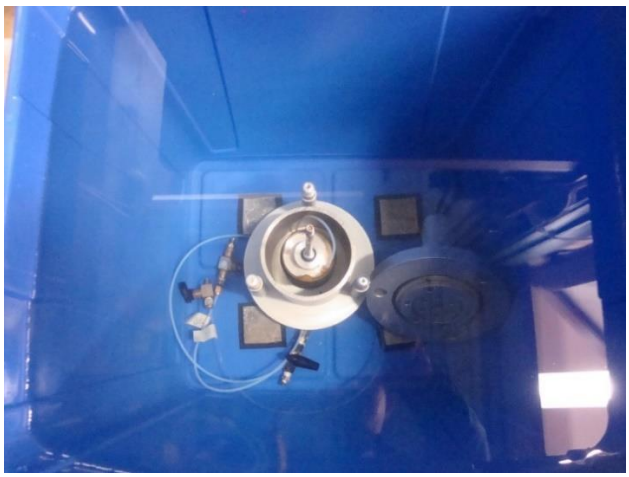

Figure 3-12 Put the triaxial cell together under water to avoid introducing air

After double checking that all connections are correct, the soil specimen is ready to be saturated by applying back pressure incrementally. The objective of the saturation

phase of the test is to fill all voids in the specimen with water without undesirable increase of effective stress on the specimen. It must be mentioned that the amount of dissolving air in solution is a function of both time and pressure. Accordingly, removing as much air as possible prior to applying back pressure decreases the pressure required for saturation. To saturate the specimen, the cell pressure and back pressure are simultaneously increased in steps with specimen drainage valves open so that the de-aired water from the burette connected to the top and bottom of the specimen may flow into the specimen. The back pressure is applied while simultaneously increasing the cell pressure and axial pressure by the same amount to keep the effective stresses constant. The axial stress increment is independently controlled and applied through a rolling diaphragm double acting piston mounted on the loading frame.

At the beginning of the saturation, the initial effective stress applied to the specimen is approximately 15-20 kPa. To avoid undesirable pre-stressing of the specimen while applying the back pressure, an increment of 20 kPa pressure is applied incrementally with a time interval of 10 minutes to allow equalization of the pore-water pressure throughout the specimen. To check for equalization after application of a back pressure increment, the drainage valves are closed and the change in pore-pressure over a one-minute interval is measured. If the change of water pressure is less than 5% of the difference between the cell pressure and the back pressure, the next back pressure increment could be added (as recommended by ASTM D7181-11). With an increase of the back pressure, the air in the specimen is compressed and partially dissolved in water, resulting in an increase in the degree of saturation of the specimen. The degree of saturation is estimated by the pore pressure parameter B as

$$B = \frac{\Delta u}{\Delta \sigma_3} \tag{3-12}$$

where Δu is the change in pore pressure in the specimen that occurs as a result of the change of $\Delta \sigma_3$ in the cell pressure under undrained conditions. The specimen is considered to be fully saturated if the value of B is equal to or greater than 0.95.

To reduce the duration of saturation stage, when the pore pressure parameter B is greater than 0.5, an increment of 50 kPa of back pressure is applied over a time interval of 30 minutes. Depending on the permeability and the type of soil investigated in this study, the magnitude of the back pressure required for the full saturation ranges from 400 to 550 kPa.

After the back pressure is increased step-by-step to approximately 400 kPa, the sample is left overnight to reach a satisfactory $B-value$ and to reduce the volumetric compliance of the cell-water system. This method effectively dissolved small amounts of entrapped air in either the cell-water or pore-water system (Vaid, 1972).

During the entire process of saturation, the effective stress in the specimen is maintained in the range of 20 to 30 kPa, and the axial deformation of the specimen, which is monitored when applying back-pressure, is in the negligible range of 0-0.005mm. The K_0-compression test is ready to start after the specimen is saturated with $B-value$ no less than 0.95.

3.6 Triaxial K_0-compression test

3.6.1 K_0-condition

The principle behind carrying out the K_0-test was to load the sample by strain control in the vertical direction at a slow rate and simultaneously measure the corresponding horizontal pressure that was required to keep the lateral deformation zero.

When a back pressure was applied to effectively dissolve entrapped air in the specimen and to fully saturate the specimen, the initial effective stresses were determined as

$$\sigma'_{v0} = \sigma_{v0} - u_{b0} \tag{3-13}$$

$$\sigma'_{h0} = \sigma_{h0} - u_{b0} \tag{3-14}$$

in which, u_{b0} is the initial back pressure required to fully saturate the specimen.

Figure 3-13 conceptually illustrates the process of a K_0-test. In this figure, σ_{v0} and σ_{h0} represent the initial axial and horizontal total stresses, respectively, with σ'_{v0} and σ'_{h0} being the corresponding initial axial and horizontal effective stresses. During a K_0-test, the axial stress increment $\Delta\sigma_v$ was measured by a load cell as the axial displacement increased. The horizontal stress increment $\Delta\sigma_h$ to keep the lateral strain zero was measured by the cell pressure transducer. Any undissipated excess pore water pressure Δu induced by the vertical compression of the soil was measured by the pressure transducers connected to the bottom end of the specimen. Although the constant axial strain rate was low enough to ensure dissipation of most excess pore pressure in the specimen, a small amount of excess pore pressure accumulated throughout the test. Therefore, the current average effective stresses were calculated by:

$$\sigma'_v = \sigma_{v0} - u_{b0} + \Delta\sigma_v - \frac{2}{3}\Delta u \tag{3-15}$$

$$\sigma'_h = \sigma_{h0} - u_{b0} + \Delta\sigma_h - \frac{2}{3}\Delta u \tag{3-16}$$

The factor $\frac{2}{3}$ was a coefficient required to determine the average non-uniform undissipated pore pressure over the height of soil sample (as recommended by ASTM D7181-11).

The K_0-value of a sample was calculated by

$$K_0 = \frac{\sigma'_h}{\sigma'_v} \tag{3-17}$$

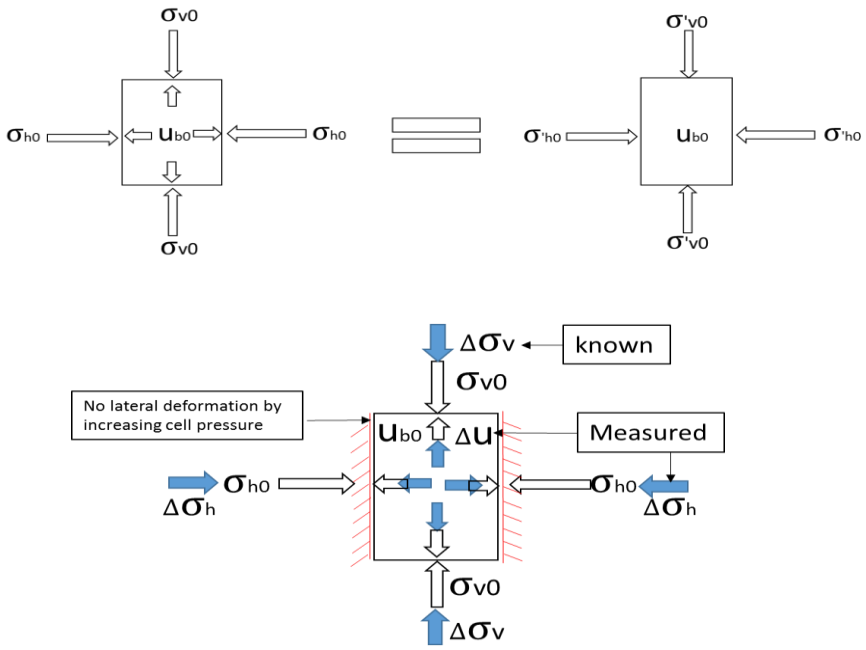

Figure 3-13 Concept of K_0-value estimation

3.6.2 Initial stress state

In routine triaxial testing, the soil specimen is often consolidated under hydrostatic pressure prior to shearing. According to Mesri and Hayat (1993), a 10-20 kPa hydrostatic pressure before conducting the drained K_0-test brings minimum disturbance to the undisturbed soil's internal structure. The initial hydrostatic stress state before conducting the K_0-test in the triaxial cell was also adopted by other researchers, such as Vaid (1972) and Keskin (2004). In this study, the initial stress state before conducting a K_0-test corresponded to an effective hydrostatic pressure of 20 kPa, which provided necessary support for the specimen and prevented undisturbed soft soils from deforming improperly or collapsing before the K_0-test.

3.6.3 Selection of the constant rate of axial strain

For a strain-controlled, K_0-compression test on a saturated specimen, the rate of axial strain should be low enough to ensure dissipation of any excess pore pressure in the specimen during loading. The selection of strain rate must consider both the effects of

the test's duration and the rate of dissipation of excess pore pressure. In general, the axial displacement rate was selected following recommendations in ASTM D4186/D4186M-12, which is the standard test method for one-dimensional consolidation properties of soils using strain-controlled loading.

During testing, pore-water drainage was permitted only from the top of the sample, while excess pore water pressure at the bottom of the specimen was monitored. If the change in excess pore water pressure was less than 5% of the cell pressure increment in a minute, the pore pressure was considered to be fully dissipated. Overall, a proper strain rate should be slow enough to ensure at least 95% dissipation of excess pore pressure in the specimen during shearing; as recommended by ASTM D4186/D4186M-12.

Depending on the type of soil, the proper strain rate may vary, according to ASTM D4186/D4186M-12. For layered soil specimens, the strain rate was generally 0.0008-mm/min (0.096%/hour). For the homogeneous sandy soil, the strain rate was much higher than that of a fine-grained layered soil, being 0.004 mm/min (0.48%/hour).

3.6.4 Measurement of the lateral strain

The lateral strain of the specimen during the K_0-compression test was checked promptly because a small generation of lateral strain in the process could have introduced a significant error in the measured K_0-value. As stated previously, the lateral strain could have be measured by a transducer installed at the periphery of the specimen. Such a transducer could have captured the deformation accurately, provided that the soil deformed uniformly.

In this study, the special design for the triaxial cell allowed an indirect deduction of the lateral strain of the fully saturated specimens during the K_0-test. More specifically, under the ideal K_0-condition, the volume of water, ΔV_w expelled from the sample must be the same as that calculated from the axial deformation of the sample; i.e.,

$\Delta V_w = A\Delta h$. Herein A is the cross-sectional area of the specimen and Δh is the axial compression of the specimen. If lateral deformation took place, the lateral strain would be calculated as

$$\varepsilon_h = \frac{1}{2}\left(\varepsilon_{vol} - \varepsilon_v\right) = \frac{1}{2}\left(\frac{\Delta V_w}{V} - \frac{\Delta h}{H}\right) \tag{3-18}$$

where ε_{vol} and ε_v are the volumetric strain and the vertical strain of the specimen, respectively.

During the K_0-test, the axial deformation and volume change of the soil sample were monitored and recorded every 15 seconds. The relation between the volumetric strain and the vertical strain of the sample during the test was tracked by a computer to provide a relation of volumetric versus vertical strain; as shown in Figure 3-14 (a). The magnitude of lateral strain can then be determined using Eq. (3-18); as shown in Figure 3-14 (b).

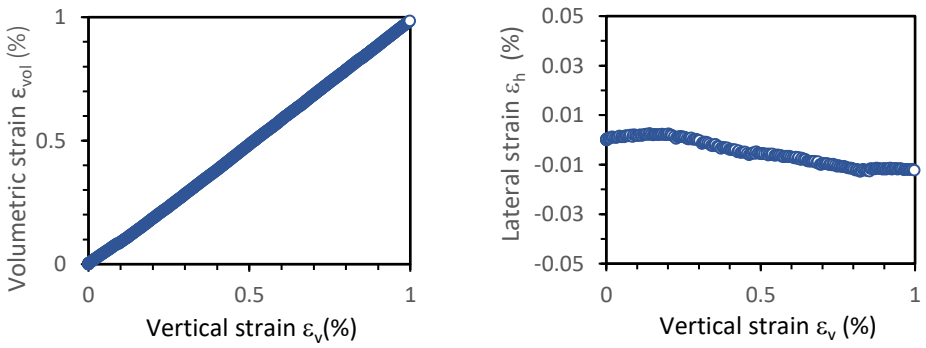

(a) (b)

Figure 3-14 Strain relations during the K_0-test for specimen #2004

3.6.5 Verification of K_0-condition and application of compliance correction

Ideally, if the compliance of the apparatus used in this study for conducting K_0-test is low enough, the K_0-condition is automatically obtained so that there is no need to make any compliance correction throughout the test. However, since limited compliance of the system exists owing to the small amount of dissolved air in the water or entrapped

air in the triaxial cell during sample installation process, a small lateral deformation is always generated and accumulated during testing, which could have had certain influence on the measured K_0-value.

As presented previously in Section 3.2.4, the initial rate of injecting water for making proper compliance correction can be estimated from theoretical analysis, based on the estimated soil properties (coefficient of volumetric compressibility m_v and K_0-value) and the axial strain rate. However, to keep an ideal K_0-condition throughout the test, the rate of injection should be adjusted according to the magnitude of lateral strain calculated from Eq. (3-18). More specifically, when the lateral strain of the sample had a potential to increase at a fast speed, based on the current ratio of volume compensation, the rate of volume compensation needed to be increased properly; otherwise, the rate of injection needed to be decreased if the soil sample was over-compressed in the lateral deformation due to more water being injected than needed.

In general, at the beginning of the K_0-test, there was no need to make any compliance correction because the sample was over-compressed in the lateral direction since the specimen was initially consolidated under the 20 kPa hydrostatic stress. As the K_0-test proceeded, the sample had a potential to approach its in-situ K_0-state and the effect of compliance of the system became more and more significant. As a result, a small lateral deformation would be generated and accumulated. When the calculated lateral strain was less than -0.005%, the compliance correction was needed by injecting a certain amount of water into the triaxial chamber to push the specimen back to its K_0-state.

The process of adjustments for the compensation correction is summarized in the flowchart; as shown in Figure 3-15. It should be mentioned that the soil mechanics sign convention is adopted; namely, compressive stress and strain are taken as positive, and the tensile stress and strain are taken as negative.

Overall, test results show that that the magnitude of lateral strain can be easily controlled in the range of $\pm 0.02\%$ by adjusting the rate of water injection into the

triaxial cell, which is smaller than $\pm 0.05\%$, the recommended amount by Shimizu et al. (2014) and the Japanese Geotechnical Standard (JGS525-2000).

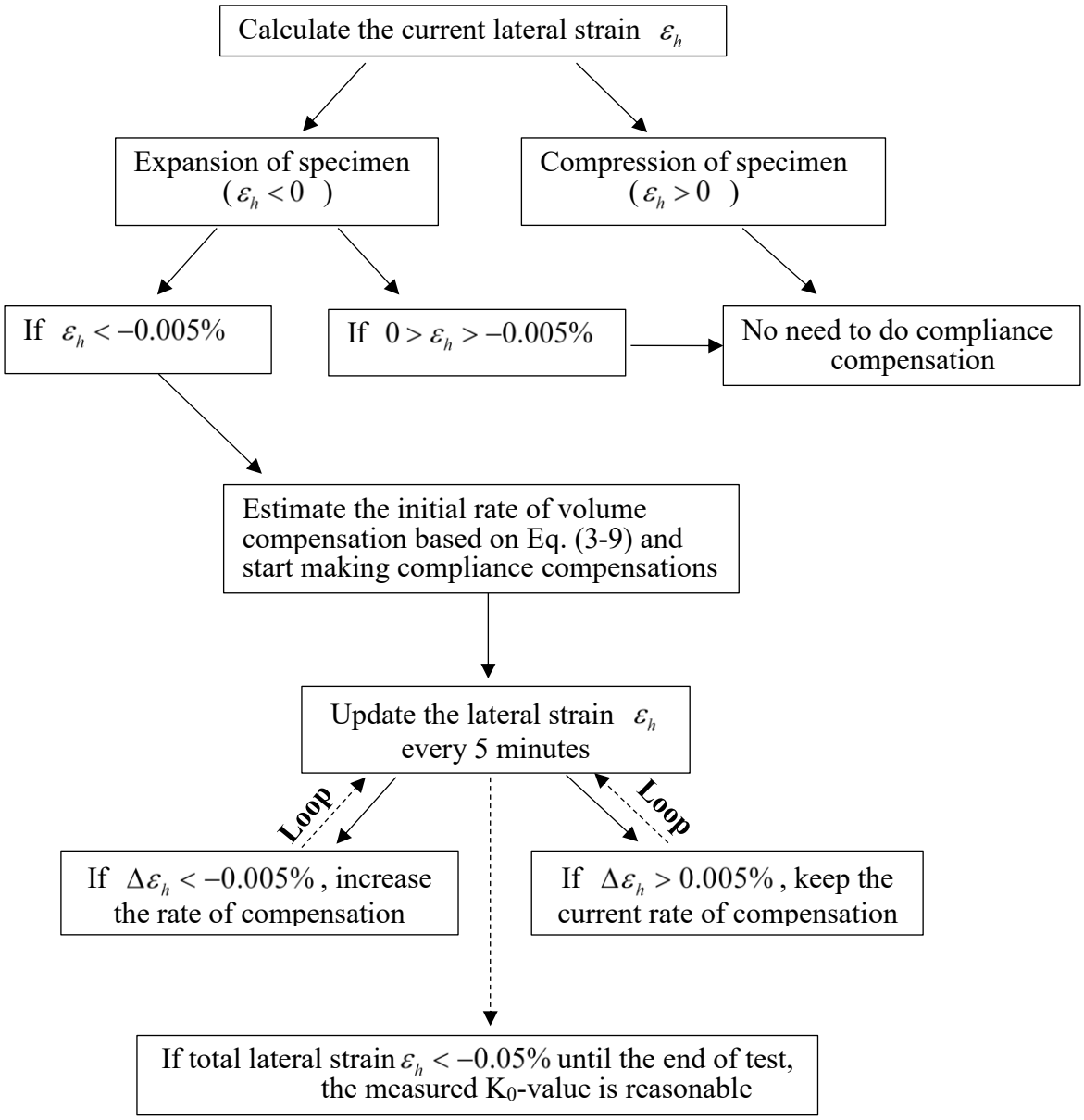

Figure 3-15 Processes of the compensation correction

3.6.6 Repeatability of drained K_0-test

To verify the repeatability of the K_0-test results, preliminary tests on two types of soil (specimen #6011 and specimen #4002) were conducted under the same conditions following the same test procedures. Figure 3-16 presents the measured K_0-value as a function of stress level, as well as the corresponding deformations.

Figure 3-16 (a) presents the measured K_0-values of three K_0-tests carried out on individual specimens trimmed from the same core located at the same depth. In other words, the specimens had similar stress history and physical properties. All three K_0-tests initially started from an isotropic stress state. With an increase of vertical effective stress induced by strain-controlled loading, the measured K_0-value decreased gradually and eventually converged to a stable value when the vertical effective stress was greater than the estimated in-situ overburden pressure. This was consistent with the conclusion drawn by Wood (1990) that the K_0-value for normally consolidated clay is independent of the magnitude of σ_v'.

Although there were some minor differences between the measured K_0-values obtained from the three tests, the repeatability of the tests was confirmed. The small differences of measured K_0-values could have resulted from a slight difference in the internal structure of tested specimens. The generated lateral strain due to the compliance of the system could also have had some influence on the measured the K_0-values. The relation between the volumetric strain and the vertical strain can be observed in Figure 3-16 (b), from which the amount of generated lateral strain can be estimated. The slopes of the three lines were controlled to be close to one by making compliance corrections.

Two repeated tests were carried out on another type of soil specimen #4002 (homogeneous sandy soil), in exactly the same way as was conducted on specimen #6011 (layered soil). Small noise and oscillation in the data can be observed in Figures 3-16 (c) and (d). Nevertheless, the control of compliance compensation was found to be excellent. The K_0-condition was satisfied because the ratio of the volumetric strain and vertical strain was always approximately one throughout the test. Finally, the measured K_0-values between two tests were nearly identical. The tests on specimens #6011 and #4002 demonstrated good repeatability and reliability of the proposed sample preparation methods and testing procedures.

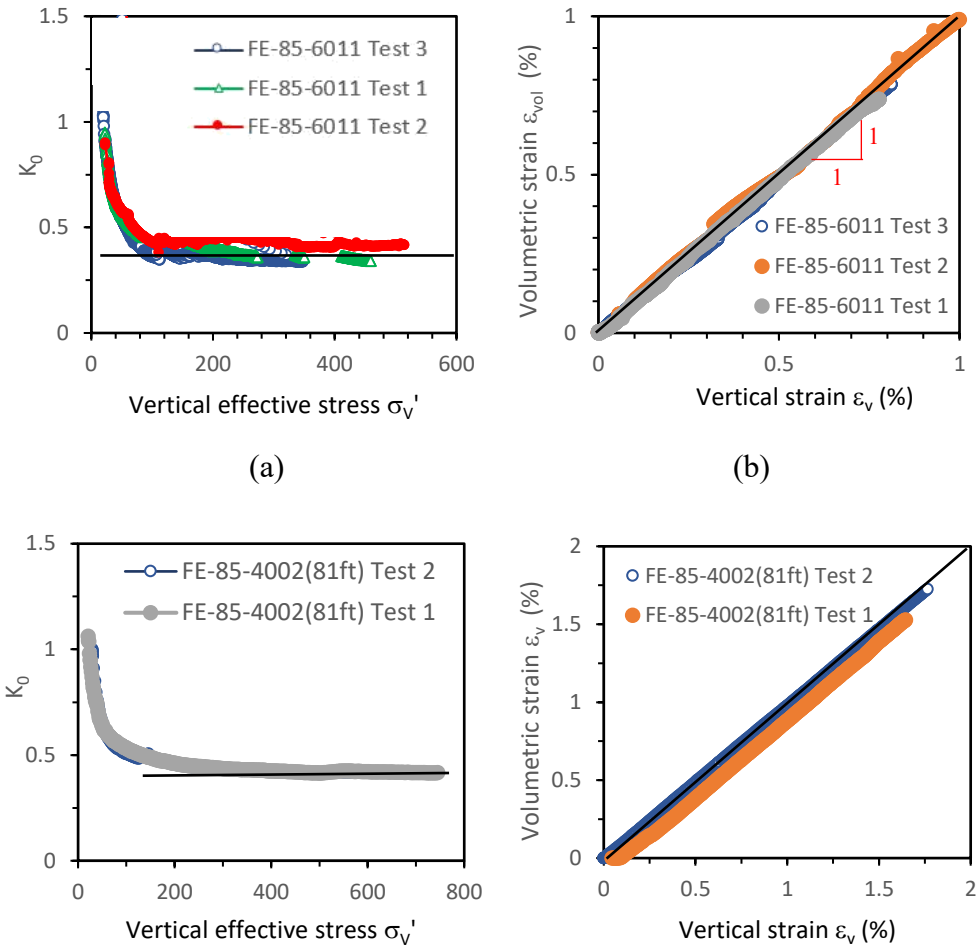

Figure 3-16 Repeatability of K_0-test results

(a) Relation of measured K_0-values and the stress level for specimen #6011

(b) Relation of volumetric and vertical strain during the K_0-test for specimen #6011

(c) Relation of measured K_0-values and the stress level for specimen #4002

(d) Relation of volumetric and vertical strain throughout the K_0-test for specimen #4002

3.7 Plane strain compression test with $\Delta\varepsilon_{zz} = 0$

The purpose of doing this test was to explore how the soil responds to lateral compression and to compare results to the normal K_0-compression test, in which the lateral strain was zero. By combining the data with that obtained from tests along two other stress paths, the cross-anisotropic soil properties can be estimated.

The plane strain compression tests were conducted using the specifically constructed rigid cell that allowed for independent control of radial and axial stresses, as well as back pressure. More specifically, the vertical strain of the cylindrical specimen was kept zero while the radial pressure (i.e., the cell pressure) was increased. The idea was to constrain the vertical strain ($\Delta\varepsilon_{zz} = 0$) by adjusting the axial pressure manually while increasing the cell pressure at a slow rate under the control of the pressure controller (i.e., GDS volume-pressure controller). The volume change of the specimen was measured during the testing. The schematic process of the plane strain test is illustrated in Figure 3-17.

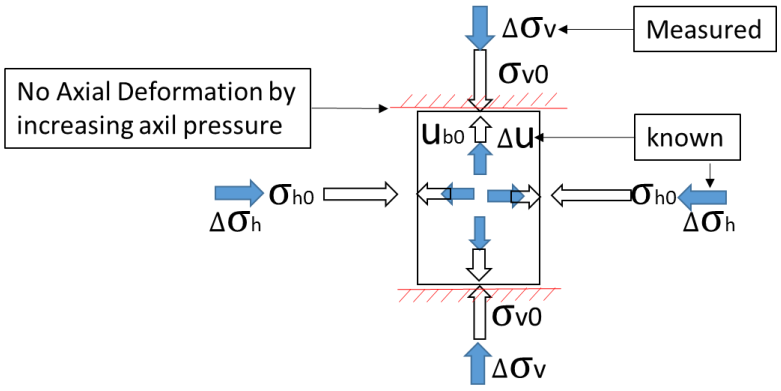

Figure 3-17 Schematic process of zero vertical strain compression test

3.8 Isotropic consolidation test with $\Delta\sigma_{xx} = \Delta\sigma_{yy} = \Delta\sigma_{zz}$

In this series of tests, consolidation under hydrostatic pressure allowed us to study the cross-anisotropic properties of soil. The consolidation test under hydrostatic pressure was carried out on saturated soil specimens by applying the same pressure in the vertical and the horizontal directions simultaneously with the drainage valve open to allow dissipation of excess pore pressure. Five levels of hydrostatic pressure were applied incrementally to determine the relation between the volumetric strain and the vertical strain of soil sample, and a load increment ratio of one was adopted. The duration of each load increment was controlled by the time the soil took to finish primary consolidation. The volume of water flowing out of the specimen was considered as the volume change of the specimen, while the axial deformation was directly measured by a LVDT attached to the loading shaft. Radial deformation was calculated from measured volume change and axial deformation of the specimen. The schematic process of the isotropic consolidation test is presented in Figure 3-18.

For an isotropic soil specimen, the principal strains of the soil specimen should be identical under hydrostatic pressure and $\Delta\varepsilon_{vol}=3\Delta\varepsilon_{v}$. For a cross-anisotropic specimen, the lateral and vertical strains would have been different under hydrostatic pressure; i.e., $\Delta\varepsilon_{vol} \neq 3\Delta\varepsilon_{v}$.

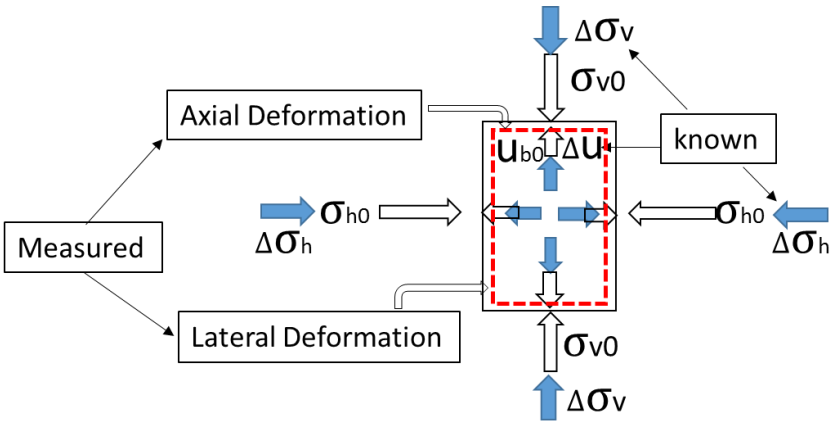

$$\Delta\sigma_{v}^{'} = \Delta\sigma_{h}^{'}$$

Figure 3-18 Isotropic consolidation test

Chapter 4 TEST RESULTS

This chapter presents the laboratory test results obtained from two strain-controlled triaxial tests (the K_0-test with $\Delta\varepsilon_{xx} = \Delta\varepsilon_{yy} = 0$ and the plane strain compression test with $\Delta\varepsilon_{zz} = 0$), as well as the hydrostatic compression tests with $\Delta\sigma_{xx} = \Delta\sigma_{yy} = \Delta\sigma_{zz}$ for different soils. Three approaches were proposed to determine the cross-anisotropic elastic properties of these soils based on the results obtained from the three types of strain and stress path tests. Compared to isotropic homogeneous soils, it is shown that multilayered soil samples tend to have stronger anisotropy with respect to stiffness (or compressibility). In addition, the influence of non-uniform lateral deformation in constituent layers and the strong varve structure of the multilayered soil on measured K_0-value are discussed.

4.1 Stress-strain responses under triaxial stress condition at small strain levels

4.1.1 Isotropic material

The mechanical properties, including the elastic properties of an isotropic material, are independent of the orientation of the frame of reference. As a result, specimens of isotropic materials display the same elastic properties irrespective of the specimen orientation. For an ideal linear elastic, isotropic material, the stress-strain relations under triaxial stress conditions are expressed as

$$\Delta\varepsilon_v = \frac{\Delta\sigma_v - 2\nu\Delta\sigma_h}{E} \tag{4-1}$$

$$\Delta\varepsilon_h = \frac{(1-\nu)\Delta\sigma_h - \nu\Delta\sigma_v}{E} \tag{4-2}$$

where ν is the Poisson's ratio, E is the elastic modulus, and the subscripts v and h stand for quantities in the vertical and horizontal directions, respectively.

The shear modulus G and bulk modulus K are related to E and ν via

$$G = \frac{E}{2(1+\nu)} \tag{4-3}$$

$$K = \frac{E}{3(1-2\nu)} \tag{4-4}$$

4.1.2 Linear Cross-anisotropic material

For a linear cross-anisotropic material, when the *x*- and *y*-axis are two orthogonal directions in the horizontal plane in which the material is isotropic, and the *z*-axis is the vertical direction, the cross-anisotropic elastic stress-strain relation is expressed as

$$\begin{pmatrix} \Delta\varepsilon_{xx} \\ \Delta\varepsilon_{yy} \\ \Delta\varepsilon_{zz} \\ \Delta\gamma_{yz} \\ \Delta\gamma_{zx} \\ \Delta\gamma_{xy} \end{pmatrix} = \begin{pmatrix} \frac{1}{E_h} & \frac{-\nu_{hh}}{E_h} & \frac{-\nu_{vh}}{E_v} & 0 & 0 & 0 \\ \frac{-\nu_{hh}}{E_h} & \frac{1}{E_h} & \frac{-\nu_{vh}}{E_v} & 0 & 0 & 0 \\ \frac{-\nu_{hv}}{E_h} & \frac{-\nu_{hv}}{E_h} & \frac{1}{E_v} & 0 & 0 & 0 \\ 0 & 0 & 0 & \frac{1}{G_{vh}} & 0 & 0 \\ 0 & 0 & 0 & 0 & \frac{1}{G_{vh}} & 0 \\ 0 & 0 & 0 & 0 & & \frac{1}{G_{hh}} \end{pmatrix} \begin{pmatrix} \Delta\sigma_{xx} \\ \Delta\sigma_{yy} \\ \Delta\sigma_{zz} \\ \Delta\tau_{yz} \\ \Delta\tau_{zx} \\ \Delta\tau_{xy} \end{pmatrix} \tag{4-5}$$

Under triaxial stress condition without shear stresses being applied, when the axial stress is in the vertical direction, which is the axis of axisymmetry, the Cartesian coordinates (*x, y, z*) can be replaced by the triaxial coordinates with (*v, h*), and Eq. (4-5) can be rewritten as

$$\begin{pmatrix} \Delta\varepsilon_h \\ \Delta\varepsilon_h \\ \Delta\varepsilon_v \end{pmatrix} = \begin{pmatrix} \frac{1}{E_h} & \frac{-\nu_{hh}}{E_h} & \frac{-\nu_{vh}}{E_v} \\ \frac{-\nu_{hh}}{E_h} & \frac{1}{E_h} & \frac{-\nu_{vh}}{E_v} \\ \frac{-\nu_{hv}}{E_h} & \frac{-\nu_{hv}}{E_h} & \frac{1}{E_v} \end{pmatrix} \begin{pmatrix} \Delta\sigma_h \\ \Delta\sigma_h \\ \Delta\sigma_v \end{pmatrix} \tag{4-6}$$

Eq. (4-6) can be further simplified by consolidating the first two columns and rows,

and by taking into account $\nu_{vh} / E_v = \nu_{hv} / E_h$, one has:

$$\begin{pmatrix} \Delta\varepsilon_h \\ \Delta\varepsilon_v \end{pmatrix} = \begin{pmatrix} \dfrac{(1-\nu_{hh})}{E_h} & -\dfrac{\nu_{vh}}{E_v} \\ \dfrac{-2\nu_{vh}}{E_v} & \dfrac{1}{E_v} \end{pmatrix} \begin{pmatrix} \Delta\sigma_h \\ \Delta\sigma_v \end{pmatrix} \tag{4-7}$$

Eq. (4-7) can be rearranged as

$$\begin{pmatrix} \Delta\varepsilon_h \\ \Delta\varepsilon_v \end{pmatrix} = \begin{pmatrix} \Delta\sigma_h & -\Delta\sigma_v & 0 \\ 0 & -2\Delta\sigma_h & \Delta\sigma_v \end{pmatrix} \begin{pmatrix} \dfrac{1-\nu_{hh}}{E_h} \\ \dfrac{\nu_{vh}}{E_v} \\ \dfrac{1}{E_v} \end{pmatrix} \tag{4-8}$$

This relation reveals that $\frac{1-\nu_{hh}}{E_h}$, $\frac{\nu_{vh}}{E_v}$ and $\frac{1}{E_v}$ can be determined directly from test results when carrying out tests along different stress paths with controlled $\Delta\sigma_h$ and $\Delta\sigma_v$.

4.2 Typical response of soil under various conditions and evidence of cross-anisotropic behaviour

4.2.1 Typical response of soil under various conditions

The results of the three types of tests (i.e., K_0-test, PSC test, and HPC test) for specimen #2004 (homogeneous sandy soil) are presented in Figures 4-1 to 4-3, respectively.

1) Drained K_0-test

Figure 4-1 (a) presents the stress path in terms of the horizontal and vertical effective stresses during the drained K_0-test. The test was started from an initial hydrostatic stress state with $\sigma'_{h0} = \sigma'_{v0} = 20\,\text{kPa}$. With the increase of axial stress, the effective stress path gradually approached the K_0 stress state as consolidation proceeded under the K_0-constraint with $\varepsilon_h = 0$. Eventually, the sample consolidated steadily

under the K_0 stress state conditions, which was supposed to be similar to the original in-situ stress state. As indicated previously, the stress ratio of horizontal effective stress and the axial effective stress σ_h' / σ_v' at the ultimate K_0 stress state was used to determine the K_0-value; as shown in Figure 4-1 (b). Figure 4-1 (c) presents the evolution of the vertical effective stress with the vertical strain of the specimen during K_0-test. The stress-strain relation was approximately linear when the vertical strain was in the range of 0-0.2%, for which the deformation of the soil specimens had not reached the K_0-state yet, as can be seen from Figures 4-1 (a) and (c). During the K_0-consolidation state, the experimental data could be described by a linear relation between $Log\ \sigma_v'$ and the vertical strain ε_v; as shown in Figure 4-1(d).

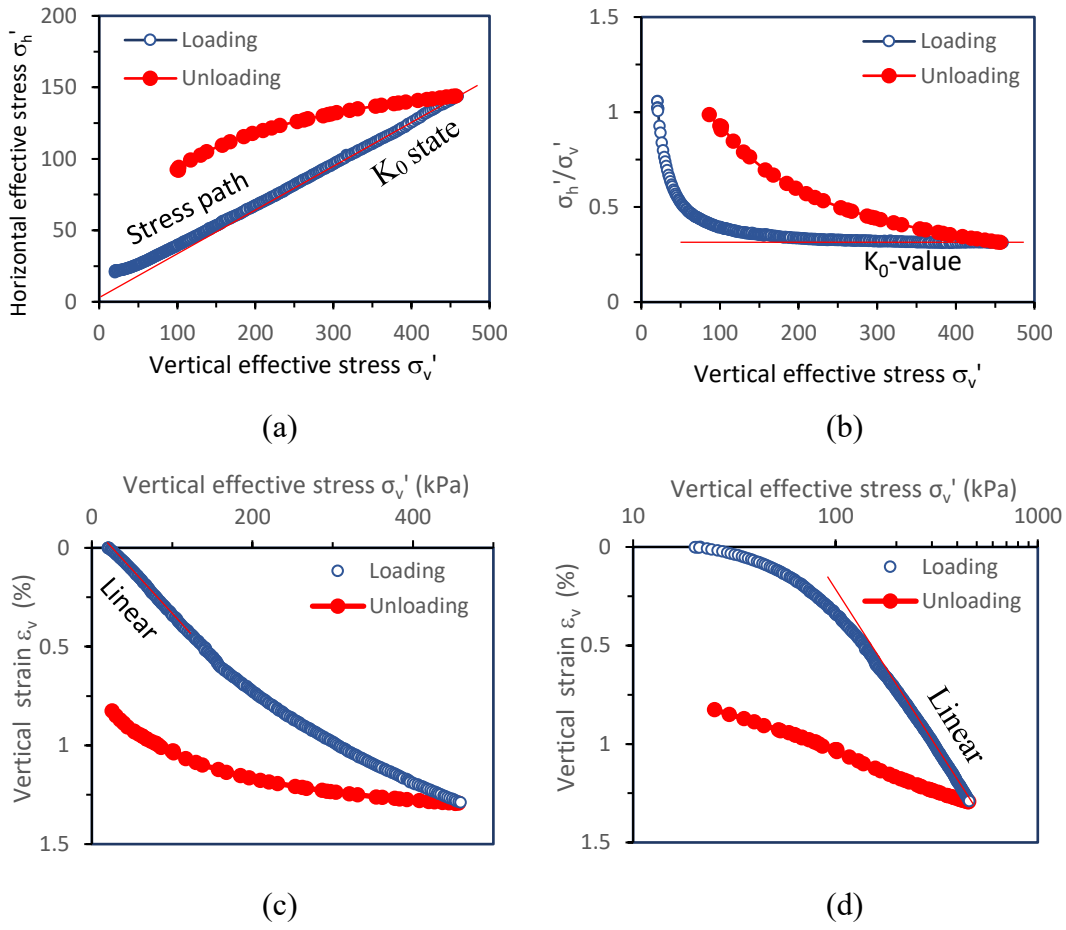

Figure 4-1 Results of the K_0-compression test for soil specimen #2004

2) Plane strain compression test

Figure 4-2 (a) presents the variation of horizontal and vertical effective stress during the PSC test with $\varepsilon_v = 0$. The stress trajectory is seen to be similar to that of the K_0-compression test. The variation of the ratio σ_h' / σ_v' as a function of the vertical effective stress can be observed in Figure 4-2 (b). Figure 4-2 (c) presents the evolution of the horizontal effective stress with the horizontal strain of the specimen during the PSC test. The stress-strain relation was approximately linear when the horizontal strain was in the range of 0-0.15%, for which the deformation of the soil specimens had not reached the K_{v0}-state yet, as can be seen from Figures 4-2 (a) and (c). During the K_{v0}-consolidation state, the experimental data could be described by a linear relation between $Log\ \sigma_h'$ and the horizontal strain ε_h; as shown in Figure 4-2(d).

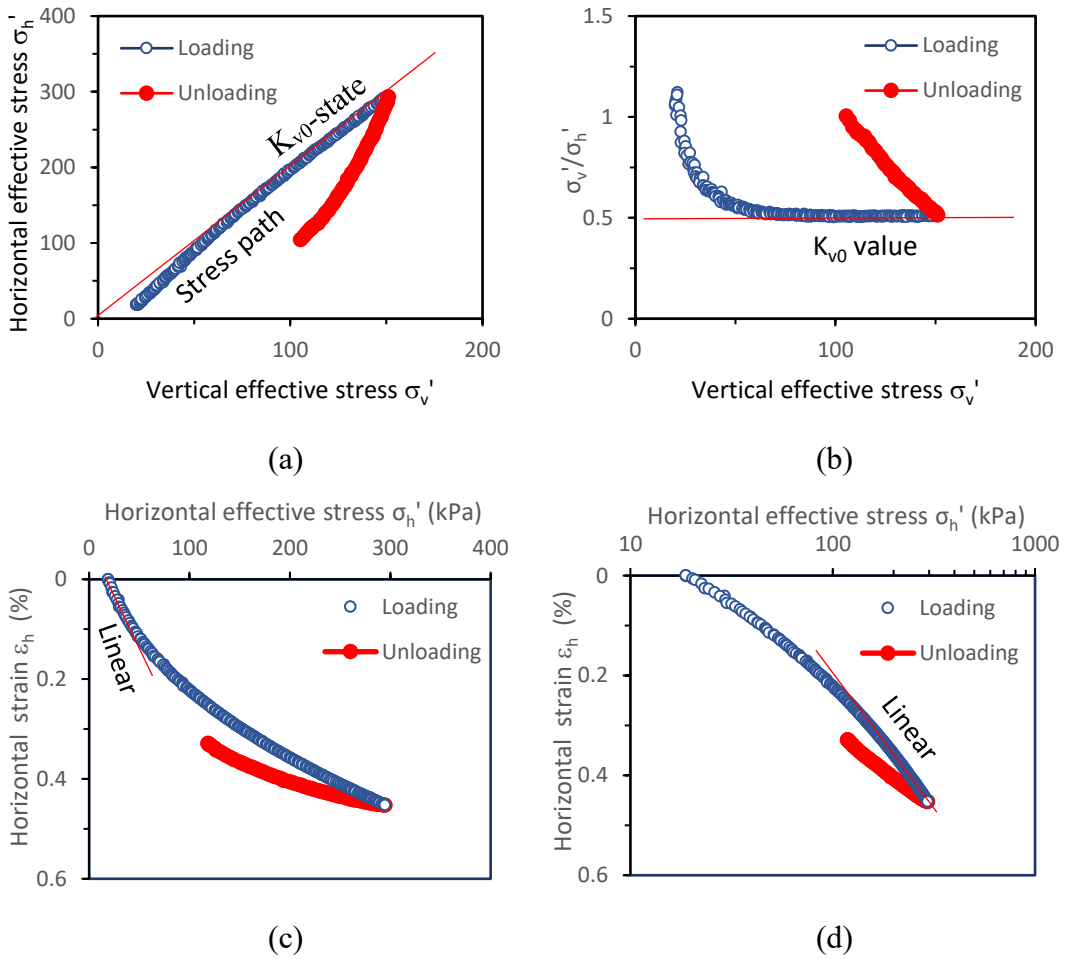

Figure 4-2 Results of the PSC test for soil specimen #2004

3) Hydrostatic pressure compression test

As can be observed from Figures 4-3 (a) and (b), the relation between hydrostatic pressure p' and vertical strain ε_v during the isotropic consolidation test is linear at small strain level (0-0.15%), while a linear relation exists between $Log\ p'$ and the vertical strain ε_v at high-stress level.

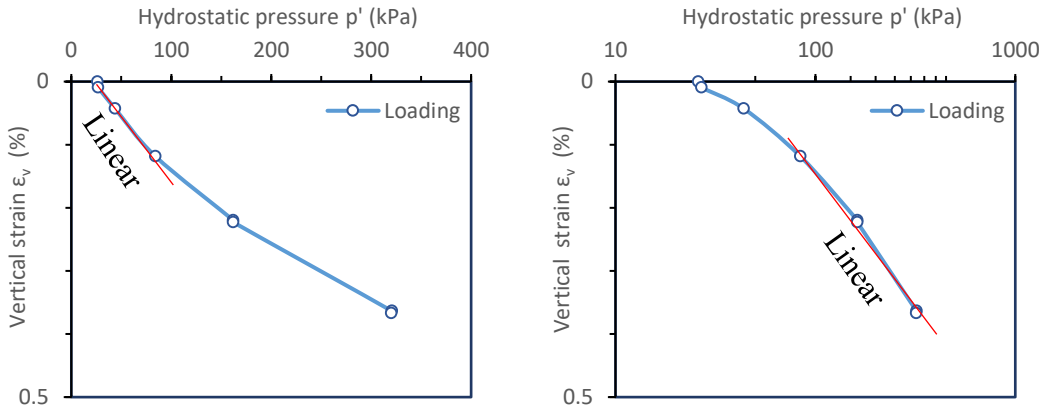

(a) (b)

Figure 4-3 Results of the hydrostatic compression test for soil specimen #2004

4.2.2 Evidence of cross-anisotropic behaviour

1) K_0-test and PSC test

The K_0-test and the PSC test are both strain-controlled loading tests with one fixed boundary condition either in the lateral direction (K_0-test with $\varepsilon_h = 0$) or vertical direction (PSC test with $\varepsilon_v = 0$). For an isotropic material, the principal effective stress ratio for the K_0-test and the PSC test can be expressed from Eqs. (4-1) and (4-2) as follows:

$$K_0 = \frac{\sigma'_h}{\sigma'_v} = \frac{\sigma'_3}{\sigma'_1} = \frac{\nu}{1-\nu} \tag{4-9}$$

$$K_{v0} = \frac{\sigma'_v}{\sigma'_h} = \frac{\sigma'_3}{\sigma'_1} = 2\nu \tag{4-10}$$

where the Poisson's ratio can be determined according to the measured stress ratio as

$$\nu = \frac{K_0}{1+K_0} \quad \text{or} \quad \nu = \frac{1}{2}K_{v0} \tag{4-11}$$

If a soil is isotropic, the Poisson's ratio ν determined from both tests should be identical. Otherwise, the soil is anisotropic. K_0 and PSC tests were carried out on three materials, including a grey sand (specimen #2004 from a depth of 18m), a clayey sand (specimen #4002 from a depth of 10m), and a layered soil (specimen #5022 from a depth of 8m). As shown in Figure 4-4, specimen #2004 looked like a homogeneous soil with uniform particle size distribution; specimen #4002 was heterogeneous with visible non-uniform particle distribution; specimen #5002 was a layered soil that had a varve structure with approximately 2-5mm thick layering.

(a) (b) (c)

Figure 4-4 Tested materials for making a comparison
(a) Homogeneous soil #2004 (b) Heterogeneous soil #4002 (c) Layered soil #5022

Figure 4-5 (a) shows the variation of the stress ratios σ_3'/σ_1' with respect to the vertical effective stress σ_v' for the K_0 and PSC tests on the grey sand (#2004), and Figure 4-5 (b) provides the corresponding stress paths. The initial state of stress was approximately isotropic. In each test, with an increase of σ_v', the ratio σ_3'/σ_1' decreased gradually to a steady-state value. The ultimate σ_3'/σ_1' for the K_0-test was 0.30, compared to 0.50 for the PSC test on the same soil. Based on Eq. (4-12), the Poisson's ratio determined by the principal effective stress ratios was $\nu = 0.24$ from the K_0-test and $\nu = 0.25$ from the PSC test, which implied that the grey sand #2004

was approximately isotropic.

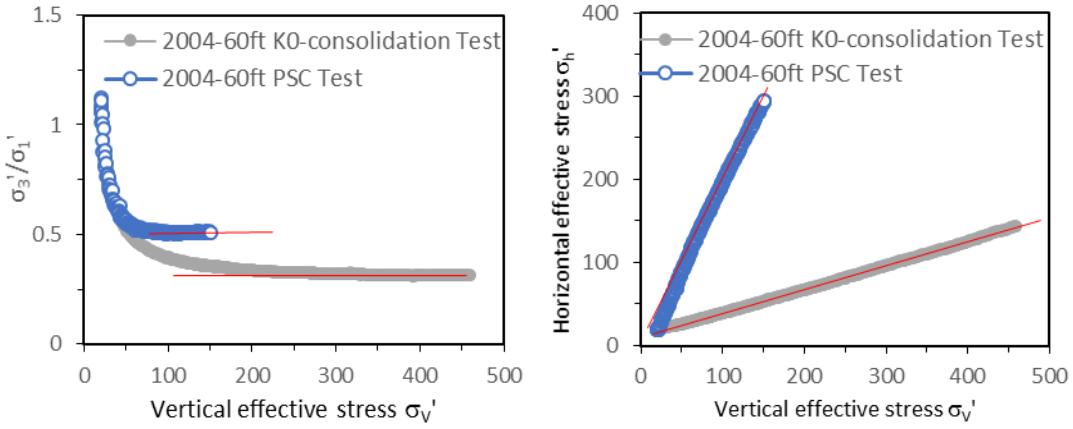

(a) (b)

Figure 4-5 Results of the K_0 and the PSC tests for the homogeneous grey sand #2004

Figure 4-6 presents the variation of the stress ratio from the K_0 and PSC tests on specimens of heterogeneous soil # 4002 and layered soil #5022. As stated previously, the soils #4002 and #5022 were expected to be anisotropic, given their appearance in Figures 4-4 (b) and (c). Table 4-1 summarizes the stress ratios and Poisson's ratios obtained from the tests using Eq. (4-12), in which ν_1 is a Poisson's ratio determined from the K_0-test, and ν_2 is a Poisson's ratio determined from the PSC test.

As can be found from Table 4-1, the values of Poisson's ratio determined from the two tests were different for both soils #4002 and #5002, which confirmed that the soils #4002 and #5002 were both anisotropic with direction dependent Poisson's ratios.

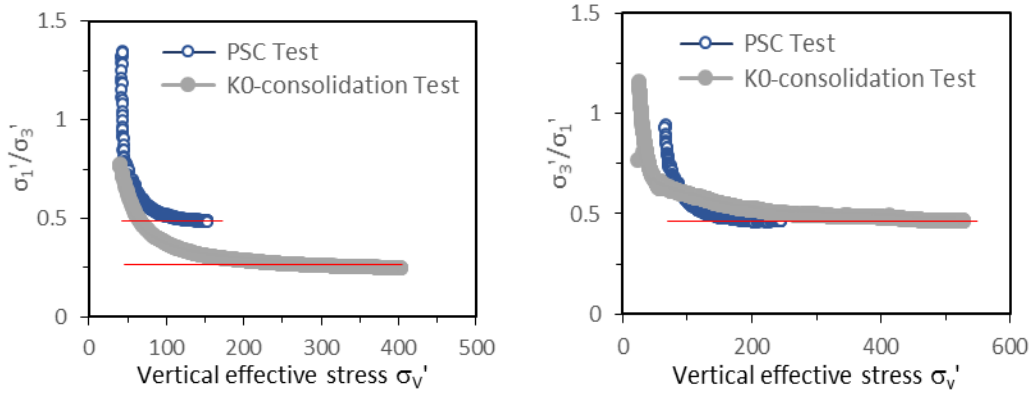

(a) (b)

Figure 4-6 Variation of stress ratio with vertical effective stress
(a)Heterogeneous soil #4002 (b) Layered soil #5022

Table 4-1 Summary of the stress ratios and Poisson's ratios

Soil Number	K_0-test: $K_0 = \sigma_3' / \sigma_1'$	ν_1	PSC test: $K_{v0} = \sigma_3' / \sigma_1'$	ν_2
Soil #2004	0.31	0.24	0.50	0.25
Soil #4002	0.23	0.18	0.50	0.25
Soil #5022	0.46	0.32	0.46	0.23

2) Hydrostatic compression tests

Five levels of hydrostatic pressure were applied incrementally to determine the relation between volumetric strain and the vertical strain. If a soil specimen is isotropic, the volumetric strain increment should be equal to three times the vertical strain increment; *i,e.,* $\Delta\varepsilon_{vol}=3\Delta\varepsilon_v$.

Figure 4-7 (a) presents the relation between the measured volumetric strain ε_{vol} and vertical strain ε_v for the soil #2004. From this figure, we see that when the vertical strain level was greater than 0.02%, the value of $\Delta\varepsilon_{vol} / \Delta\varepsilon_v$ was 3.12, which is very close to 3 for an isotropic material. Figure 4-4 (b) provides the variation $\Delta\varepsilon_{vol} / \Delta\varepsilon_v$ during consolidation. At the beginning of the test, the ratio of $\Delta\varepsilon_{vol} / \Delta\varepsilon_v$ was greater than six, which was out of the reasonable range. This was attributed to measurement errors from either the displacement transducer or the volume change transducer. As the consolidation test proceeded with an increase of the vertical strain, the ratio $\Delta\varepsilon_{vol} / \Delta\varepsilon_v$ gradually approached three. As a result, one could conclude that soil #2004 was practically isotropic, which is consistent with the conclusion obtained based on the K_0- and PSC tests.

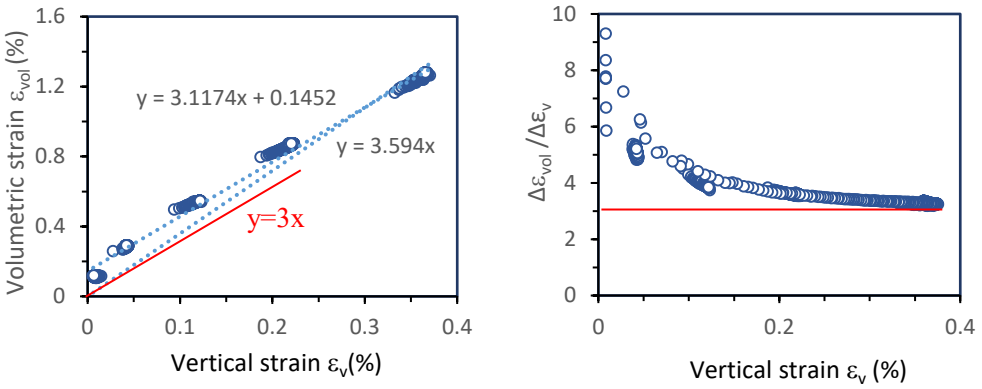

(a) (b)

Figure 4-7 Hydrostatic compression test for the homogeneous soil #2004

For the heterogeneous soil (specimen #4002), the test results corresponding to Figure 4-8 yielded $\Delta\varepsilon_{vol} / \Delta\varepsilon_v \approx 4$, or equivalently $\Delta\varepsilon_h / \Delta\varepsilon_v \approx 1.5$, which implies that the specimen was anisotropic and the stiffness in the vertical direction was higher than that in the horizontal direction.

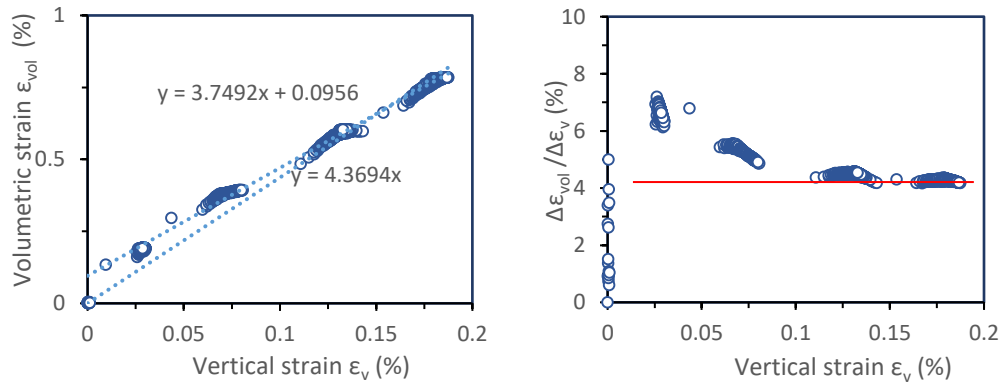

(a) (b)

Figure 4-8 Hydrostatic compression test results for the heterogeneous soil #4002

For the layered soil #5022, a strong anisotropic characteristic was expected. As can be seen from Figure 4-6, the measured data was $\Delta\varepsilon_{vol} / \Delta\varepsilon_v$=1.697 , which corresponded to $\Delta\varepsilon_h$=0.35$\Delta\varepsilon_v$. This implies that the layered soil was highly anisotropic. More specifically, the stiffness in the horizontal direction was higher than that in the

vertical direction.

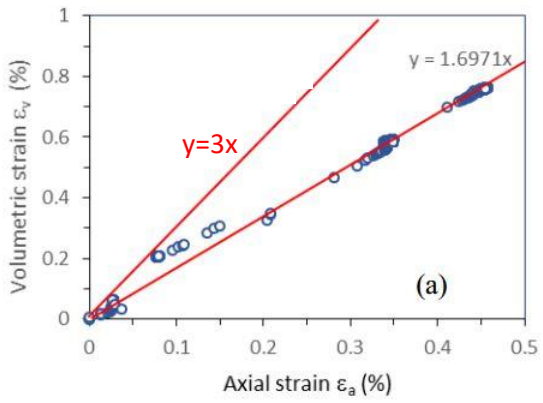

Figure 4-9 Hydrostatic compression test results for the layered soil #5022

4.3 Characterization of cross-anisotropic elastic soil properties

Even though the test results of the three soils presented in Figures 4-5 to 4-9 from the K_0-test, PSC test, and consolidation test under hydrostatic pressure only provided the evidence for a soil's anisotropy, further analyses must be conducted to determine the cross-anisotropic elastic parameters of soil. Three approaches are presented in this section. Thereafter, the value of elastic properties were examined to ensure that the compliance matrix in Eq. (4-6) is positive definite that is a fundamental requirement for non-negative strain energy. To fulfill this requirement, the inequality provided by Raymond (1970) in Eq. (2-5) must be satisfied.

4.3.1 Approach A to determine cross-anisotropic elastic parameters

The elastic properties can be determined from the measurement of stress and strain increments in the triaxial tests. For conventional triaxial compression tests with constant confining pressure (i.e., $\Delta\sigma_h = 0$), according to Eq. (4-8) the stress-strain relation for a cross-anisotropic elastic material is

$$\begin{pmatrix} \Delta\varepsilon_h \\ \Delta\varepsilon_v \end{pmatrix} = \begin{pmatrix} -\Delta\sigma_v & 0 \\ 0 & \Delta\sigma_v \end{pmatrix} \begin{pmatrix} \frac{\nu_{vh}}{E_v} \\ \frac{1}{E_v} \end{pmatrix} \tag{4-12}$$

from which E_v and ν_{vh} can be determined from the measured data.

For a triaxial test with $\Delta\sigma_v = 0$, one obtains the following relations from Eq. (4-8) as

$$\begin{pmatrix} \Delta\varepsilon_h \\ \Delta\varepsilon_v \end{pmatrix} = \begin{pmatrix} \Delta\sigma_h & 0 \\ 0 & -2\Delta\sigma_h \end{pmatrix} \begin{pmatrix} \dfrac{1-\nu_{hh}}{E_h} \\ \dfrac{\nu_{vh}}{E_v} \end{pmatrix} \tag{4-13}$$

in which E_h and ν_{hh} are coupled and cannot be uniquely determined.

For a triaxial test along a stress path with $\Delta\sigma_h \neq 0$ and $\Delta\sigma_v \neq 0$, four elastic parameters (E_h, E_v ν_{hh}, and ν_{vh}) cannot be readily determined from the two relations in Eq. (4-8) for a single stress path test. Additional equations are required to determine all the cross-anisotropic elastic properties, which also requires necessary assumptions to decouple ν_{hh} and E_h from $\dfrac{1-\nu_{hh}}{E_h}$ (Liu, 2010). Tuturmluer and Seyhan (2003) indicate that one can perform three slightly different but very close stress path tests (i.e., described in *q-p* stress space as $\Delta q / \Delta p = k$ and $k \pm 0.1$, respectively) to obtain the required number of equations. In this study, tests along three stress paths (i.e., K_0-test, PSC test, and HPC test) were carried out to provide sufficient data for determining the cross-anisotropic elastic properties of soil. When applying Eq. (4-8) to each individual test, six equations in total can be obtained as follows

$$\begin{pmatrix} \Delta\varepsilon_h^{(1)} \\ \Delta\varepsilon_v^{(1)} \\ \Delta\varepsilon_h^{(2)} \\ \Delta\varepsilon_v^{(2)} \\ \Delta\varepsilon_h^{(3)} \\ \Delta\varepsilon_v^{(3)} \end{pmatrix} = \begin{pmatrix} \Delta\sigma_h^{(1)} & -\Delta\sigma_v^{(1)} & 0 \\ 0 & -2\Delta\sigma_h^{(1)} & \Delta\sigma_v^{(1)} \\ \Delta\sigma_h^{(2)} & -\Delta\sigma_v^{(2)} & 0 \\ 0 & -2\Delta\sigma_h^{(2)} & \Delta\sigma_v^{(2)} \\ \Delta\sigma_h^{(3)} & -\Delta\sigma_v^{(3)} & 0 \\ 0 & -2\Delta\sigma_h^{(3)} & \Delta\sigma_v^{(3)} \end{pmatrix} \begin{pmatrix} \dfrac{1-\nu_{hh}}{E_h} \\ \dfrac{\nu_{vh}}{E_v} \\ \dfrac{1}{E_v} \end{pmatrix} \tag{4-14}$$

which can be written as

$$\boldsymbol{\varepsilon} = \mathbf{A}\mathbf{X} \tag{4-15}$$

where $\mathbf{A}$, $\mathbf{X}$ and $\boldsymbol{\varepsilon}$ can be identified when comparing Eq. (4-14) and Eq. (4-15).

Eq. (4-14) is an over-determined system of linear equations with redundancies because it has six equations for three unknowns ($\frac{1-\nu_{hh}}{E_h}$, E_v, and ν_{vh}). Stress and strain increments obtained from three stress path tests at small strain level (0-0.2%) were substituted to the matrices $\boldsymbol{\varepsilon}$ and $\mathbf{A}$ in Eq. (4-14), and the least squares method was used to determine the unknowns in $\mathbf{X}$ by solving $\mathbf{A^T\varepsilon = A^TAX}$. After solving these three components ($\frac{1-\nu_{hh}}{E_h}$, E_v, and ν_{vh}) in $\mathbf{X}$, the following assumption explored by Graham and Houlsby (1983) was used to decouple ν_{hh} and E_h from $\frac{1-\nu_{hh}}{E_h}$;i.e.,

$$\sqrt{\frac{E_h}{E_v}} = \frac{\nu_{hh}}{\nu_{vh}} \tag{4-16}$$

Finally, all elastic properties (E_v, E_h, ν_{vh}, ν_{hv} and ν_{hh}) could be determined. For more details about the mathematic manipulations for determining all the elastic properties, the reader is referred to Liu (2010).

4.3.2 Approach B to determine cross-anisotropic elastic parameters.

For a cross-anisotropic material, the effective stress ratio can be inferred from a K_0-test ($\varepsilon_h = 0$) together with Eq. (4-7) as

$$K_0 = \frac{\sigma'_h}{\sigma'_v} = \frac{E_h}{E_v}\frac{\nu_{vh}}{1-\nu_{hh}} = \frac{\nu_{hv}}{1-\nu_{hh}} \tag{4-17}$$

while for the PSC test with $\varepsilon_v = 0$, the effective stress ratio becomes

$$K_{v0} = \frac{\sigma'_v}{\sigma'_h} = 2\nu_{hv}\frac{E_v}{E_h} = 2\nu_{vh} \tag{4-18}$$

where ν_{vh} can be determined directly once the effective stress ratio K_{v0} is known from the experimental data of the PSC test. Substituting Eqs. (4-17) and (4-18) into Eq. (4-7), one obtains

$$\begin{pmatrix} \Delta\varepsilon_h \\ \Delta\varepsilon_v \end{pmatrix} = \begin{pmatrix} \dfrac{K_{v0}}{2K_0E_v} & -\dfrac{K_{v0}}{2E_v} \\ \dfrac{-K_{v0}}{E_v} & \dfrac{1}{E_v} \end{pmatrix} \begin{pmatrix} \Delta\sigma_h \\ \Delta\sigma_v \end{pmatrix} \tag{4-19}$$

where E_v is the only unknown in the over-determined system of linear equations once the K_0 and K_{v0} are obtained from the experimental data of the K_0-test and PSC test, respectively. When applying Eq. (4-19) to each individual test (K_0-test and PSC test), four equations in total can be obtained as follows:

$$\begin{pmatrix} \Delta\varepsilon_h^{(1)} \\ \Delta\varepsilon_v^{(1)} \\ \Delta\varepsilon_h^{(2)} \\ \Delta\varepsilon_v^{(2)} \end{pmatrix} = \begin{pmatrix} \dfrac{K_{v0}}{2K_0E_v} & -\dfrac{K_{v0}}{2E_v} & 0 & 0 \\ \dfrac{-K_{v0}}{E_v} & \dfrac{1}{E_v} & 0 & 0 \\ 0 & 0 & \dfrac{K_{v0}}{2K_0E_v} & -\dfrac{K_{v0}}{2E_v} \\ 0 & 0 & \dfrac{-K_{v0}}{E_v} & \dfrac{1}{E_v} \end{pmatrix} \begin{pmatrix} \Delta\sigma_h^{(1)} \\ \Delta\sigma_v^{(1)} \\ \Delta\sigma_h^{(2)} \\ \Delta\sigma_v^{(2)} \end{pmatrix} \tag{4-20}$$

Stress and strain increments selected from the K_0-test and PSC test at the strain levels, where the K_0 and K_{v0} states have been reached are substituted into Eq. (4-20), and then the least squares method similar to that adopted in approach A can be used to determine E_v. Finally, Eq. (4-17) obtained from the K_0-test is combined with the constraints in Eqs. (2-4) and (4-16) to determine the remaining properties E_h, ν_{hv}, and ν_{hh}.

4.3.3 Approach C to determine cross-anisotropic elastic parameters.

For a cross-anisotropic elastic material, the earth pressure coefficient at rest for $\varepsilon_h = 0$ can be inferred from Eq. (4-7) as

$$K_0 = \frac{\sigma_h'}{\sigma_v'} = \frac{E_h}{E_v}\frac{\nu_{vh}}{1-\nu_{hh}} = \frac{\nu_{hv}}{1-\nu_{hh}} \tag{4-21}$$

and the constrained modulus that is defined as $M_{vz} = \sigma_v' / \varepsilon_v\big|_{\varepsilon_h=0}$ can be related to other elastic properties through

$$\frac{1}{M_{vz}} = \frac{1}{E_v} - 2K_0\frac{\nu_{hv}}{E_h} = \frac{1}{E_h}\left(\frac{E_h}{E_v} - \frac{2\nu_{hv}^2}{1-\nu_{hh}}\right) \tag{4-22}$$

Both K_0 and M_{vz} can be determined from the measured stresses and strains from the K_0-test directly. For the PSC test with ε_v=0, the plane strain constraint requires

$$\varepsilon_v = \frac{\sigma_v'}{E_v} - 2\frac{\nu_{hv}}{E_h}\sigma_h' = 0$$

The relation between the lateral stain and lateral stress is obtained from Eq. (4-6) as

$$\varepsilon_h = \frac{1}{E_h}\left[\left(1-\nu_{hh}\right)\sigma_h' - \nu_{hv}\sigma_v'\right] = \frac{\sigma_h'}{E_h}\left[\left(1-\nu_{hh}\right) - 2\frac{E_v\nu_{hv}^2}{E_h}\right] \tag{4-23}$$

It follows that the K_{v0} and M_{vx} can be related to the other elastic properties as

$$K_{v0} = \frac{\sigma_v'}{\sigma_h'} = 2\nu_{hv}\frac{E_v}{E_h} \tag{4-24}$$

$$\frac{1}{M_{vx}} = \frac{\varepsilon_h}{\sigma_h'} = \frac{1}{E_h}\left[\left(1-\nu_{hh}\right) - \frac{2E_v\nu_{hv}^2}{E_h}\right] \tag{4-25}$$

Both K_{v0} and M_{vx} can be determined from the measured stresses and strains from the PSC test. According to Eq. (4-8), the stress-strain relations in the hydrostatic compression test are

$$\varepsilon_h = \frac{1}{E_h}(1-\nu_{hh}-\nu_{hv})\ \sigma,\ \varepsilon_v = \left(\frac{1}{E_v} - \frac{2\nu_{hv}}{E_h}\right)\ \sigma \tag{4-26}$$

in which σ is the applied hydrostatic pressure. The volumetric strain can, therefore, be expressed as

$$\varepsilon_{vol} = 2\varepsilon_h + \varepsilon_v = \frac{1}{E_h}\left[2\left(1-\nu_{hh}-2\nu_{hv}\right)+\frac{E_h}{E_v}\right]\sigma \tag{4-27}$$

The ratio of volumetric strain and vertical strain follows as

$$\frac{\varepsilon_{vol}}{\varepsilon_v} = \frac{2(1-\nu_{hh}-2\nu_{hv})+E_h/E_v}{E_h/E_v-2\nu_{hv}} \tag{4-28}$$

This ratio can be determined from the measured volume change and axial deformation of the sample in a hydrostatic test.

When K_0, M_{vz}, K_{v0}, M_{vx}, and $\varepsilon_{vol}/\varepsilon_v$ are determined directly from the three tests (i.e., K_0-test, PSC test, and HPC test) while taking into account the constraints in Eqs. (2-4) and (4-16), all cross-anisotropic elastic properties of the soil (E_v, E_h, ν_{hv}, and ν_{hh}) can be determined through the algebra manipulation of the equations. There are five equations for four unknowns, implying that the equations are not independent.

More specifically, Eq. (4-22) and Eq. (4-25) are not independent, while Eq. (4-24) and Eq. (4-28) are also not independent. Referring to Eq. (4-22), one has

$$\frac{1}{M_{vz}} = \frac{1}{E_v} - 2K_0\frac{\nu_{hv}}{E_h} = \frac{1}{E_h}\left(\frac{E_h}{E_v}-\frac{2\nu_{hv}^2}{1-\nu_{hh}}\right)$$
$$= \frac{\nu_{vh}}{E_v}\left(\frac{1}{\nu_{vh}}-2K_0\right) = \frac{1}{E_v}\left(1-K_{v0}K_0\right)$$

Similarly, one obtains from Eq. (4-25) that

$$\frac{1}{M_{vx}} = \frac{\varepsilon_h}{\sigma_h'} = \frac{1}{E_h}\left[\left(1-\nu_{hh}\right)-\frac{2E_v\nu_{hv}^2}{E_h}\right]$$
$$= \frac{1}{E_h}\left[\frac{\nu_{hv}}{K_0}-2\nu_{vh}\nu_{hv}\right] = \frac{1}{E_v}\left[\frac{K_{v0}}{2K_0}-\frac{K_{v0}^2}{2}\right]$$

One observes that in both Eqs. (4-22) and (4-25), the only unknown is E_v.

With regard to Eqs. (4-24) and (4-28), they can be rewritten as

$$K_{v0} = \frac{\sigma_v'}{\sigma_h'} = 2\nu_{hv}\frac{E_v}{E_h} = 2\nu_{vh}$$

$$\frac{\varepsilon_{vol}}{\varepsilon_v} = \frac{2(1-\nu_{hh}-2\nu_{hv})+E_h/E_v}{E_h/E_v-2\nu_{hv}} = \frac{2(1/K_0-2)+1/\nu_{vh}}{1/\nu_{vh}-2}$$

When K_{v0} and $\varepsilon_{vol}/\varepsilon_v$ are determined from laboratory tests, the above two equations both have one only unknown ν_{vh}.

An optimization method (the least squares method) has to be used for the dependent equations to determine elastic properties E_v and ν_{vh}. Other elastic properties E_h, ν_{hv}, and ν_{hh} can be determined through Eqs. (2-4), (4-16), and (4-21).

4.3.4 Selection of experimental data to determine cross-anisotropic elastic properties

Referring to representative results of tests presented in Figures 4-1, 4-2, and 4-3, the experimental stress-strain relations are generally non-linear and stress-level dependent. Therefore, it is reasonable to argue that the cross-anisotropic elastic properties of a soil are functions of stress state, strain level, and other influencing factors (i.e., stress history and stress path). In other words, for the approaches adopted in this study, the elastic cross-anisotropic properties depend on the stress-strain level at which the data are selected for the determination of these material properties.

In general, approach A can be used for data at any stress level, as long as the stress or strain level in the different tests are the same. It should be noted, however, a soil can be considered approximately elastic in the small strain level range (0-0.2%), as can be observed in Figure 4-1, 4-2, and 4-3. Above this strain level, the results obtained from approach A should be considered as tangential elastic properties at the corresponding strain level.

When approaches B and C are used to determine the elastic properties of a soil, the data used was selected from the stress or strain level, where the sample is either at the K_0 stress state in K_0-test or the K_{v0} stress state in PSC test. It could be argued that the data should be picked from the unloading branch of the tests to define the elastic

stress and strain increments because the elastic strain is recoverable and can be measured more accurately with the absence of irrecoverable plastic strain. However, this had been found impractical for the two strain-controlled tests (i.e., K_0-test with $\varepsilon_h = 0$ and PSC test with $\varepsilon_v = 0$) through several trial tests. The experimental operations turned out to be too complex with regard to controlling the stress paths. Regardless, the results from the trial tests on the unloading part were analyzed, attempting to determine the elastic cross-anisotropic properties. As might have been expected, the determined properties were not reasonable because the thermodynamic constraints provided by Eqs. (2-5) and (2-6) were not satisfied. As a result, only the test results obtained from the loading process are presented in the following part. At this point, since the strain level of the soil specimen is controlled in a relatively small range during the tests, the generation of the plastic strain is assumed to be negligible.

4.3.5 Summary of results

A series of tests were performed on five soils to determine their cross-anisotropic elastic properties using three approaches presented in the previous section, with the results being summarized in Table 4-2.

As expected, the grey sand (#2004) was approximately isotropic. The elastic modulus in the vertical direction E_v is close to the elastic modulus in the horizontal direction E_h , with $E_h / E_v = 0.92 \pm 0.01$ determined from the three approaches. Three Poisson's ratios are close to one other, with $\overline{\nu_{vh}} = 0.255$ $\overline{\nu_{hv}} = 0.234$, $\overline{\nu_{hh}} = 0.241$. This conclusion supports the previous investigation conducted by the consolidation test under hydrostatic pressure that the volumetric strain increment of the sample must be equal to three times the vertical strain increment (i.e., $\Delta\varepsilon_{vol}=3\Delta\varepsilon_v$) for an isotropic consolidation test if the soil is isotropic. The same conclusion can be applied to the sandy silt (#3002), which can also be considered as a homogeneous,

isotropic soil, with $E_h / E_v = 0.98$, $\overline{\nu_{vh}} = 0.279$, $\overline{\nu_{hv}} = 0.270$, and $\overline{\nu_{hh}} = 0.273$.

The silty clay (#4002) is a heterogeneous soil with $E_h / E_v = 0.80 - 0.86$ and $\nu_{hh} / \nu_{hv} = 0.88 - 0.93$. More specifically, the elastic modulus in the vertical direction E_v is approximately 20% higher than that in the horizontal direction E_h. This conclusion is consistent with the previous investigation in Section 4.2.2 with respect to anisotropy.

It is also noted that the cross-anisotropic elastic properties obtained from approaches B and C are close to each other, but differences are observed in the results obtained by using approach A. This difference between the results obtained from the approach A and the approach B/C is attributed to the different stress levels at which the experimental data was interpreted.

The layered soil (#5022) has strong anisotropy of stiffness, with the elastic modulus E_h in the direction parallel to the layering being 40% higher than the value of E_v in the vertical direction at stress levels corresponding to K_0-state determined from approaches B and C. At the small strain levels, the E_h / E_v ratio determined from approach A is as high as 1.90. The results clearly show the influence of stress/strain level on the cross-anisotropy of the layered soil. It is also noted that the values of E_v determined from the three approaches are almost the same, while the significant difference is observed between E_h and E_v. In other words, the lower the stress level, the higher the difference in elastic modulus in directions parallel and perpendicular to the layering. As far as the Poisson's ratio is concerned, the lower the stress level, the higher the ratio of ν_{hh} / ν_{hv}.

For another layered soil (#3030), the degree of anisotropy is lower with the ratio of E_h / E_v being approximately 1.3. This series of tests confirms that the layered soil has stronger stiffness in the horizontal direction than that in the vertical direction. It

should be noted that a good consistency with respect to the elastic moduli (E_h and E_v) and Poisson's ratio ν_{hv} determined from the three approaches was achieved. For the other two Poisson's ratios ν_{vh} and ν_{hh} determined from the three approaches, a 10% difference is observed.

Overall, the stiffness difference between the vertical and horizontal directions can be significantly different from one soil to another, depending on soil type. More specifically, for homogeneous and isotropic soils #2004 and #3002, the elastic modulus tends to be direction independent, with the same elastic modulus in the vertical and horizontal directions. For heterogeneous soil #4002, the stiffness in the vertical direction is slightly greater than that in the horizontal direction, with elastic modulus in the vertical direction being approximately 20% higher than that in the horizontal direction. For layered soils #5022 and #3030, the elastic modulus in the horizontal direction is approximately 40% greater than that in the vertical direction owing to the strong varve structure characteristics.

Table 4.2 also compares the soil properties determined by approaches A and B, and C. Generally, a good agreement between the three methods is achieved with respect to the Poisson's ratios. Although the magnitude of the elastic modulus determined by three approaches are slightly different, the ratio of E_h / E_v is consistent. The difference of the elastic modulus obtained from the three methods is attributed to a fact that the stress-strain relation obtained from the tests are non-linear and the data used (stresses and strain increments) is at different strain levels.

Since approach A made use of the least square method to do a linear regression for the tests results, the data selected from all the tests had to be at the same strain level. Otherwise, the elastic properties determined by this approach would not be reasonable due to the significant numerical random errors.

Approach B only manipulated the data from two stress path tests, in which the values for K_0 and K_{v0} were determined when the sample eventually steadily

consolidated along the K_0 and K_{v0} lines. The stresses and strains increments used in Eq. (4-20) had to be selected from the strain level, where the stress state of the sample was at the K_0 and K_{v0} states. Therefore, approach B was not applicable to use the stresses and strains increments selected from the measured data at small stain level for solving elastic properties of soil.

In addition to the K_0 and K_{v0} values defined in method B, Method C further defined two constrain modulus M_{vz} and M_{vx} with clear physical meanings. After all the parameters were determined from measured data (K_0 , K_{v0} , M_{vz} and M_{vx}), the following process to solve the elastic properties was a algebraic operation, which made calculation process more efficient. The data used (stresses and strains increments) were selected in the same range as method B conducted.

Table 4-2 Summary of estimated elastic cross-anisotropic properties

	Soil number	E_h / E_v	ν_{hh} / ν_{vh}	E_v （MPa）	E_h （MPa）	ν_{vh}	ν_{hv}	ν_{hh}
Method A	#2004(60ft)	0.91	0.92	28.51	26.00	0.255	0.232	0.235
Method B	#2004(60ft)	0.92	0.93	39.20	36.10	0.255	0.235	0.245
Method C	#2004(60ft)	0.93	0.95	42.00	40.00	0.255	0.234	0.244
Method A	#3002(15ft)	0.98	0.99	28.20	27.60	0.256	0.253	0.250
Method B	#3002(15ft)	0.96	0.98	29.87	28.70	0.290	0.280	0.285
Method C	#3002(15ft)	0.96	0.98	34.00	32.60	0.290	0.278	0.284
Method A	#4002(30ft)	0.86	0.93	42.68	36.90	0.257	0.222	0.239
Method B	#4002(30ft)	0.80	0.88	54.57	43.00	0.250	0.193	0.220
Method C	#4002(30ft)	0.80	0.88	58.00	46.00	0.250	0.195	0.220
Method A	#5022(81ft)	1.93	1.40	83.30	160.63	0.203	0.391	0.282
Method B	#5022(81ft)	1.44	1.20	83.61	120.21	0.233	0.335	0.280
Method C	#5022(81ft)	1.45	1.21	82.16	119.00	0.230	0.333	0.277
Method A	#3030(91ft)	1.20	1.10	31.00	37.00	0.280	0.340	0.301
Method B	#3030(91ft)	1.30	1.13	33.00	43.00	0.238	0.320	0.270
Method C	#3030(91ft)	1.30	1.15	30.50	40.00	0.240	0.310	0.273

Material properties determined by approach A are compared with those of other researchers' work shown in Table 4-3. The purpose is to demonstrate the applicability of the method. It is difficult to make a direct comparison with respect to the magnitude of material properties and the degree of the anisotropy because the test materials are totally different. All the parameters determined in this study appear to be in a reasonable range, compared to the data of other types of soils. The anisotropy of the soils in this study, evaluated in terms of E_h / E_v and ν_{hh} / ν_{vh} ranges over 0.86-1.93 and 0.92-1.4, respectively.

Generally, the elastic modulus determined by the current study is lower than the value determined by others. One of the reasons for this difference could be related to the fact that the elastic stiffness is a function of stress state and strain level; with the increase of the strain level, the corresponding stiffness of soil decreases. (Clayton, 2011). The strain level investigated in this study was in the range of 0.1-1.0%., compared to that of other studies which had the strain in the range of 0.001%-0.01%. Another possible reason for the discrepancy is that the majority of the researchers adopted dynamic cyclic loading approach rather than static loading for the tests, which was used in this study. In the dynamic cyclic loading approach, the recoverable elastic strain is measured more accurately without the interference of the irrecoverable plastic strain, which contributes to a higher elastic modulus.

It also needs to be mentioned that disturbance produced from sample preparation or experimental work itself would bring some effects to the final results even though the soil specimen is assumed to be undisturbed. The soil stiffness determined in the laboratory is expected to be smaller than the actual stiffness of soil in-situ (Clayton, 2011).

Table 4-3 Comparison of results

Soil number	Description	E_h / E_v	ν_{hh} / ν_{vh}	E_v （MPa）	E_h （MPa）	ν_{vh}	ν_{hv}	ν_{hh}	Strain level (%)
#2004(60ft)	Grey sand	0.91	0.92	28.51	26.00	0.255	0.232	0.235	0.1~1
#3002(15ft)	sandy silt	0.98	0.99	28.20	27.60	0.256	0.253	0.250	0.1~1
#4002(30ft)	Silty clay	0.86	0.93	42.86	36.90	0.257	0.222	0.239	0.1~1
#5022 (85ft)	Layered soil	1.93	1.40	83.30	160.63	0.203	0.391	0.282	0.1~1
#3030(91ft)	Layered soil	1.20	1.10	31.00	37.00	0.280	0.340	0.301	0.1~1
Liu Ying （2010）	Granular material	0.16	0.40	132.60	20.70	0.660		0.260	0.01~0.1
Nishimura （2014）	Ma13(Marine Deposit)	1.61	0.16	12.30	19.80	0.063	0.010	0.110	0.001~0.01
	Ma12(Marine Deposit)	1.88	-4.00	110.00	207.60	0.030	0.056	0.120	0.001~0.01
	Ma12R(MarineDeposit)	1.92	-1.42	58.20	111.50	0.014	0.027	-0.02	0.001~0.01
Kuwano (2002)	Ham river sand	0.54	0.20	520.00	280.00	0.350	0.190	0.070	0.001~0.01
Ling (2000)	Gault clay	1.00		550p'	2186p'	0		-0.04	0.001~1
Stokoe (1991)	M-dense mortar sand	1.25	0.72	242.90	304.00	0.201	0.251	0.145	0.001~1
Bellotti (1996)	Dry Ticino sand	1.21	0.97	287.90	349.40	0.177	0.215	0.172	0.001~1
Gaspare(2007b)	Bender element triaxial	1.95	-0.20	122.00	238.00	0.100	0.710	-0.02	0~0.001
(London Clay)	Static HCA Tests	2.11	-0.76	112.00	236.00	0.250	0.490	-0.19	0.001~0.1

4.4 Experimental error analysis

4.4.1 The influence of the non-uniform ε_r in layered soil specimen

As indicated previously, the varve structure of layered soil #6011; as shown in Figure 4-10 (a) and (b), contributed to strong anisotropy with respect to the average elastic soil properties of this soil. As illustrated in Figure 4-10 (c), such structural characteristics may result in non-uniform lateral deformation of the specimen in triaxial tests with flexible boundaries, including the K_0-test in the rigid cell used in this study. This is because the lateral deformation of the specimen was not controlled in the K_0-test directly. Instead, the zero lateral strain was achieved by ensuring that the volumetric strain and vertical strain are the same since $\Delta\varepsilon_h = \left(\Delta\varepsilon_{vol} - \Delta\varepsilon_v\right)/2$. For a layered soil specimen, the condition $\Delta\varepsilon_{vol} = \Delta\varepsilon_v$ is satisfied on the average so that

$$\Delta V = \frac{1}{4}\pi D^2 \Delta u_a \tag{4-29}$$

and

$$\pi D \sum_{i=1}^{n} h_i \Delta u_{ri} = 0 \tag{4-30}$$

where D, ΔV and Δu_a are the diameter, the total volume change and the total axial deformation of the specimen, h_i and Δu_{ri} are the thickness and the radial (lateral) deformation of the *i*-th layer of the specimen. In other words, $\Delta \varepsilon_{vol} = \Delta \varepsilon_v$ on the average does not guarantee zero lateral deformation of each individual layer; as illustrated in Figure 4-10 (c). The local non-zero lateral strain in different constituent layers would have had an influence on the results.

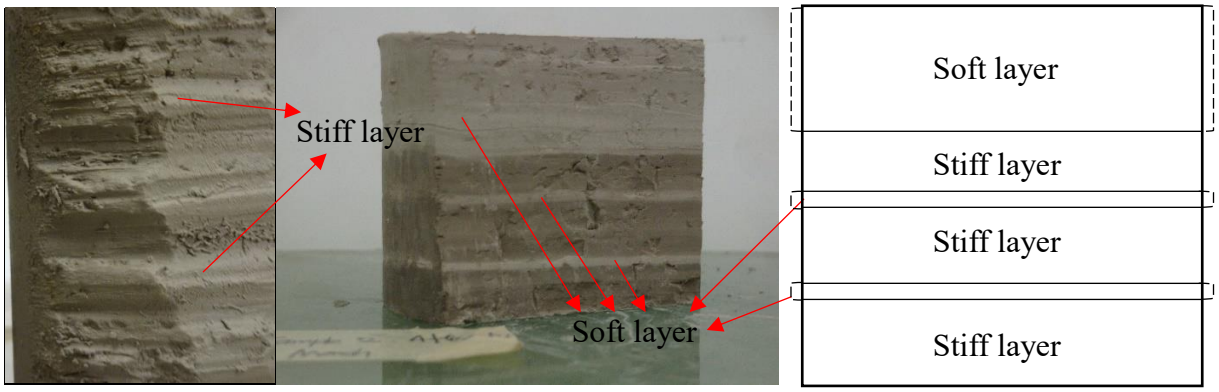

(a) (b) (c)

Figure 4-10 Composition of the layered soil specimen #6011

Figure 4-11 compares the diameter change of the layered soil specimen of # 6011 before and after the K_0-test. As shown in Figure 4-12 (b), the lateral deformation of the specimen was non-uniform, since the change of the diameter in each individual layer after the K_0-test was slightly different.

(a) Before K_0-test (b) After K_0-test

Figure 4-11 Diameter change of the soil specimen #6011 before and after the tests

4.4.2 Influences of varve structure in layered soil

As can be observed from Figures 3-7 and 3-8, the layered soil had strong varve structure characteristic, compared to the homogeneous soil. An equivalent homogeneous approach was adopted to deal with the complexity of the multilayered characteristic when conducting the experimental investigation as this study was more interested in the average response of soil. However, when a thick or weak silt layer with approximately 20 mm thickness exists in a multilayered system, for example, specimen #1004 shown in Figure 3-8 (b), such layer dominates the overall behaviour of the multilayered medium and influences the K_0-test result.

By comparing the effective stress paths in the loading stage of the K_0-test for homogeneous soil #2004 and layered soil #1004 in Figures 4-12 and 4-13, we observe that the stress trajectory of the layered soil specimen is not as smooth as that of the homogenous soil specimen, which could be attributed to the change of the internal structure due to different characteristic of constituent layers or the non-uniform deformation on the outer boundary. The unsmooth stress path, in turn, confirms that a homogeneous approach is only applicable when the thickness of each constituent layer must be much smaller than the characteristic length of the multilayered medium.

During the unloading stage for the K_0-test on homogeneous soil #2004, the measured horizontal effective increases with the decrease of the vertical effective stress.

This is consistent with the conclusion drawn by Mayne (1972) that the K_0-value of the over-consolidated soil increases with the increase of over-consolidated ratio; as illustrated in Eq. (2-25). For the layered soil #1004, however, the measured horizontal effective stress during the unloading process almost holds constant with the decrease of the vertical effective stress. The different response of the layered soil #2004 during the unloading processes could also be attributed to the influence of the strong varve structure.

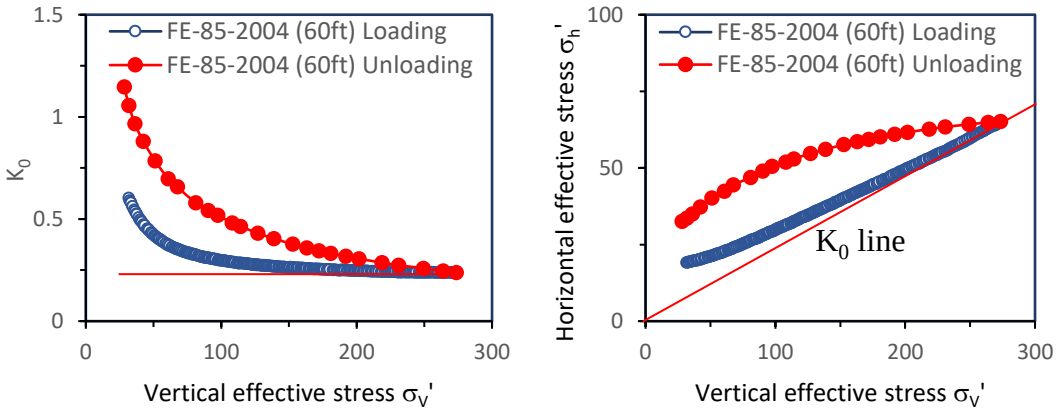

Figure 4-12 K_0-compression test results for the specimen #2004

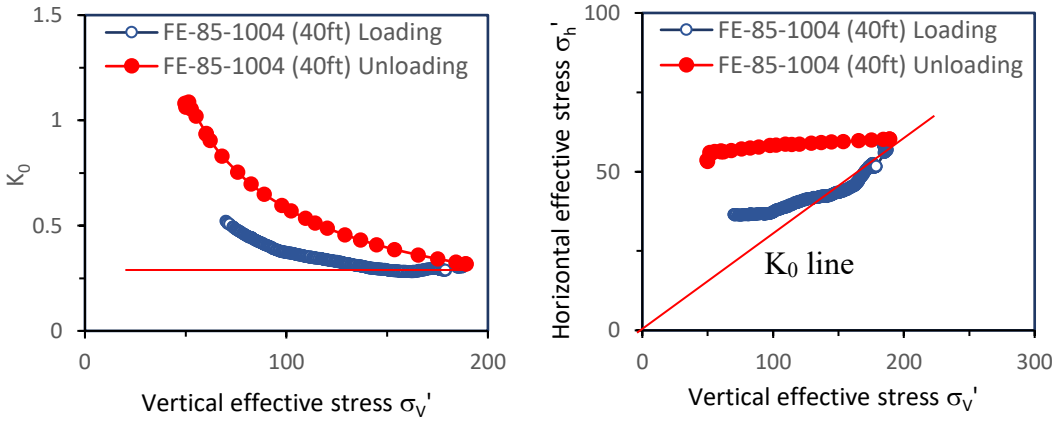

Figure 4-13 K_0-compression test results for the specimen #1004

Chapter 5 EQUIVALENT ELASTIC PROPERTIES OF MULTILAYERED SOIL: NUMERICAL MODELING AND THEORETICAL ANALYSIS

This chapter presents the numerical modeling of K_0-test using FEM, in which two strategies are used to determine the average strain of the elements on the lateral boundary. In addition, this chapter provides a theoretical homogenisation approach to determine the equivalent cross-anisotropic elastic properties for a multilayered medium. The applicability of the approach is examined by analyzing a multilayered medium with two constituent materials that are both isotropic. A parameter sensitivity analysis is performed to investigate the dependence of the equivalent cross-anisotropic properties on the Poisson's ratio and elastic modulus of each constituent layer in a multilayered medium.

5.1 A three parameters cross-anisotropic constitutive model

The stress-strain relation of a linearly isotropic material can be expressed as

$$\begin{pmatrix} \Delta\sigma_{xx} \\ \Delta\sigma_{yy} \\ \Delta\sigma_{zz} \\ \Delta\tau_{xy} \\ \Delta\tau_{xz} \\ \Delta\tau_{yz} \end{pmatrix} = \begin{pmatrix} \lambda+2\mu & \lambda & \lambda & & & \\ \lambda & \lambda+2\mu & \lambda & & & \\ \lambda & \lambda & \lambda+2\mu & & & \\ & & & \mu & & \\ & & & & \mu & \\ & & & & & \mu \end{pmatrix} \begin{pmatrix} \Delta\varepsilon_{xx} \\ \Delta\varepsilon_{yy} \\ \Delta\varepsilon_{zz} \\ \Delta\gamma_{xy} \\ \Delta\gamma_{xz} \\ \Delta\gamma_{yz} \end{pmatrix} \tag{5-1}$$

in which λ and μ are Lame constants, which can be related to the elastic modulus E and the Poisson's ratio ν via $\lambda = \dfrac{E\nu}{(1+\nu)(1-2\nu)}$ and $\mu = G = \dfrac{E}{2(1+\nu)}$.

For a cross-anisotropic material that is isotropic in the horizontal plane (i.e., the ***x-y*** plane), Graham and Houlsby (1983) introduced an anisotropic factor α as a measure of the degree of anisotropy. The factor α is defined as the ratio of direct stiffness in

the horizontal direction and the vertical direction; i.e., $\alpha = \sqrt{E_h / E_v} = \nu_{hh} / \nu_{vh}$.

Let $E_v = E^*$ and $\nu_{vh} = \nu^*$, the other parameters can be expressed as a function of E^*, ν^* and α, such as $E_h = \alpha^2 E^*$, $\nu_{hh} = \alpha\nu^*$, and $\nu_{hv} = \alpha^2\nu^*$. Therefore, the stress-strain relation of a cross-anisotropic elastic material is expressed as

$$\begin{pmatrix} \Delta\sigma_{xx} \\ \Delta\sigma_{yy} \\ \Delta\sigma_{zz} \\ \Delta\tau_{xy} \\ \Delta\tau_{xz} \\ \Delta\tau_{yz} \end{pmatrix} = \frac{E^*}{(1+\nu^*)(1-2\nu^*)} \begin{pmatrix} \alpha^2(1-\nu^*) & \alpha^2\nu^* & \alpha\nu^* & & & \\ \alpha^2\nu^* & \alpha^2(1-\nu^*) & \alpha\nu^* & & & \\ \alpha\nu^* & \alpha\nu^* & 1-\nu^* & & & \\ & & & \frac{\alpha^2(1-2\nu^*)}{2} & & \\ & & & & \frac{\alpha(1-2\nu^*)}{2} & \\ & & & & & \frac{\alpha(1-2\nu^*)}{2} \end{pmatrix} \begin{pmatrix} \Delta\varepsilon_{xx} \\ \Delta\varepsilon_{yy} \\ \Delta\varepsilon_{zz} \\ \Delta\gamma_{xy} \\ \Delta\gamma_{xz} \\ \Delta\gamma_{yz} \end{pmatrix} \quad (5\text{-}2)$$

where the ***x***- and ***y***-axes correspond to two orthogonal directions in the horizontal plane in which the material is isotropic, and ***z***-axis is in the vertical direction.

An axisymmetric problem in terms of both the geometry and loading can be simplified to a two-dimensional description. Examples of the axisymmetric problem include a triaxial compression test of a cylindrical soil sample and the deformation of a semi-infinite half space subjected to a uniformly distributed load on a circular area (e.g., a circular footing). For an axisymmetric problem, the stress-strain relation can be alternatively expressed as

$$\begin{pmatrix} \Delta\sigma_r \\ \Delta\sigma_z \\ \Delta\tau_{rz} \\ \Delta\sigma_\theta \end{pmatrix} = \frac{E^*}{(1+\nu^*)(1-2\nu^*)} \begin{pmatrix} \alpha^2(1-\nu^*) & \alpha\nu^* & 0 & \alpha^2\nu^* \\ \alpha\nu^* & 1-\nu^* & 0 & \alpha\nu^* \\ 0 & 0 & \frac{\alpha(1-2\nu^*)}{2} & 0 \\ \alpha^2\nu^* & \alpha\nu^* & 0 & \alpha^2(1-\nu^*) \end{pmatrix} \begin{pmatrix} \Delta\varepsilon_r \\ \Delta\varepsilon_z \\ \Delta\gamma_{rz} \\ \Delta\varepsilon_\theta \end{pmatrix} \quad (5\text{-}3)$$

where r, z, θ indicate the radial, longitudinal, circumferential directions, respectively. This constitutive equation has been introduced into a basic FEM code. It should be noted that the r- and θ- axis are in the horizontal plane while z- axis is in the vertical direction; as shown in Figure 5-1.

When carrying out FEM simulations for the axisymmetric problem, the axisymmetric system is often discretized using quadrilateral torus elements because they can be used to simulate complex surfaces and are simple to work with in FEM. The vertical cross section of the quadrilateral torus is shown in Figure 5-1.

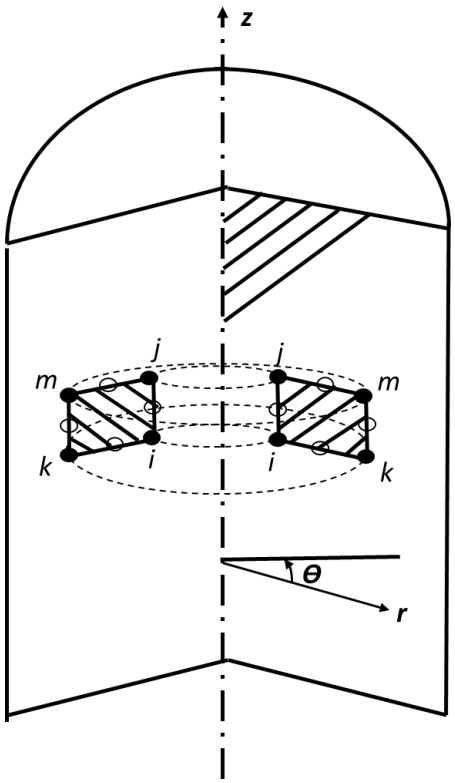

Figure 5-1 An axial-symmetrical triangular torus element

5.2 FEM simulation for K_0-test.

5.2.1 Numerical process

In this section, the experimental process to determine the K_0-values of soils using a rigid cell was simulated by FEM. More specifically, the experimental K_0-test was considered to be an axisymmetric problem since the geometry of the sample and loading were axial symmetric with respect to the vertical direction. The modified three-parameter anisotropic constitutive equations were adopted. All equivalent elastic cross-anisotropic properties of a multilayered medium determined by the proposed homogenous experimental approach were adopted to conduct numerical simulations.

Soil samples with the same dimension as that in the actual specimen used in laboratory tests were discretized with 8-node quadrilateral elements. For basic FEM discretization and assembly processes, the reader is referred to Zienkiewicz (2005). The geometry of the specimen and the finite element mesh are illustrated in Figure 5-2. Roller boundary condition was considered along the interface between the bottom edge of the sample and the base of the triaxial cell since the contact surface between them was considered to be frictionless.

Three stages were considered when numerically simulating the K_0-test; as illustrated in Figure 5-2. In stage I, the soil sample was loaded in the vertical direction step-by-step by the desired surface traction q_1 that was equal to the applied axial effective stress in the experimental K_0-test while applying a small pressure q_2 (1 kPa) to the outer boundary of the sample in the lateral direction. In stage II, the soil sample tended to deform in the vertical and lateral directions due to the applied vertical pressure q_1. The lateral deformation of the sample due to the applied loading was calculated. In stage III, the lateral deformation of the sample was eliminated by applying extra lateral pressure q_3 to push the sample back to its initial radius. The extra pressure applied in the horizontal direction in stage III was equivalent to the lateral pressure required to keep zero lateral deformation of the sample. The numerical K_0-value of the sample was determined as $K_{0,numerical} = q_3 / q_1$.

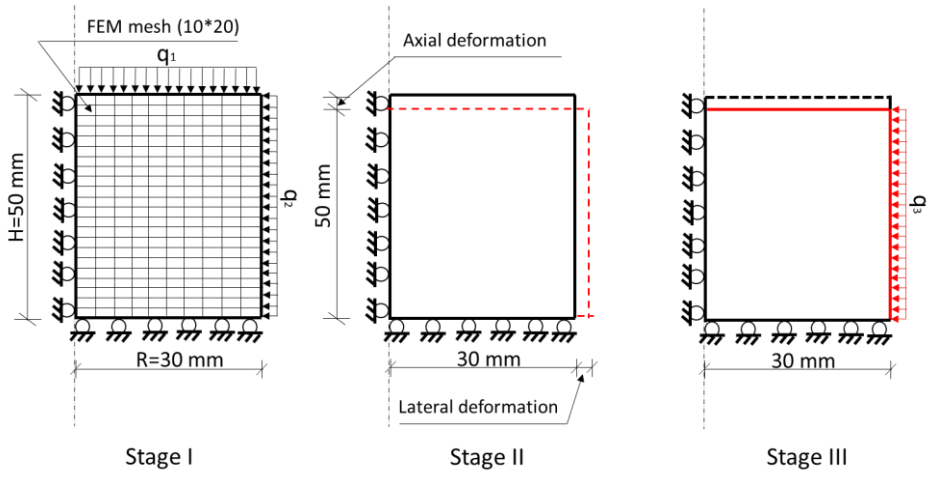

Figure 5-2 K_0-test numerical simulation process

Two methods were used to determine the numerical K_0-value of multilayered soils. In Method 1, the multilayered soil sample was considered as an equivalent homogeneous cross-anisotropic elastic material. In Method 2, the multilayered soil sample was considered as an assembly of layers of isotropic material with different elastic constants.

In Method 1, the equivalent homogenous cross-anisotropic elastic properties of test soils used in numerical simulations are summarized in Table 5-1, which are the same as those determined by approach A in the experimental study.

Table 5-1 Cross-anisotropic elastic properties of test soils

Soil number	$\alpha = E_h / E_v$	E_v （MPa）	E_h （MPa）	ν_{vh}	ν_{hv}	ν_{hh}
#2004(60ft)	0.91	28.51	26.00	0.255	0.232	0.235
#3002(15ft)	0.96	29.87	28.70	0.290	0.280	0.285
#4002(30ft)	0.86	42.68	36.90	0.257	0.222	0.239
#5022(81ft)	1.44	83.61	120.21	0.233	0.335	0.280
#3030(91ft)	1.20	31.00	37.00	0.280	0.340	0.301

Table 5-2 compares the numerical K_0-values obtained from the Method 1 for different soils when using the isotropic and anisotropic constitutive models with the experimental K_0-values and theoretical K_0-values calculated by using Eq. (4-21), respectively. A good agreement among the theoretical, numerical and experimental results is achieved, especially for soils #2004 and #3002 that are weekly anisotropic. For the two layered soils #5022 and #3030, consistent results are obtained between theoretical analysis and experimental data. However, the numerical K_0-values are much lower than those determined by theoretical and experimental approaches. On the other hand, for the heterogeneous soil #4002 and the layered soil #5022, a significant difference between the experimental K_0-values and the numerical K_0-values is observed. This was attributed to the inaccurate equivalent elastic properties of the soils determined from the experimental study. The discrepancy also reflects the nature of

layered soil and the fact that care needs to be taken when applying the equivalent cross-anisotropic homogenization approach to the layered soils. However, it is obvious that the anisotropic model gives better numerical K_0-values than the isotropic model, especially for the layered soil.

Table 5-2 Comparison between experimental K_0 values and numerical K_0 values

Soil Type	Theoretical K_0-value	Experimental K_0-value	Numerical K_0-value		Relative error (%)	
			Isotropic	Anisotropic	Isotropic	Anisotropic
#2004	0.323	0.330	0.344	0.327	4.2	0.9
#3002	0.392	0.390	0.410	0.400	5.1	2.6
#4002	0.292	0.250	0.346	0.320	38.4	28.0
#5022	0.465	0.460	0.304	0.365	33.9	20.7
#3030	0.486	0.460	0.390	0.425	15.2	7.6

5.2.2 Approach A to determine average strain on the lateral boundary

As introduced in the previous section, when performing FEM simulations for the K_0-test during stage II, the average lateral strain of sample on the outer boundary had to be calculated. For homogeneous soils in Method 1, the lateral displacement pattern on the outer boundary was uniform, which makes the calculation process straightforward. However, in Method 2 for layered soils with different elastic material properties for each layer, a non-uniform lateral displacement pattern on the outer boundary was found; as demonstrated in Figure 5-3 via a numerical simulation.

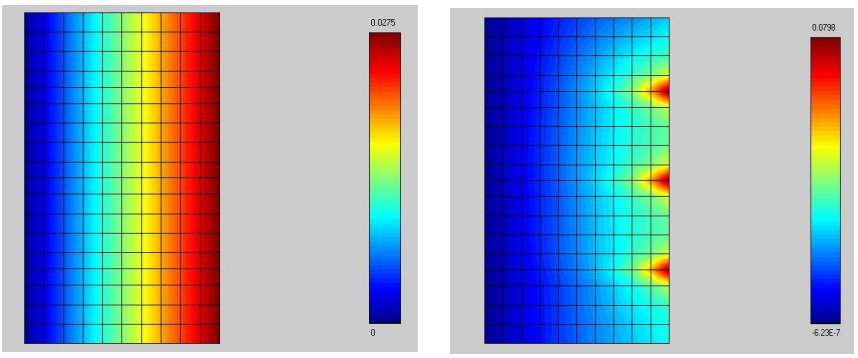

(a) Homogeneous soil (Method 1) (b) Layered soil (Method 2)

Figure 5-3 Comparison of the lateral displacement patterns

As stated previously, in Method 1, the layered soil was regarded as an equivalent homogeneous soil with equivalent cross-anisotropic elastic properties determined from laboratory tests. The K_0-value of the layered soil is then considered the same as that of the equivalent homogeneous cross-anisotropic soil. This approach gives reasonable results when comparing the numerical K_0-values to the experimental K_0-values. However, it should be mentioned that the limitation of the proposed experimental approach (K_0-test) for layered soils is that the local lateral strain in each layer could be non-zero although the average lateral strain of the specimen was close to zero. Similarly, for a numerical K_0-test, in order to better capture the characteristics of layered soils (i.e., different elastic properties in each constituent layer), average strain quadrilateral elements were used for numerical calculation (Stolle, 1992).

Stolle (1992) described an average strain gradient strategy, which allowed evaluating the average strain within an element. The average lateral strain on the boundary can be evaluated with the help of Gauss's theorem. Let us start by considering the element stiffness matrix equation for a two-dimensional problem

$$\mathbf{K} = t \int_A \mathbf{B}^{\mathrm{T}}\mathbf{D}\mathbf{B}\,\mathrm{d}A \tag{5-4}$$

where $\mathbf{B}$ is the usual strain-displacement matrix, $\mathbf{D}$ is the constitutive matrix, A represents the area over which integration takes place and t is the element thickness. In FEM simulations, Eq. (5-4) can be rewritten as

$$\mathbf{K} = t \sum_i \left(\bar{\mathbf{B}}_{\mathbf{i}}^{\mathrm{T}}\mathbf{D}\bar{\mathbf{B}}_{\mathbf{i}}\right) A_i \tag{5-5}$$

where $\bar{\mathbf{B}}_\mathbf{i}$ is constant over element subdomain A_i; that is, the strain is constant over A_i. The average strain $\bar{\varepsilon}_{kj}$ of elements subdomain A_i can be evaluated with the help of Gauss's theorem

$$\bar{\varepsilon}_{kj} = \frac{1}{2A_i}\int_{A_i}(u_{k,j}+u_{j,k})\,\mathrm{d}A = \frac{1}{2A_i}\oint_{S_i}(u_k n_j + u_j n_k)\,\mathrm{dS} \tag{5-6}$$

where the index notation is applied with u_k representing the displacement and n_j the direction cosine associated with the line integral along S_i. Repeated indices do not imply summation here.

For the axial-symmetric K_0-test explored in this study, the average strain on the lateral boundary can be determined as

$$\bar{\varepsilon}_x = \frac{1}{2V}\oint_{S_i} u_x n_x \mathrm{dS} = \frac{\pi}{V}\int u_x n_x |J| r\ \mathrm{ds} \tag{5-7}$$

We replace Eq. (5-7) with the Gauss's integration scheme by substituting $n_x = \frac{\Delta y}{l}$ and $|J| = \frac{l}{2}$ as

$$\begin{aligned}\bar{\varepsilon}_x &= \frac{\pi}{V}\sum_{j=1}^{3} u_x n_x r |J| W_j \\ &= \frac{\pi}{V}\sum_{i=1}^{3}\sum_{j=1}^{3}(u_{xi}N_{js})\frac{\Delta y}{2}(X_j N_{js})W_j\end{aligned} \tag{5-8}$$

where $|J|$ is the determinant of Jacobian transformation matrix, l is the length of an element, V is the total volume of the domain, u_{xi} is the nodal displacement in the *x*-direction of the element on the boundary at node *i*, N_{js} is the shape function of the boundary element at integration point *j*, Δy is the length of element on the boundary in the *y*-direction, X_j is the global coordinate of integration point *j*, N_{js} is the shape

function at integration point *j*, and W_j is the weighting factor at integration point *j*.

5.2.3 Approach B to determine the average lateral displacement

This is an alternative approach to numerically calculate the average lateral strain of layered soils on the outer boundary when conducting the K_0-test using Method 2. This scheme averages the radial displacement in different layers along the outer boundary by using a weighting factor, which is a sum of the height of all elements on the boundary. The mathematical expression is

$$\bar{u}_x = \frac{\int_H u dy}{\sum_{i=1}^{n} h_i} \tag{5-9}$$

where H is the total height of the sample, u is the lateral displacement, n is the total number of layers, h_i is the thickness of layer ***i***.

The Integral in Eq. (5-9) is evaluated numerically by using the Gauss integration scheme with three Gauss integration points. After obtaining the average lateral displacement $\bar{u}_x$, the average lateral strain is then determined as $\bar{\varepsilon}_x = \frac{\bar{u}_x}{R}$, in which R is the radius of the sample.

Approach B has clear physical meaning and is easy to understand, compared to approach A with more complex mathematics. However, to confirm its applicability for layered materials, a comparison was made between these two approaches. For a selected layered material with the same material properties, both approaches were used to calculate the average lateral strain of the sample when conducting the numerical K_0-test at stage I. After the lateral strain of the sample was calculated by two approaches, the numerical K_0-tests proceeded to the next two stages. Table 5-2 compares the numerical K_0-values based on the average lateral strain calculated by the two approaches. The agreement between the calculated K_0-values using the two approaches

confirms that approach B is also applicable to determine the lateral strain of a layered sample when conducting a numerical K_0-test.

Table 5-3 comparisons between approach A and B

Soil Type	Numerical K_0-value	
	Approach A	Approach B
#2004	0.340	0.335
#3002	0.410	0.408
#4002	0.350	0.348
#5022	0.300	0.300
#3030	0.392	0.390
#6011	0.330	0.330

5.3 A theoretical equivalent homogenisation approach for the multilayered medium

In the previous section, the layered materials were considered in Method 1 as equivalent homogeneous cross-anisotropic materials, and numerical simulations of K_0-tests were conducted on homogeneous equivalent soils to compare with the experimental K_0-tests. However, approximately 20 percent difference was observed when comparing the numerical K_0-values to the experimental K_0-values. This discrepancy is related to the equivalent cross-anisotropic elastic properties used in numerical simulations. It is expected that improved determination of the equivalent cross-anisotropic elastic properties may provide better results for the numerically calculated K_0-values.

To better capture the equivalent material characteristics of a multilayered soil, especially the elastic properties at small strain levels, a physically meaningful homogenization theoretical approach is presented in this section to determine the elastic properties of the equivalent material. This approach, which follows the work of Salamon (1968), makes use of the Reuss and the Voigt models, and conducts a theoretical analysis for two special cases of deformation; i.e.,K_0-compression test with $\varepsilon_{xx} = \varepsilon_{yy} = 0$ and plane strain compression test with $\varepsilon_{yy} = 0$ and $\sigma_{zz} = 0$.

5.3.1 K_0-compression test with $\varepsilon_{xx} = \varepsilon_{yy} = 0$

Let us first examine a multilayered system that is constrained in the lateral direction with $\varepsilon_{xx} = \varepsilon_{yy}$=0 and loaded in the vertical direction by $\sigma_{zz} = \sigma_v$; as shown in Figure 5-4. Each layer is isotropic with the directional independent elastic modulus E_i and the Poisson's ratio ν_i. By applying the Voigt model's assumption that all layers have the same vertical stress $\sigma_{zzi} = \sigma_v$, the lateral stresses of different layers are different owing to the zero lateral strain $\varepsilon_{xxi} = \varepsilon_{yyi}$=0. Since the material in each constituent layer is isotropic and linearly elastic, the lateral stresses in the ***x***-and ***y***-directions in the *i*-th layer must be equal such that ($\sigma_{xxi} = \sigma_{yyi} = \sigma_{hi}$).

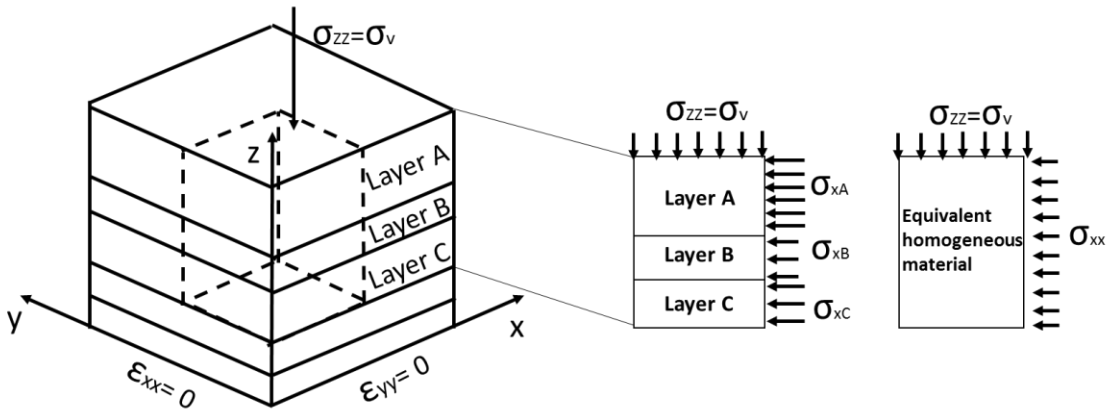

Figure 5-4 K_0 compression of a layered material

Applying the lateral constraint to Eq. (4-2) for an ideal isotropic material, the lateral stress in layer ***i*** is determined as

$$\sigma_{hi} = \frac{\nu_i}{1-\nu_i}\sigma_v \tag{5-10}$$

For an equivalent homogeneous, cross-anisotropic elastic material, the lateral stress can be calculated from Eq. (4-21) as

$$\sigma_h = \frac{\nu_{hv}}{1-\nu_{hh}}\sigma_v \tag{5-11}$$

For the layered soil sample, the equilibrium condition in the lateral directions requires $\sigma_h = \sum \varphi_i \sigma_{hi}$, which yields

$$\frac{\nu_{hv}}{1-\nu_{hh}} = \sum \frac{\varphi_i \nu_i}{1-\nu_i} \tag{5-12}$$

This equation builds the connection between Poisson's ratios of the equivalent cross-anisotropic elastic material, and the Poisson's ratio of each layer using the weighting factor φ_i that is the volume fraction or normalized thickness of layer ***i***. Eq. (5-12) can also be used to determine the average earth pressure coefficient K_0 of layered soil. Referring to Eq. (4-21) and applying Eq. (5-12), one has

$$K_0 = \frac{\sigma_h}{\sigma_v} = \frac{\nu_{hv}}{1-\nu_{hh}} = \sum \frac{\varphi_i \nu_i}{1-\nu_i} = \sum \varphi_i K_{0i} \tag{5-13}$$

where $K_{0i} = \frac{\nu_i}{1-\nu_i}$ is the coefficient of earth pressure at-rest K_0 of constituent soil layer ***i***.

As derived previously in Eq. (4-22), the constrained elastic modulus of an equivalent cross-anisotropic material under the K_0-condition (as illustrated in Figure 5-4) is expressed as

$$\frac{1}{M_{vz}} = \frac{1}{E_v} - \frac{2\nu_{hv}^2}{(1-\nu_{hh})E_h} \tag{5-14}$$

On the other hand, the constrained elastic modulus of the isotropic material in each individual layer is

$$\frac{1}{M_{vzi}} = \frac{1}{E_i} - \frac{2\nu_i^2}{(1-\nu_i)E_i} \tag{5-15}$$

Applying the rule of mixture adopted in the Reuss model that is in the form of

$$\frac{1}{M_{vz}} = \sum \frac{\varphi_i}{M_{vzi}} \tag{5-16}$$

we have,

$$\frac{1}{E_v}-\frac{2\nu_{hv}^2}{\left(1-\nu_{hh}\right)E_h}=\sum\varphi_i\left(\frac{1}{E_i}-\frac{2\nu_i^2}{E_i\left(1-\nu_i\right)}\right) \tag{5-17}$$

5.3.2 Plane strain compression with $\varepsilon_{yy}=0$, $\sigma_{zz}=0$ and $\Delta\sigma_{xx}\neq 0$

The second case to examine is a layered system that experiences plane strain compression with $\varepsilon_{yyi}=\varepsilon_{yy}=0,$ and $\sigma_{zz}=\sigma_v=0$; as illustrated in Figure 5-5.

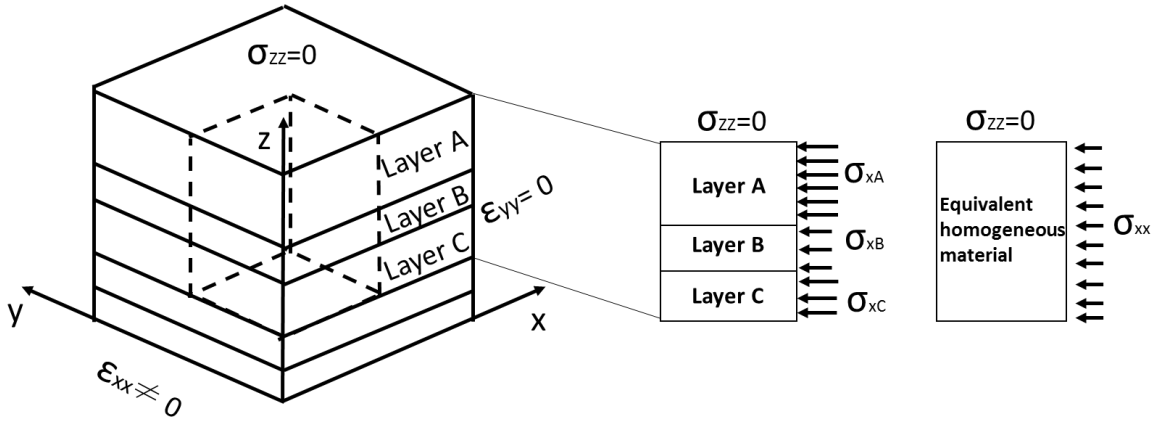

Figure 5-5 Plane-strain compression of a layered material

For the equivalent cross-anisotropic material, when applying $\varepsilon_{yyi}=\varepsilon_{yy}=0$ and $\sigma_v=0$ to the general stress-strain relation in Eq. (4-5), one has

$$\varepsilon_{xx}=\frac{\sigma_{xx}}{E_h}-\nu_{hh}\frac{\sigma_{yy}}{E_h} \tag{5-18}$$

$$\varepsilon_{yy}=-\frac{\nu_{hh}\sigma_{xx}}{E_h}+\frac{\sigma_{yy}}{E_h}=0 \tag{5-19}$$

where σ_{xx} and σ_{yy} are the average stresses in the equivalent homogeneous material. The following expressions can be obtained from Eqs. (5-18) and (5-19) as

$$\sigma_{xx} = \frac{E_h}{1-\nu_{hh}^2}\varepsilon_{xx},\ \sigma_{yy} = \nu_{hh}\sigma_{xx} \tag{5-20}$$

On the other hand, for an individual isotropic material layer, the lateral stress is determined as

$$\sigma_{xxi} = \frac{E_i}{1-\nu_i^2}\varepsilon_{xxi},\ \sigma_{yyi} = \nu_i\sigma_{xxi} \tag{5-21}$$

in which the lateral strain of each layer is equal to the average lateral strain of the equivalent material ($\varepsilon_{xxi} = \varepsilon_{xx}$). Owing to the different material properties, the constraint in the lateral direction $\varepsilon_{xxi} = \varepsilon_{xx}$ results in different lateral stresses in each constituent layer. The equilibrium equation in the lateral direction yields

$$\sigma_{xx} = \sum \varphi_i \sigma_{xxi},\ \sigma_{yy} = \sum \varphi_i \sigma_{yyi} \tag{5-22}$$

which is the same as that in the Voigt model. Substituting Eqs. (5-21) and (5-22) into Eq. (5-20), the following equations are obtained

$$\frac{E_h}{1-\nu_{hh}^2} = \sum \frac{\varphi_i E_i}{1-\nu_i^2},\ \frac{E_h \nu_{hh}}{1-\nu_{hh}^2} = \sum \frac{\varphi_i E_i \nu_i}{1-\nu_i^2} \tag{5-23}$$

It follows that

$$E_h = (1-\nu_{hh}^2)\sum \frac{\varphi_i E_i}{1-\nu_i^2},\quad \nu_{hh} = \left(\sum \frac{\varphi_i \nu_i E_i}{1-\nu_i^2}\right)\left(\sum \frac{\varphi_i E_i}{1-\nu_i^2}\right)^{-1} \tag{5-24}$$

Eq. (5-23) can be alternatively obtained by making use of the Voigt model for the elastic modulus in the ***x***-direction. More specifically, according to Eqs. (5-20) and (5-21), for this specific plane strain condition with $\varepsilon_{yyi} = \varepsilon_{yy} = 0$ and $\sigma_{zz} = 0$, the elastic modulus in the ***x***-direction for the equivalent homogeneous material and each individual layer are

$$\bar{E}_x = \frac{\sigma_{xx}}{\varepsilon_{xx}} = \frac{E_h}{1-\nu_{hh}^2},\ \bar{E}_{xi} = \frac{\sigma_{xxi}}{\varepsilon_{xxi}} = \frac{E_i}{1-\nu_i^2} \tag{5-25}$$

After applying $\bar{E}_x = \varphi_i \bar{E}_{xi}$, Eq. (5-23) is recovered.

Another parameter ν_{vh} can be easily determined by invoking the symmetrical constraint of the constitutive matrix for a cross-anisotropic material, which is given in Eq. (2-4) as $\nu_{vh}=\left(E_v / E_h\right)\nu_{hv}$.

In summary, the above presentation makes use of the Voigt and the Reuss models to develop a homogenisation approach to determine the equivalent elastic properties of a layered system composed of isotropic constituent layers. By investigating the behaviour of two testing configurations (i.e., the K_0-compression and the plane-strain compression), four independent elastic properties of the equivalent cross-anisotropic material can be connected to the isotropic elastic properties of each constituent layer as

$$\begin{aligned}
&\nu_{hh}=\frac{\sum\frac{\varphi_i\nu_i E_i}{1-\nu_i^2}}{\sum\frac{\varphi_i E_i}{1-\nu_i^2}}, \quad \nu_{hv}=\left(1-\nu_{hh}\right)\sum\frac{\varphi_i\nu_i}{1-\nu_i}\\
&E_h=\left(1-\nu_{hh}^2\right)\sum\frac{\varphi_i E_i}{1-\nu_i^2}, \quad \frac{1}{E_v}=\sum\frac{\varphi_i}{E_i}\left(1-\frac{2\nu_i^2}{1-\nu_i}\right)+\frac{2\nu_{hv}^2}{\left(1-\nu_{hh}\right)E_h} \qquad (5\text{-}26)\\
&\nu_{vh}=\left(E_v / E_h\right)\nu_{hv}
\end{aligned}$$

The remaining shear moduli of equivalent materials (G_{hh}, G_{hv}, and G_{vh}) are not considered in this study. The expressions in Eq. (5-26) show that if the elastic material properties and the volume fraction of each isotropic constituent material are given, the cross-anisotropic material properties of the homogeneous medium that is equivalent to the layered material system can be determined theoretically. Once again it must be stressed that this method is only applicable when the thickness of each layer is small, compared to the overall thickness of a sample.

Guo and Stolle (2016) explored the special features of the equivalent homogenized medium by examining several special cases in terms of the elastic properties of each individual layer. They found that the expression for the cross-anisotropic properties of the equivalent medium can be simplified, and is different from the regular cross-anisotropic medium. More specifically, it was found that the equivalent material has only three elastic constants when the Poisson's ratio of all layers are equal, while the

general cross-anisotropic material has five. Moreover, if the elastic modulus of all layers were the same, the equivalent medium would have four independent elastic constants. These special features reveal that although a multilayered medium with isotropic constituent layers can be considered as an equivalent homogeneous cross-anisotropic material, it is different from a 'general' cross-anisotropic material, and the cross-anisotropic properties of the equivalent material are more restrictive than those for the 'general' cross-anisotropic material.

5.4 Multilayered medium with two constituent materials

The analyses in the last section present equations to determine the cross-anisotropic elastic properties of the equivalent material, given that the elastic properties and the volume fraction of each isotropic constituent material. This section presents a parametric study on a multilayered medium with two constituent materials that are both isotropic to demonstrate the influence of individual layer properties on the equivalent material properties.

5.4.1 Equivalent cross-anisotropic elastic properties

Referring to Eq. (5-26), the equivalent elastic properties of a layered medium composed of two isotropic constituent materials are summarized as

$$
\begin{aligned}
&\nu_{hh}=\frac{\frac{E_1}{E_2}\varphi_1\nu_1\left(1-\nu_2^2\right)+\varphi_2\nu_2\left(1-\nu_1^2\right)}{\frac{E_1}{E_2}\varphi_1\left(1-\nu_2^2\right)+\varphi_2\left(1-\nu_1^2\right)},\quad \nu_{hv}=\left(1-\nu_{hh}\right)\left(\frac{\varphi_1\nu_1}{1-\nu_1}+\frac{\varphi_2\nu_2}{1-\nu_2}\right)\\
&E_h=\left(1-\nu_{hh}^2\right)\left(\frac{E_1\varphi_1}{1-\nu_1^2}+\frac{E_2\varphi_2}{1-\nu_2^2}\right),\qquad \nu_{vh}=\left(E_v/E_h\right)\nu_{hv}\\
&\frac{1}{E_v}=\frac{\varphi_1}{E_1}\left(1-\frac{2\nu_1^2}{1-\nu_1}\right)+\frac{\varphi_2}{E_2}\left(1-\frac{2\nu_2^2}{1-\nu_2}\right)+\frac{2\nu_{hv}^2}{\left(1-\nu_{hh}\right)E_h}\\
&K_0=\frac{\sigma_h}{\sigma_v}=\frac{\nu_{hv}}{1-\nu_{hh}}=\frac{\varphi_1\nu_1}{1-\nu_1}+\frac{\varphi_2\nu_2}{1-\nu_2}=\varphi_1K_{01}+\varphi_2K_{02}
\end{aligned}
\tag{5-27}
$$

These equations show that if the elastic properties and normalized thickness of two

constituent layers are known, the cross-anisotropic elastic properties of equivalent homogeneous material can be determined theoretically. For such a layered medium, the value of the equivalent Poisson's ratio ν_{hh} depends on the ratio of elastic moduli of the constituent layer but is independent of the absolute values of these moduli; as observed in Eq. (5-27).

Referring to Eqs. (2-20) and (2-21), the Voigt average E_{Voigt} and the Reuss average E_{Reuss} can be determined for the layered system with two constituent isotropic materials as

$$E_{Voigt} = \varphi_1 E_1 + \varphi_2 E_2 \tag{5-28}$$

$$\frac{1}{E_{Reuss}} = \frac{\varphi_1}{E_1} + \frac{\varphi_2}{E_2} \tag{5-29}$$

in which, φ_1, φ_2 is the normalized thickness , and $\varphi_1 + \varphi_2 = 1$

To make comparisons more clear, the Voigt average E_{Voigt} was used to normalize the horizontal elastic modulus E_h of the equivalent material, and the Reuss average E_{Reuss} was used to normalize the vertical elastic modulus E_v of the equivalent material. It needs to be mentioned that the Voigt average E_{Voigt} and the Reuss average E_{Reuss} provide the upper and lower bounds for the elastic moduli of a composite material rather than the actual elastic modulus.

Figure 5-6 presents the variation of the normalized modulus E_h / E_{Voigt} as a function of the normalized thickness and the difference between constituent layers in terms of the Poisson's ratio or the elastic modulus. It is clear that a good agreement between E_h of the equivalent material developed by the proposed approach and the Voigt average E_{Voigt} is achieved. The maximum variation of the E_h / E_{Voigt} is less than 3% for $E_1 / E_2 = 5$ with various ν_2 / ν_1. A similar observation can be made when

examining Figure 5-6 (b), where E_1 / E_2 varies from 1 to 5 for constant $\nu_2 / \nu_1 = 2$.

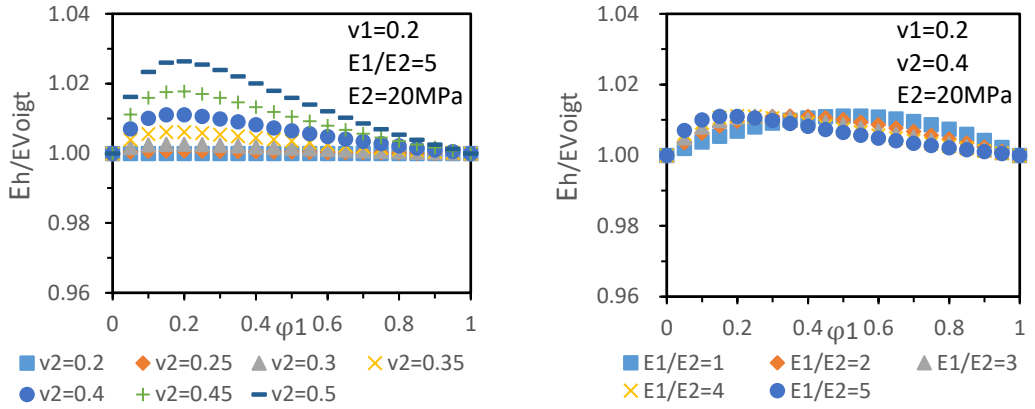

(a) (b)

Figure 5-6 Comparison of E_h with the Voigt averages E_{Voigt}

On the other hand, when examining Figure 5-7, a considerable difference between E_v of the equivalent material and the Reuss average E_{Reuss} is observed. More specifically, the Reuss average E_{Reuss} tends to underestimate the elastic modulus E_v considerably, depending on the properties of the constituent layers. The difference between E_v and E_{Reuss} increases as the difference of the material properties between the constituent layers grows. Compared to horizontal elastic modulus E_h, the value of E_v is more sensitive to the difference of the material properties between constituent layers.

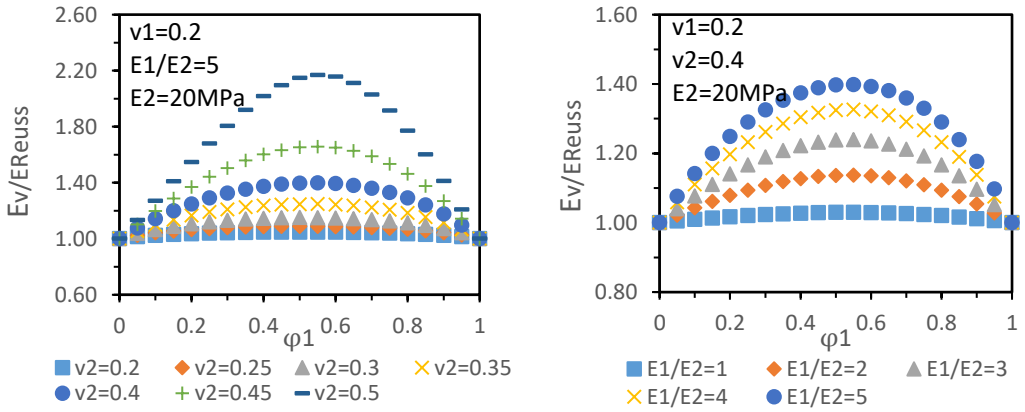

(a) (b)

Figure 5-7 Comparison of E_v with the Reuss average E_{Reuss}

In engineering practice, the Voigt average modulus and the Reuss average modulus are considered appropriate to provide theoretical upper and lower bounds on elastic modulus for a composite material composed up of different constitutive layers. Now we examine the applicability of these averages as the bounds for the vertical and horizontal elastic modulus of the equivalent material.

Figure 5-8 compares E_h and E_v with E_{Voigt} and E_{Reuss} with various volume fraction φ_1, and all the modulus are normalized by E_2 for a clear comparison. One observes that all vertical and horizontal elastic moduli of the equivalent materials determined by the proposed approach lie between curves corresponding to the upper band E_{Voigt} and the lower band E_{Reuss}. In addition, the value of E_v is sensitive to the contrast of the Poisson's ratios of different constituent layers. More specifically, as the difference between the Poisson's ratios of the constituent layers increases, the increase of E_v with φ_1 becomes significantly nonlinear. As shown in Figure 5-8 (a), the variation of φ_1 causes a small increase of E_v at lower values of φ_1 (i.e., $0 < \varphi_1 < 0.5$). However, an increase of φ_1 tends to induce a significant increase of E_v at higher values of φ_1 (i.e., $0.5 < \varphi_1 < 1$). On the other hand, the value of horizontal elastic modulus E_h of the equivalent material is independent of the difference between the Poisson's ratios of the constituent layers; as shown in Figure 5-8 (b). A close agreement between the Voigt average E_{Voigt} and E_h is observed, regardless of the difference between the Poisson's ratios of the constituent layers.

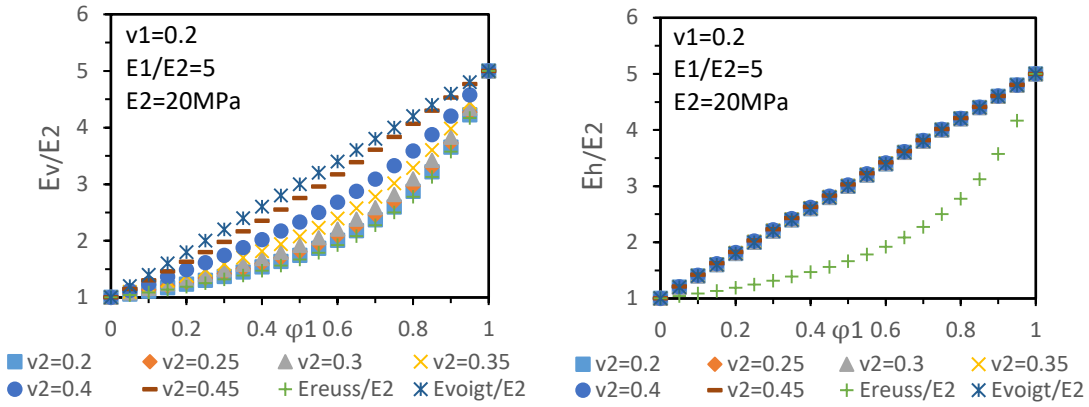

(a) (b)

Figure 5-8 The upper and lower bounds of elastic moduli of a layered material A

Another example with different elastic constants of constituent materials is examined for the applicability of the Reuss averages E_{Reuss} and the Voigt averages E_{Voigt} as the bounds for the elastic moduli of the equivalent material; as shown in Figure 5-9. Compared to the results shown in Figure 5-8 for the layered material A with two constituent layers, the same conclusion can be drawn for the layered material B. These two examples clearly prove that the Voigt averages E_{Voigt} and Reuss averages E_{Reuss} provide the upper and lower bounds for the elastic moduli of a multilayered material; i.e., $E_{Reuss} \le E \le E_{Voigt}$.

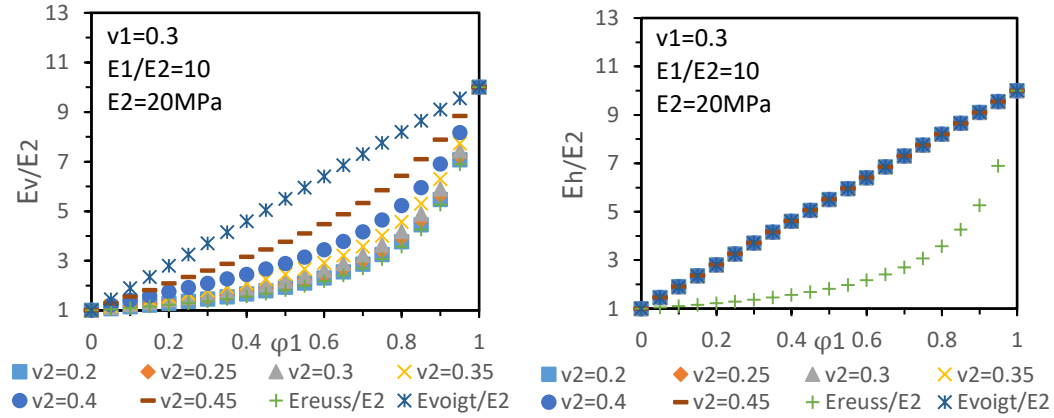

(a) (b)

Figure 5-9 The upper and lower bounds of the elastic moduli of a layered material B

Figure 5-10 presents the variation of the vertical and the horizontal elastic moduli of the equivalent medium as functions of the ratio of elastic modulus and volume fraction of constituent layers, when $v_1 = 0.2$, $v_2 = 0.4$, and $E_2 = 20\,\text{MPa}$. As the ratio of elastic modulus E_1 / E_2 and volume fraction of the stiffer material φ_1 increases, the vertical and horizontal elastic moduli (i.e., E_v and E_h) of the equivalent medium both increase, but at a different rate with respect to φ_1. When the volume fraction φ_1 of the stiffer layer increases from 0 to 0.5, E_v increases slightly slower than E_h with respect to φ_1. However, an opposite trend is observed when the volume fraction of the stiffer material is greater than 0.5. It should be noted that E_h of the equivalent medium always increases linearly as a function of the volume fraction of the stiffer constituent layer, regardless of the difference between the elastic modulus of the constituent layer. However, E_v of the equivalent medium increases non-linearly as a function of φ_1.

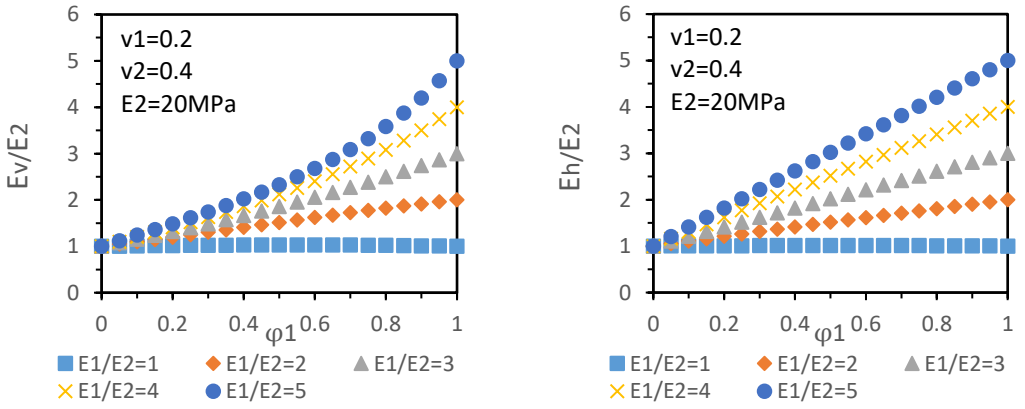

(a) (b)

Figure 5-10 Comparison of E_v and E_h of the equivalent medium

Figure 5-11 presents the variation of the K_0-values of the equivalent material as a function of the normalized thickness and the difference between constituent layers in terms of the Poisson's ratio or the elastic modulus. It is clear that the K_0-values of the equivalent material vary linearly with normalized thickness φ_1 for given elastic constants of constituent layers (i.e., Poisson's ratio and elastic modulus). More specifically, when the difference between the Poisson ratios of constituent layers increases with the normalized thickness, the variation of the K_0-values of the equivalent material follow the relation $K_0 = \frac{\varphi_1 \nu_1}{1-\nu_1} + \frac{\varphi_2 \nu_2}{1-\nu_2} = \varphi_1 K_{01} + \varphi_2 K_{02}$; as shown in Figure 5-11 (a). On the other hand, the K_0-values of the equivalent material is independent of the difference between the elastic modulus of the constituent layers; as shown in Figure 5-11(b). The same variation trend of the K_0-values of the equivalent material is obtained for given $\nu_1 = 0.2$ and $\nu_2 = 0.4$, regardless of various ratios of elastic modulus of constituent layers E_1 / E_2.

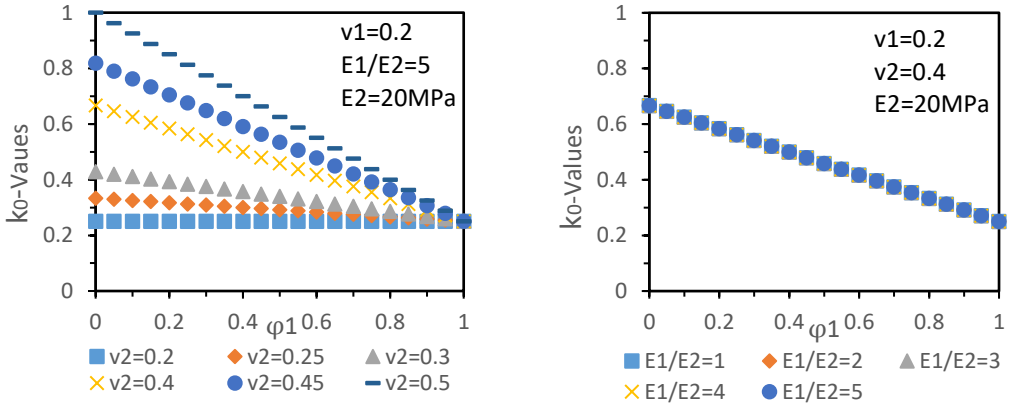

(a) (b)

Figure 5-11 K_0-values of the equivalent medium

The ratio of horizontal elastic modulus and vertical elastic modulus E_h / E_v can be used as a measure to the degree of anisotropy of the equivalent material with respect to stiffness. Figure 5-12 presents the variation of E_h / E_v of the equivalent material as functions of the material properties and volume fraction of constituent materials for selected cases. More specifically, when $v_1 = 0.2$, $v_2 = 0.4$, and $E_2 = 20\,\text{MPa}$, as the difference between the elastic modulus of constituent layers increases(i.e., E_1 / E_2 increases) for a given volume fraction φ_1, the value of E_h / E_v increases; as shown in Figure 5-12 (a). However, when the difference between the elastic modulus of constituent layers is small (i.e., $1 < E_1 / E_2 < 2$), the value of the degree of anisotropy remain approximately constant, which is close to one. It should be noted that the value of E_h / E_v is also affected by the volume fraction of the constituent material.

On the other hand, Poisson's ratio of each constitutive layer plays a different role in affecting the magnitude of the horizontal and vertical elastic modulus of the equivalent medium. For the select elastic modulus ratio $E_1 / E_2 = 5$, as the difference between the Poisson's ratio of constituent layers increases, the value of E_h / E_v decreases for a given volume fraction φ_1; as shown in Figure 5-12 (b).

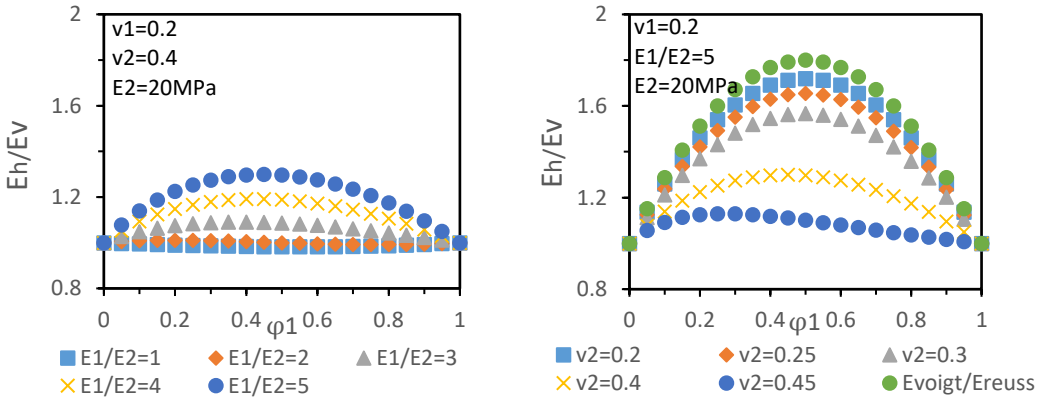

(a) (b)

Figure 5-12 Degree of anisotropy of the equivalent medium

In summary, the applicability of the Voigt average E_{Voigt} and the Reuss average E_{Reuss} as the upper and lower bounds for the effective elastic modulus of the multilayered material composed of two isotropic constituent layers was examined through two examples. Regarding the horizontal elastic modulus of the equivalent material, a good agreement between E_h developed by the proposed approach and the Voigt average E_{Voigt} was achieved. On the other hand, the Reuss average E_{Reuss} appeared to underestimate the vertical elastic modulus E_v of the composite material considerably, depending on the properties of the constituent layers.

The linear variation of the K_0-values of the equivalent material with normalized thickness and elastic constants of the constituent layers was illustrated. The variation trend was consistent with the expectation coming from the theoretical analysis.

It has been demonstrated that the degree of anisotropy of the equivalent homogeneous material increased, with the increase of the difference between the elastic constants of constitutive layers for a constant volume fraction. However, it should be noted that the difference between the Poisson ratios of the constituent layers plays a different role in affecting the magnitude of the degree of anisotropy, compared to the influence of the difference between the elastic modulus of the constituent layers

Chapter 6 CONCLUSION AND FUTURE WORK

6.1 Summary and conclusion

This study includes experimental, theoretical, and numerical aspects, and it provides an insight into the anisotropic behaviour of the layered soil in the elastic range. It has been shown that when the thickness of each constitutive layer is much smaller than the characteristic length of the multilayered medium, the layered material can be considered as the 'equivalent' cross-anisotropic homogenisation material. The cross-anisotropic elastic material properties can be determined by the proposed experimental program. It must be stressed out that the proposed approach is only applicable for the layered soil with a horizontal layered structure, in which the layer thicknesses are narrow when compared to the overall height of the sample.

In the experimental program, this study extended Vaid's work (1971) to conduct K_0-compression test in the rigid triaxial cell with flexible lateral boundary for the determination of the K_0-value of the normally consolidated soil, and the error induced by the compliance of the cell-water system that always exists in the previous study were matigated by attaching a compliance correction system (i.e., GDS controller) to the triaxial cell. A good performance of the experimental setup adopted was confirmed by the consistency and repeatability of the test results for the two types of selected soils (i.e., the homogeneous soil and the layered soil).

The selected soils were considered as the cross-anisotropic soils, whose elastic properties were determined by the proposed approach through the manipulation of the elastic theory and combining the measured data obtained from three stress-path tests (i.e., the K_0-compression test, the plane strain compression test, and the hydrostatic pressure compression test). The least squares method was used to eliminate the mathematical redundancy induced by more stress-strain relations obtained from the various stress-path tests than the equations required.

Based on the material properties determined by the experimental study, numerical simulations (i.e., the numerical K_0-test) were conducted to compare with the test results. A good consistency was achieved between the numerically generated data and the experimentally measured data, which in turn demonstrates the applicability of the proposed approach to determine the cross-anisotropic elastic constant of the soil.

This study made use of the Reuss and the Voigt approximations and proposed a simple, yet physically meaningful approach to determine the equivalent cross-anisotropic elastic properties for the multilayered medium. The explicit expressions for the elastic constants of the equivalent cross-anisotropic material were given in terms of the elastic properties and volume fraction of the constitutive layers.

The applicability of the approach was examined by analyzing a multilayered medium with two constituent materials that were both isotropic. The anisotropic behaviour of the multilayered material (i.e., stiffness anisotropy) was analyzed by conducting the parameters sensitivity analysis, in which Poisson's ratio and elastic modulus of each constitutive layer are different. The conclusion is that with the increase of the difference between elastic properties of constitutive layers for a condition of constant volume fractions, the degree of anisotropy of the equivalent homogeneous material increased. That is, the equivalent homogeneous material would be gradually stiffer in the horizontal direction than in the vertical direction.

6.2 Recommendations for future work

The following work is considered necessary in the future:

- Add bender elements to and local strain measurement sensors into the proposed testing system for determining the shear moduli and providing a better measurement for the actual deformation of the sample during loading.
- Further experiments on the horizontally cut layered soil sample with a vertical bedding plane with comparison of the tests.
- Further experiments on the tested layered material for the determination of

strength parameters and failure mechanism.

- Further experiments on layered soils with inclined and vertical layered structures and comparison of the test results to those of layered soil with a horizontal layered structure obtained from this study.

Reference

Abdelhamid,M.S., and Krizek, R,J. (1976). At rest lateral earth pressure of a consolidating clay. *ASCE Journal of the Geo-technical Engineering Division,* 102(GT7): pp.721-738.

Abelev, A. and Lade, P. (2003). Effects of Cross Anisotropy on Three-Dimensional Behaviour of Sand. I: Stress–Strain Behaviour and Shear Banding. *J. Eng. Mech.*, 129(2), pp.160-166.

Atkinson, J., Richardson, D. and Stallebrass, S. (1990). Effect of recent stress history on the stiffness of overconsolidated soil. *Géotechnique*, 40(4), pp.531-540.

Bellotti, R., Jamiolkowski, M., Presti, D. and O'Neill, D. (1996). Anisotropy of small strain stiffness in Ticino sand. *Géotechnique*, 46(1), pp.115-131.

Bishop,A,W., and Henkel,D.J., (1962). The measurement of soil properties in the triaxial test. *2nd edn. London:Edward Arnold*.

Bishop, A. and Hight, D. (1977). The value of Poisson's ratio in saturated soils and rocks stressed under undrained conditions. *Géotechnique*, 27(3), pp.369-384.

Campanella.R.G. and Vaid.Y.P (1972) A Simple K_0 Triaxil Cell. *Canadian Geotechnical Journal*, 9(3), pp.249-260.

Chaney, R., Demars, K., Hoque, E., Tatsuoka, F. and Sato, T. (1996). Measuring Anisotropic Elastic Properties of Sand Using a Large Triaxial Specimen. *Geotech. Test. J.*, 19(4), p.411.

Chaney, R., Demars, K., Kuwano, R., Connolly, T. and Jardine, R. (2000). Anisotropic

Stiffness Measurements in a Stress-Path Triaxial Cell. *Geotech. Test. J.*, 23(2), p.141.

Clayton, C. (2011). Stiffness at small strain: research and practice. *Géotechnique*, 61(1), pp.5-37.

Clayton, C. and Heymann, G. (2001). Stiffness of geomaterials at very small strains. *Géotechnique*, 51(3), pp.245-255.

Davis,E.H. and Poulos,H.G.(1963). Triaxial testing and three-dimensional settlement analysis. Fourth Australia-New Zealand Conference on Soil Mechanics &Foundation Engineering. pp233-243

David Suits, L., Sheahan, T., Zeng, X. and Grolewski, B. (2005). Measurement of Gmax and Estimation of K_0 of Saturated Clay Using Bender Elements in an Oedometer. *Geotech. Test. J.*, 28(3), p.11318.

Eliadorani,A.A. and Vaid,Y.P.(2005). The measurement of K0, the coefficient of earth pressure at rest by strain path loading technique. Proc.16th Int. Conf. On. Soil Mech. and Geotechnical Engineering, ICSMGE, Osaka, Vol.2, pp.345-348.

Fahad Alshawmar. (2008). Evaluation of Compressibility, Anisotropy and At-rest Lateral Earth Pressure in Champlain Sea Clays. Master thesis, Carleton University, Ottawa, Canada.

Farhad Vatandoost.(2009).On the elastic properties of the equivalent transversely isotropic material. Master thesis, McMaster University, Hamilton, Canada.

Gasparre, A., Nishimura, S., Minh, N., Coop, M. and Jardine, R. (2007). The stiffness of natural London Clay. *Géotechnique*, 57(1), pp.33-47.

Gerrard, C. (1982). Equivalent elastic moduli of a rock mass consisting of orthorhombic layers. *International Journal of Rock Mechanics and Mining Sciences & Geomechanics Abstracts*, 19(1), pp.9-14.

Graham, J. and Houlsby, G. (1983). Anisotropic elasticity of a natural clay. *Géotechnique*, 33(3), pp.354-354.

Guo,P and Stolle, D.(2016). A physically meaningful homogenization approach to determine equivalent elastic properties of layered material. *Canadian Geotechnical Journal.*

Hornung, U.1997. Homogenization and porous media (*interdisciplinary applied mathematics*).Springer-Verlag, New York.

Hoque, E. and Tatsuoka, F. (1998). Anisotropy in Elastic Deformation of Granular Materials. *SOILS AND FOUNDATIONS*, 38(1), pp.163-179.

Jaky,J.(1944). "The coefficient of earth pressure at rest. *Journal of the Society of Hungarian Architects and Engineering*, pp.355-358

Japanese Geotechnical Society Standards (JGS0525-2000): Method for K_0-consolidation undrained triaxial compression test on soils with pore water pressure measurement, *Standard for Laboratory Tests on Geo-materials*, pp.604-609.

Jardine, R., Symes, M. and Burland, J. (1984). The Measurement of soil stiffness in the triaxial apparatus. *Géotechnique*, 34(3), pp.323-340.

Jiang, G., Tatsuoka, F., Flora, A. and Koseki, J. (1997). Inherent and stress-state-induced anisotropy in very small strain stiffness of a sandy gravel. *Géotechnique*, 47(3), pp.509-521.

Knodel, P., Kirkgard, M. and Lade, P. (1991). Anisotropy of Normally Consolidated San Francisco Bay Mud. *Geotech. Test. J.*, 14(3), p.231.

Kuwano, R. and Jardine, R. (2002). On measuring creep behaviour in granular materials through triaxial testing. *Canadian Geotechnical Journal*, 39(5), pp.1061-1074.

Kuwano, R. and Jardine, R. (2002). On the applicability of cross-anisotropic elasticity to granular materials at very small strains. *Géotechnique*, 52(10), pp.727-749.

Kuwano, R. and Jardine, R. (2002). On the applicability of cross-anisotropic elasticity to granular materials at very small strains. *Géotechnique*, 52(10), pp.727-749.

Ladd,R.S.1965. Use of electrical pressure transducers to measure soil pressure. *Massachusetts Institute of Technology Research Report* R65-48,No.180.

Lings, M. (2001). Drained and undrained anisotropic elastic stiffness parameters. *Géotechnique*, 51(6), pp.555-565.

Lings, M., Pennington, D. and Nash, D. (2000). Anisotropic stiffness parameters and their measurement in a stiff natural clay. *Géotechnique*, 50(2), pp.109-125.

Lirer, S., Flora, A. and Nicotera, M. (2010). Some remarks on the coefficient of earth pressure at rest in compacted sandy gravel. *Acta Geotechnica*, 6(1), pp.1-12.

Liu.Y (2010). Stress-path dependency of resilient behaviour of granular materials. Ph.D. Thesis, Civil Engineering Department at McMaster University.

Lo, S. and Chu, J. (1991). The measurement of K0 by triaxial strain path testing. *SOILS AND FOUNDATIONS*, 31(2), pp.181-187.

Mayne, P. and Kulhawy, F. (1983). K_0-OCR relationships in soil. *International Journal of Rock Mechanics and Mining Sciences & Geomechanics Abstracts*, 20(1), p.A2.

Mesri, G. and Hayat, T. (1993). The coefficient of earth pressure at rest. *Canadian Geotechnical Journal*, 30(4), pp.647-666.

Milton,G.W.(2004). The theory of composite. Cambridge University Press, Cambridge, UK.

Minh,A.N., Nishimura,S., Takahashi,A, and Jardine,R.J., (2011). On the control systems and instrumentation required to investigate the anisotropy of stiff clays and mudrocks through hollow cylinder test. *Proc.5th Int. Symp. Deform Charact .Geomater., Seoul.*, pp.287-294.

Niemunis, A., Karcher, C. and Theile, T. (2000). An averaging procedure for layered materials. *International Journal for Numerical and Analytical Methods in Geomechanics*, 24(10), pp.837-851.

Nishimura, S. (2014). Assessment of anisotropic elastic parameters of saturated clay measured in triaxial apparatus: Appraisal of techniques and derivation procedures. *Soils and Foundations*, 54(3), pp.364-376.

Nishimura, S. (2014). Cross-anisotropic deformation characteristics of natural sedimentary clays. *Géotechnique*, 64(12), pp.981-996.

Northcutt, S. and Wijewickreme, D. (2013). Effect of particle fabric on the coefficient of lateral earth pressure observed during one-dimensional compression of sand. *Canadian Geotechnical Journal*, 50(5), pp.457-466.

Okochi, Y. and Tatsuoka, F. (1984). Some factors affecting K_0-values of sand

measured in triaxial cell. *Soils and Foundations*, 24(3), pp.52-68.

Postma, G. (1955). Wave propagation in a stratified medium. *Geophysics*, 20(4), pp.780-806.

Pyrah, I. (1996). One-dimensional consolidation of layered soils. *Géotechnique*, 46(3), pp.555-560.

Ratananikom, W., Likitlersuang, S. and Yimsiri, S. (2013). An investigation of anisotropic elastic parameters of Bangkok Clay from vertical and horizontal cut specimens. *Geomechanics and Geoengineering*, 8(1), pp.15-27.

Reuss, A. (1929). Berechnung der Fließgrenze von Mischkristallen auf Grund der Plastizitätsbedingung für Einkristalle . *ZAMM - Zeitschrift für Angewandte Mathematik und Mechanik*, 9(1), pp.49-58.

Salamon, M. (1968). Elastic moduli of a stratified rock mass. *International Journal of Rock Mechanics and Mining Sciences & Geomechanics Abstracts*, 5(6), pp.519-527.

Santana.T, and Candeias .M, (2015). K0 measurement in sand using back volume change. *Soil and Rocks*, 38(1), pp.3-8.

Seed.H.B. and R.L. McNeill, (1957). Soil Deformation under Repeated Stress Applications. *Proceeding, Conference on Soils for Engineering Purposes*, Universidad de Mexico.

Seyhan, U., Tutumluer, E. and Yesilyurt, H. (2005). Anisotropic Aggregate Base Inputs for Mechanistic Pavement Analysis Considering Effects of Moving Wheel Loads. *J. Mater. Civ. Eng.*, 17(5), pp.505-512.

Skrzypek, J.J. and Ganczarski, A.W.(2015). Mechanics of anisotropic materials. Springer Cham Heidelberg New York Dordrecht Lonton

Stolle, D. (1992). Average strain quadrilateral elements. *Communications in Applied Numerical Methods*, 8(8), pp.505-510.

Stolle, D. and Guo, P. (2007). A look at the use of an equivalent homogeneous medium. *Canadian Geotechnical Journal*, 44(5), pp.507-519.

Voigt, W. (1907). Bestimmung der Elastizitätskonstanten von Aragonit. *Annalen der Physik,* 329(12), pp.290-304.

Wanatowski, D. and Chu, J. (2007). K_0 of sand measured by a plane-strain apparatus. *Canadian Geotechnical Journal,* 44(8), pp.1006-1012.

Wardle, L. and Gerrard, C. (1972). The “equivalent” anisotropic properties of layered rock and soil masses. *Rock Mechanics Felsmechanik Mécanique des Roches*, 4(3), pp.155-175.

Wood,D.M.(1990). Soil Behaviour and Critical State Soil Mechanics. Cambridge University Press, Cambridge, pp.462

Yamanouchi, T. and Yasuhara, K. (1974). A Consideration on the Coefficient of Earth Pressure at Rest in Clayey Soils. *SOILS AND FOUNDATIONS*, 14(2), pp.113-118.

Yu, S. and Dakoulas, P. (1993). General Stress-Dependent Elastic Moduli for Cross-Anisotropic Soils. *Journal of Geotechnical Engineering*, 119(10), pp.1568-1586.

Zdravkovic, L. and Jardine, R. (1997). Some anisotropic stiffness characteristics of a silt under general stress conditions. *Géotechnique*, 47(3), pp.407-437.

Zienkiewicz, O., Taylor, R. and Nithiarasu, P. (2014). The Finite Element Method for

Fluid Dynamics. 1st ed. Oxford, [et al.]: Butterworth-Heinemann.

Appendix

1) Sample calculation for estimating the error of the K_0-value induced by the compliance of the cell-water system

Following Vaid (1971), the actual increase in horizontal stress (i.e., the cell pressure) is determined as $\Delta\sigma_c' = K_0\Delta\sigma_v'\eta$.

Considering a clay is consolidated under K_0-condition from a slurry (i.e., initial effective stress are essentially zero) to a vertical effective stress σ_v', the magnitude of horizontal effective stress can be calculated by a summation of the above equation as

$$\Delta\sigma_c' = K_0\int_0^{\sigma_v'} d\sigma_v'\ \eta$$

where $\eta = \dfrac{1}{1+\dfrac{1.5}{V}\dfrac{C}{m_v}}$

m_v can be related to the compression index C_c that is constant with pressure for most normally consolidated clays. Assuming the average void ratio of the soil equal to unity, one has

$$m_v = \frac{0.22C_c}{\sigma_m'},\quad \sigma_m' = \frac{1}{3}\sigma_v'(1+2K_0),\quad m_v = \frac{0.22C_c}{\sigma_v'}\frac{3}{1+2K_0}$$

$$\Delta\sigma_c' = K_0\int_0^{\sigma_v'} d\sigma_v'\ \eta = K_0\int_0^{\sigma_v'} \frac{1}{1+\dfrac{1.5C}{V}\dfrac{(1+2K_0)\sigma_v'}{0.22\times 3C_c}}d\sigma_v' = K_0\int_0^{\sigma_v'} \frac{1}{1+X\sigma_v'}\,d\sigma_v'$$

$$X = \frac{1.5C}{V}\frac{(1+2K_0)}{0.22\times 3C_c}$$

$$\Delta\sigma_c' = K_0\int_0^{\sigma_v'} d\sigma_v'\ \eta = \frac{K_0}{X}In\left(1+X\sigma_v'\right)$$

In the apparatus adopted in this study, the compliance C was estimated to be in the range of 0.15-0.20 cm^3/100 kPa. Considering a clay sample (60.9 cm in diameter $\times$ 50 cm in high, V=145 cm^3) with $K_0 = 0.5$ and C_c=0.2 consolidated to σ_v'=6 kg/cm^2,

one has when C=0.15 cm^3/100 kPa

$$X=\frac{1.5C}{V}\frac{(1+2K_0)}{0.22\times 3C_c}=\frac{1.5\times 0.15}{145}\frac{2}{0.66\times 0.2}\approx\frac{1}{42}$$

$$\Delta\sigma_c'=K_0\int_0^{\sigma_v'}d\sigma_v'\ \ \eta=\frac{K_0}{X}In\left(1+X\sigma_v'\right)=42K_0In\left(1+\frac{\sigma_v'}{42}\right)=2.804$$

$$\left(K_0\right)_m=\frac{\Delta\sigma_c'}{\Delta\sigma_v'}=\frac{2.804}{6}=0.467$$

$$Error=\frac{\left|K_0-(K_0)_m\right|}{K_0}\times 100\%=\frac{0.5-0.467}{0.5}*100\%\approx 6\%$$

When C=0.2 cm^3/100 kPa

$$X=\frac{1.5C}{V}\frac{(1+2K_0)}{0.22\times 3C_c}=\frac{1.5\times 0.2}{145}\frac{2}{0.66\times 0.2}\approx\frac{1}{32}$$

$$\Delta\sigma_c'=K_0\int_0^{\sigma_v'}d\sigma_v'\ \ \eta=\frac{K_0}{X}In\left(1+X\sigma_v'\right)=32K_0In\left(1+\frac{\sigma_v'}{32}\right)=2.75$$

$$\left(K_0\right)_m=\frac{\Delta\sigma_c'}{\Delta\sigma_v'}=\frac{2.75}{6}=0.458$$

$$Error=\frac{\left|K_0-(K_0)_m\right|}{K_0}\times 100\%=\frac{0.5-0.458}{0.5}\times 100\%\approx 9\%$$

2) Estimating the initial rate of injecting water for making proper compliance compensations

Change in volume of the sample: $\Delta V_1 = m_v V \frac{1}{3}(\Delta\sigma_v' + 2\sigma_c')$

Expansion of the lateral pressure system is $\Delta V_2 = C\sigma_c'$

In comparison, the change in volume of a sample in the presence of a $C = 0$ lateral pressure system is $\Delta V_3 = m_v V \frac{1}{3}(\Delta\sigma_v' + 2K_0\sigma_v') = m_v V \frac{1}{3}(1+2K_0)\Delta\sigma_v'$

$$\Delta V_2 = \Delta V_3 - \Delta V_1 = \frac{2}{3} m_v V (K_0 \Delta\sigma_v' - \Delta\sigma_c')$$

Alternatively, $\Delta V_3 = m_v V \frac{1}{3}(1+2K_0)\Delta\sigma_v' = \varepsilon_v V$; $\varepsilon_v = m_v \frac{1}{3}(1+2K_0)\Delta\sigma_v'$,

$$\Delta\sigma_v' = \frac{3\varepsilon_v}{m_v(1+2K_0)}$$

$$\Delta V_2 = C\Delta\sigma_c' = 2\varepsilon_h V$$

$$\Delta V_1 = m_v V \frac{1}{3}(\Delta\sigma_v' + 2\sigma_c') = m_v V \frac{1}{3}\left[\frac{3\varepsilon_v}{m_v(1+2K_0)} + \frac{4\varepsilon_h V}{c}\right]$$

$$2\varepsilon_h V = \frac{2}{3} m_v V (K_0 \Delta\sigma_v' - \Delta\sigma_c') = \frac{2}{3} m_v V \left[K_0 \frac{3\varepsilon_v}{m_v(1+2K_0)} - \frac{2\varepsilon_h V}{c}\right],$$

$$\left(1 - \frac{2m_v V}{3c}\right)\varepsilon_h = \frac{K_0 \varepsilon_v}{1+2K_0}, \quad \frac{\varepsilon_h}{\varepsilon_v} = \frac{K_0}{1+2K_0}\left(1 + \frac{2m_v V}{3c}\right)^{-1}$$

$$\frac{\dot{V}_2}{\dot{h}} = \frac{2\varepsilon_h V}{\varepsilon_v H} = \frac{\varepsilon_h}{\varepsilon_v} 2A, \quad \dot{V}_2 = \frac{\varepsilon_h}{\varepsilon_v} 2A\dot{h}$$